

# Block copolymers as (single-ion conducting) lithium battery electrolytes

Alexander Mayer<sup>1,2</sup> , Dominik Steinle<sup>1,2</sup> , Stefano Passerini<sup>1,2,\*</sup>  and Dominic Bresser<sup>1,2,\*</sup> 

<sup>1</sup> Helmholtz Institute Ulm (HIU), Helmholtzstrasse 11, D-89081 Ulm, Germany

<sup>2</sup> Karlsruhe Institute of Technology (KIT), PO Box 3640, D-76021 Karlsruhe, Germany

E-mail: [dominic.bresser@kit.edu](mailto:dominic.bresser@kit.edu) and [stefano.passerini@kit.edu](mailto:stefano.passerini@kit.edu)

## Abstract

Solid-state batteries are considered the next big step towards the realization of intrinsically safer high-energy lithium batteries for the steadily increasing implementation of this technology in electronic devices and particularly, electric vehicles. However, so far only electrolytes based on poly(ethylene oxide) have been successfully commercialized despite their limited stability towards oxidation and low ionic conductivity at room temperature. Block copolymer (BCP) electrolytes are believed to provide significant advantages thanks to their tailorable properties. Thus, research activities in this field have been continuously expanding in recent years with great progress to enhance their performance and deepen the understanding towards the interplay between their chemistry, structure, electrochemical properties, and charge transport mechanism. Herein, we review this progress with a specific focus on the block-copolymer nanostructure and ionic conductivity, the latest works, as well as the early studies that are frequently overlooked by researchers newly entering this field. Moreover, we discuss the impact of adding a lithium salt in comparison to single-ion conducting BCP electrolytes along with the encouraging features of these materials and the remaining challenges that are yet to be solved.

Keywords: block copolymer, electrolyte, single-ion conductor, ionic conductivity, lithium battery

(Some figures may appear in colour only in the online journal)

## Abbreviations

A, B, C,	abbreviations for different blocks in block copolymers	CV	cyclic voltammetry
ATRP	atom transfer radical polymerization	DIS	disordered state
bcc	body-centered cubic packing	EC	ethylene carbonate
BCP(E)	block copolymer (electrolytes)	EFTEM	energy-filtered transmission electron microscopy
C	cylinders	EO	ethylene oxide
CFRP	controlled free radical polymerization	G	gyroidal or bicontinuous
CP	copolymer	hcp	hexagonal close packing
		HEX-C	hexagonally packed cylinders
		HOMO	highest occupied molecular orbital
		HPL	hexagonally perforated lamellae

\* Authors to whom any correspondence should be addressed.

IL	ionic liquid	PO	propylene oxide
ISO	poly(isoprene)- <i>b</i> -poly(styrene)- <i>b</i> -poly(ethylene oxide) triblock copolymer	PP	poly(propylene)
L	lamellae	PPO	poly(propylene oxide)
LCO	lithium cobalt oxide	PS	poly(styrene)
LFP	lithium iron phosphate	PSTFSiLi	lithiated poly(styrene sulfonyl(trifluoromethanesulfonyl) imide)
Li	lithium	PVdF-HFP	poly(vinylidene difluoride- <i>co</i> -hexafluoropropylene)
LiBOB	lithium bis(oxalato)borate	RAFT	reversible addition-fragmentation chain-transfer polymerization
LiMA	lithiated methacrylic acid	ROMP	ring-opening metathesis polymerization
LiOTf/LiTf	lithium trifluoromethanesulfonate, lithium triflate	RT	room temperature
LiTFSI	lithium bis(trifluoromethanesulfonyl)imide	S	spheres
LUMO	lowest unoccupied molecular orbital	SANS	small angle neutron scattering
MDS	molecular dynamics simulation	SAXS	small angle x-ray scattering
NCM	LiNi <sub>x</sub> Co <sub>y</sub> Mn <sub>z</sub> O <sub>2</sub> , lithium nickel cobalt manganese oxide	SEC (GPC)	size exclusion chromatography (gel permeation chromatography)
NMP(T)	nitroxide-mediated polymerization (technique)	SEI	solid electrolyte interface
OCV	open circuit voltage	SEO	poly(styrene)- <i>b</i> -poly(ethylene oxide) diblock copolymer
ODT	order–disorder transition	SEM	scanning electron microscopy
OOT	order–order transition	SIC	single-ion conducting/conductor
P2VPy	poly(2-vinylpyridine)	SPE	solid polymer electrolyte
P3HT	poly(3-hexylthiophene)	(S)TEM	(scanning) transmission electron microscopy
PBPA	poly(bisphenol A carbonate)	THF	tetrahydrofuran
PC	propylene carbonate	TMC	trimethylene carbonate
PCL	poly( $\epsilon$ -caprolactone)	VTF	Vogel–Tammann–Fulcher
PDMS	poly(dimethyl siloxane)	WAXS	wide angle x-ray scattering
PDTC	poly(2,2-dimethyltrimethylene carbonate)	XRD	x-ray diffraction
PE	poly(ethylene)	XPCS	x-ray photon correlation spectroscopy
PEGDME	poly(ethylene glycol dimethyl ether)	<b>Symbols</b>	
PEI	poly(iminoethylene)	<i>B</i>	pseudo-activation energy, J
PEO	poly(ethylene oxide)	<i>k<sub>B</sub></i>	Boltzmann constant, J K <sup>-1</sup>
PFG-NMR	pulsed field gradient nuclear magnetic resonance spectroscopy	<i>M<sub>n</sub> /M<sub>PEO</sub></i>	number average molar mass of a polymer/ the PEO block, g mol <sup>-1</sup>
PFS	poly(pentafluorostyrene)	<i>M<sub>w</sub></i>	mass average molar mass of a polymer, g mol <sup>-1</sup>
PI	poly(isoprene)	<i>N</i>	degree of polymerization (number of polymer units), dimensionless
PIL	poly(ionic liquid)	<i>r</i>	molar ratio of lithium ions with respect to EO moieties, dimensionless
PLMA	poly(lauryl methacrylate)	<i>T</i>	temperature, K or °C
PMAN	poly(methacrylonitrile)	<i>T<sub>0</sub></i>	equilibrium temperature, °C
PMAALi	lithiated poly(methacrylic acid)	<i>T<sub>g</sub></i>	glass transition temperature, °C
PMMA	poly(methyl methacrylate)	<i>t<sub>Li</sub><sup>+</sup></i>	lithium ion transference number, dimensionless
PMTFSiLi	lithiated poly(3-sulfonyl(trifluoromethanesulfonyl)imide propyl methacrylate)	<i>T<sub>m</sub></i>	melting temperature, °C
PnBMA	poly( <i>n</i> -butyl methacrylate)		
POEM/POEGMA	poly[oligo(ethylene glycol)methacrylate]		
POSS	polyhedral oligomeric silsesquioxane		

## Greek letters

$\alpha$	tortuosity factor, dimensionless
$\varepsilon_{ij}$	contact energy between the monomer segments $i$ and $j$ ,
$\sigma(T)$	ionic conductivity, $\text{S cm}^{-1}$
$\chi N$	segregation strength
$\chi_0$	Flory–Huggins interaction parameter, dimensionless
$\chi_{\text{eff}}$	effective interaction parameter, dimensionless
$\varphi_A/\varphi_B$ or $f_A/f_B$	volume fraction of polymer A or B, dimensionless

## 1. Introduction

For our modern everyday lifestyle rechargeable batteries are indispensable. Especially the Li-ion battery (LIB) technology revealed to be the battery system of choice to meet the increasing energy performance requirements of portable electronic devices like laptops, smartphones, etc. In addition, it is the most suitable technology to power hybrid and electric vehicles (EVs) reducing the anthropogenic  $\text{CO}_2$  emissions [1–4]. However, future increase in energy density (i.e. driving range with respect to their application in EVs) is limited by the weight and volume of the electrode active materials (plus the required electrolyte and electrochemically inactive components). Recently, this has triggered a renewed interest in the investigation of metallic lithium for the negative electrode, despite the initial safety issues related to the formation of dendritic structures and the resulting accidental short circuits [5, 6]. In this regard, the electrolyte, physically separating the two electrodes, plays a pivotal role for the battery safety not least with respect to its potential flammability and toxicity, including also potential decomposition products [7–9]. Solid electrolytes such as polymers are considered the standard for inherently safer batteries in combination with lithium metal anodes by preventing cell leakage upon mechanical abuse, providing limited flammability and reducing, if not suppressing, lithium dendrite formation [9, 10].

The idea of implementing polymers as battery electrolytes is not a new approach but was proposed in 1973 by Fenton *et al* [11], who studied the structural properties of alkali metal salts dissolved in poly(ethylene oxide) (PEO). In 1978, Armand first reported such ‘SPEs’ for lithium batteries [12–14]. This work initiated substantial research activities towards SPEs, including the search for an improved mechanistic understanding of the ion transport phenomena [15–18]. It was established that the ionic conductivity rose with an increasing fraction of the amorphous domains in the polymer electrolyte above the glass transition temperature  $T_g$  [18–20]. As a result, the conventional model for describing the occurring charge transport became the ‘free volume model’, correlating the thermal movement of the polymer

chain segments (i.e. the segmental relaxation) with the ionic motion [21, 22]. This correlation can be expressed by the VTF equation (equation (1)):

$$\sigma(T) = \sigma_0 \cdot \frac{1}{\sqrt{T}} \cdot \exp\left(-\frac{B}{k_B \cdot (T - T_0)}\right), \quad (1)$$

where  $k_B$  is the Boltzmann constant,  $T$  the temperature in Kelvin,  $B$  the pseudo-activation energy, which corresponds to the Arrhenius-type activation energy  $E_a$ , and  $T_0$  the equilibrium  $T_g$  of the polymer (controlled for kinetic effects) [17, 18, 23]. This equation was originally developed to describe the temperature dependence of glassy materials’ viscosity [24–26], but also emerged to be applicable for the description of the temperature-dependent ionic conductivity of SPEs above the  $T_g$ , since the viscosity is directly linked to charge transport via the segmental relaxation [17].

In the case of PEO, the charge transport along the amorphous domains benefits from the advantageous spatial distance between the electron-pair donating oxygen atoms and the low energy barrier for the bond rotation, facilitating  $\text{Li}^+$  complexation and segmental relaxation [10, 27]. The ionic conductivity remains limited to values of about  $10^{-5} \text{ S cm}^{-1}$  at RT, which is far below the conductivity of common liquid organic electrolytes ranging between  $10^{-3}$  and  $10^{-2} \text{ S cm}^{-1}$  [28] or gel polymer electrolytes, in which the polymer (e.g. poly(vinylidene difluoride), PVdF) essentially serves as a matrix (comparable to a classic separator) to host the liquid organic electrolyte, usually ranging between  $10^{-3}$  and  $10^{-4} \text{ S cm}^{-1}$  [29]. While the latter type of electrolytes provides advantages concerning safety, as the intimate interaction of the polymer matrix and the liquid electrolyte hinders cell leakage, the compatibility with metallic lithium electrodes remains limited owing to the reactivity of the liquid electrolyte [9]. Thus, targeting improved ionic conductivities in ‘classic’ polymer-based electrolytes led to a plethora of synthetic strategies and modifications in order to, e.g. lower the  $T_g$  and suppress the crystallization of the polymer matrix. This includes the incorporation of solid (ceramic) nanoparticles such as  $\text{Al}_2\text{O}_3$ ,  $\text{SiO}_2$ , and  $\text{ZrO}_2$ , which increase ionic conductivity by up to several orders of magnitude [10, 28, 30], depending on their surface chemistry (i.e. acidity) and the resulting interaction between the polymer and the conducting salt [31, 32]. Another strategy is based on the incorporation of liquid plasticizers such as organic solvents [33, 34] or ionic liquids [35–37] to facilitate the segmental motion and thus the charge transport within the polymer matrix. In addition, the ionic conductivity could be improved by up to several orders of magnitude. Although, any additional phase whether solid or liquid has a significant impact on the mechanical properties, especially if large amounts are added [28]. The mechanical properties are of great importance with respect to the desired flexibility and processability as polymer-based electrolytes and the resulting battery cells will be ideally fabricated by a roll-to-roll assembly [10, 28]. Moreover, based on their computational studies Newman and Monroe reported that there is an upper threshold in shear modulus for polymer electrolytes, beyond which the dendrite-

causing progressive surface roughening can be suppressed [38]. According to their study a polymer with a Poisson's ratio like PEO should exhibit a shear modulus of at least twice the one of Li metal (i.e. >7 GPa) to effectively prevent the undesired dendritic lithium growth upon cycling. The shear modulus of common polymer electrolytes is about 3–4 orders of magnitude lower than that. Besides, high shear moduli or very stiff polymers are usually characterized by rather poor adhesion, which leads to a disadvantageous contact with the electrodes. This aspect has also been termed the 'modulus-versus-adhesion-dilemma' [39].

An alternative means to overcome dendritic lithium deposition is based on the work reported by Newman and co-workers [40] as well as the studies by Brissot, Chazalviel and co-workers [41–43], who showed that the reversed cell polarization occurring for classic dual-ion conductors (i.e. electrolytes in which both anion and cation are mobile) has a detrimental impact on the overall cell performance and the potential formation of dendritic lithium deposits. When charging the battery cell, the lithium cations are shuttling to the negative electrode and depleted as a metallic layer, while the electrolyte anions move to the positive electrode as a consequence of the electric field, resulting in a reversed polarization effect. The application of a current beyond the diffusion capability of the cations (i.e. beyond the limiting current density) leads to a depletion of their concentration at the interface with the electrode down to eventually zero. This phenomenon is considered to be one of the potential reasons for dendritic lithium deposition, since the newly arriving cations are preferentially deposited at surface protrusions. The Sand's time describes the time needed to access this state under such conditions and is therefore a potential measure for non-uniform metal plating [44]. Consequently, increasing the  $\text{Li}^+$  transference number ( $t^+$ ) to unity, e.g. by covalently tethering the anionic function to the polymer backbone - therefore the use of the term single-ion ( $\text{Li}^+$ ) conductor - has emerged as a viable solution to circumvent these issues [45, 46].

Recently, the combination of chemically different organic groups with tailored functional properties in block copolymers (BCPs), that may permit for simultaneous yet suitable mechanical and charge transport characteristics, has received increased attention [44, 46–62]. In this approach, soft ionophilic blocks for the charge transport are coupled with more rigid ionophobic blocks for the mechanical stability. Due to the different nature of the blocks, these BCPs have the tendency to self-organize in phase-separated domains of each block, resulting in a variety of possible polymer structures.

Herein, we review the development of such self-organizing BCPs as electrolytes (BCPEs) for lithium batteries. A brief overview on the characteristics and thermodynamics of BCPs and BCPEs, including the impact of adding the conducting lithium salt are discussed. Based on a selected, well-investigated model compound we provide a comprehensive description of the major developments and fundamental insights into this system, representative of BCPEs in general.

We summarize additional BCPEs reported in the literature with varying chemical compositions and functionalities, concluding with a brief overview on the activities to develop single-ion conducting BCPEs with or without the addition of small molecules to enhance the  $\text{Li}^+$  transport. Finally, we summarize the discussed findings and offer a short perspective towards advanced electrolyte systems.

## 2. General characteristics and thermodynamics of BCPs and BCP electrolytes

BCPs consist of two or more blocks, which are covalently linked together forming the copolymer (CP). In the case of two chemically different blocks, the number of distinct blocks per polymer molecule classifies them into:

Diblock CPs (di – BCPs):  $[A_m - B_n]$

Triblock CPs (tri – BCPs):  $[A_m - B_n - A_m]$

Multiblock CPs (multi – BCPs):  $[(A_m - B_n)_p]$

with A and B being the different blocks,  $m$  and  $n$  being the number of repeat units for the corresponding block, and  $p$  as the number of repeat units for the diblock unit [63]. In addition to (common) linear BCPs more complex molecular architectures and block arrangements have been discovered, including branched, star-like and cyclic structures. The common synthesis methods to obtain such BCPs are living polymerization techniques e.g. the anionic polymerization, specifically for the preparation of diblock or triblock CPs with a controlled block length [63, 64]. For the synthesis of multi-BCPs, step-growth polymerization strategies have been reported such as the polycondensation of prepolymers/telechels with appropriate end-groups [63, 64]. Recently, advanced CFRP techniques like ATRP, RAFT method and NMP have been successfully utilized for the preparation of BCPs permitting a greater variety for their design [65].

The single blocks are frequently designed to be sufficiently different in their chemical nature, making them immiscible and enabling facile phase separation. A classic example is the group of  $A_m-B_n-A_m$ -type triblock thermoplastic elastomers, with A being a rather hard and brittle poly(styrene) (PS) block and B a relatively flexible and soft poly(butadiene) or poly(isoprene) block characterized by a low  $T_g$ . Due to their immiscibility, the different blocks (of several polymer chains) phase-separate into A-type and B-type domains with a characteristic nanostructure. In fact, the interaction between different polymer chains and their 'joint' phase separation acts as a physical 'crosslinker'. Such BCPs are very impact-resistant, as any mechanical stress is dissipated over the (rubbery) soft part, while the robustness is maintained by the hard PS domains [65, 66].

The phase separation phenomenon and self-assembly of different nanostructures can be understood by studying the underlying thermodynamics as described by the Flory–Huggins solution theory, which has been independently

developed by Flory [67] and Huggins [68, 69] in 1942 (see also [65] for more details). Derived from their theoretical considerations, the Flory–Huggins parameter  $\chi$  has been introduced as a versatile method to describe the thermodynamics of the phase separation occurring in polymers [70, 71]. This parameter delineates the interaction energy between the two polymers or, more precisely, between a monomer segment of polymer A and a monomer segment of polymer B (analogous to the interaction between a polymer segment and a solvent molecule with regard to the theoretical considerations for polymers in solution) and can be expressed by equation (2):

$$\chi = \frac{1}{k_B T} \left[ \varepsilon_{AB} - \frac{1}{2}(\varepsilon_{AA} + \varepsilon_{BB}) \right] \quad (2)$$

with  $\varepsilon_{ij}$  representing the contact energy between the corresponding monomer segments of polymers A and B (negative values indicate a gain in energy) and  $k_B$  the Boltzmann constant. Negative values for  $\chi$  indicate a relatively stronger interaction between A and B ( $\varepsilon_{AB}$  dominates), while positive values are related to stronger interactions between segments of the same polymer, i.e. between A and A as well as B and B (the term  $(\varepsilon_{AA} + \varepsilon_{BB})$  dominates) [71]. If the enthalpic contribution to the Gibbs free energy of mixing dominates over the entropic contribution, phase separation occurs at the macroscale for a mixture of homopolymers and at the microscale for BCPs, since the different blocks are covalently bonded [71]. To precisely describe such a phase separation, it has been meaningful to introduce the product of the Flory–Huggins parameter and  $N$ , the overall degree of polymerization, i.e.  $\chi N$ , as an indicator [71, 72]. If  $\chi$  and/or  $N$  increases, the enthalpic contribution increasingly dominates until a certain threshold is reached to initiate microphase segregation, which is commonly referred to as the ODT. In the case of symmetric di-BCPs with  $\varphi_A = \varphi_B = 0.5$ , ODT occurs for  $\chi N \approx 10.5$  as predicted by Leibler [73] as well as Fredrickson and Helfand [74]. It should be noted at this point that  $\chi$  is temperature-dependent and correlates with  $T^{-1}$  (equation (2)), which is related to the increase in entropy with an increase in temperature. A ‘constant’ temperature, the impact of the design of the BCPs and the volume fraction of the different blocks are factors that must be considered (discussed in section 3). Typically, for asymmetric BCPs, the blocks with the relatively lower volume fraction form spherical or cylindrical domains within a matrix composed of the other block with the higher volume fraction. If the volume fraction of the two blocks is similar, the lamellar nanostructure is formed. In the case that the driving force for the phase separation is low, reflected by a low  $\chi N$  value, bicontinuous (for two different blocks) nanostructures are obtained also referred to as gyroid phase [65, 75]. This evolution is commonly depicted as a phase diagram by plotting  $\chi N$  as a function of the volume fraction of A,  $\varphi_A$  sometimes also denoted by  $f$ , which describes the ratio of the two blocks [75, 76]. In figure 1, the (theoretical) phase diagram for  $A_m-B_n$  di-BCPs is exemplarily presented, as reported by

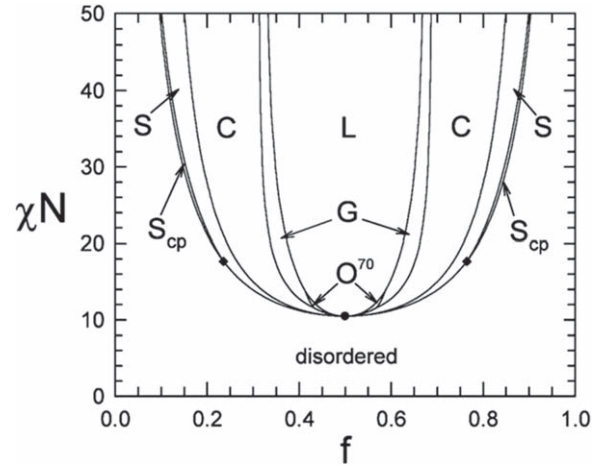


**Figure 1.** Exemplary phase diagram for melts of  $A_m-B_n$  di-BCPs, correlating  $\chi N$  and  $f$  to depict the thermodynamic stability regions of the ordered bcc spherical (S), hcp spherical ( $S_{cp}$ ), cylindrical (C), lamellar (L), gyroid (G), and  $Fddd$  ( $O^{70}$ ) phases. The diamonds indicate a triple point which is difficult to resolve and the dot a critical point (see the original publication by Matsen [77] for further details). Reprinted with permission from [77]. Copyright 2012 American Chemical Society.

Matsen [77]. For a certain fraction  $\varphi_A$ , bcc spheres (S) or hcp spheres ( $S_{cp}$ ) of A are formed in a continuous matrix of B. When  $\varphi_A$  further increases, cylindrical (C) domains are formed. For  $\varphi_A \approx 0.5$ , a lamellar (L) or gyroid (G) nanostructure is observed; for certain architectures the newly discovered  $Fddd$  ( $O^{70}$ ) phase. If  $\varphi_A$  exceeds 0.5, the organization is inverted [65, 71, 75, 78]. The general (potential) evolution of the different phases as a function of  $\varphi_A$  is schematically illustrated in figure 2(a) [78]. Nevertheless, the degree of segregation depends on  $\chi N$ , i.e. the higher  $\chi N$ , the stronger the segregation and the smaller the contact area between the different domains. The evolution and appearance of the different phases is also highly dependent on the polymer architecture [77, 79] and becomes extremely difficult to predict for more complex BCPs such as linear  $A_m-B_n-C_o$  systems [80]. In contrast, the microphase segregation behavior of multi-BCPs ( $A_m-B_n$ ) $_p$  follows essentially the behavior of di-BCPs [81, 82]. What’s more, relatively larger  $\chi N$  values are required for the phase separation, since the number of ‘diblock units’  $A_m-B_n$  within the same polymer chain increases (as indicated by the subscript  $p$ ), which promotes the entropic contribution to the overall free energy [83]. In comparison to di-BCPs, multi-BCPs provide superior mechanical properties thanks to the covalent bonding between the alternating different blocks [81], as reflected by an increase of the tensile modulus  $E$  [84].

Regarding the potential application of BCPs for lithium battery electrolytes, another important factor that affects the previous considerations is the introduction of a conducting lithium salt. For instance, it has been observed that the ODT temperature increases when incorporating  $\text{LiCF}_3\text{SO}_3$  into a lamellar PS-PEO-based di-BCP, accompanied by an increased domain spacing  $d$  [86]. The introduction of a conducting salt leads to an effective increase of the Flory–Huggins parameter,

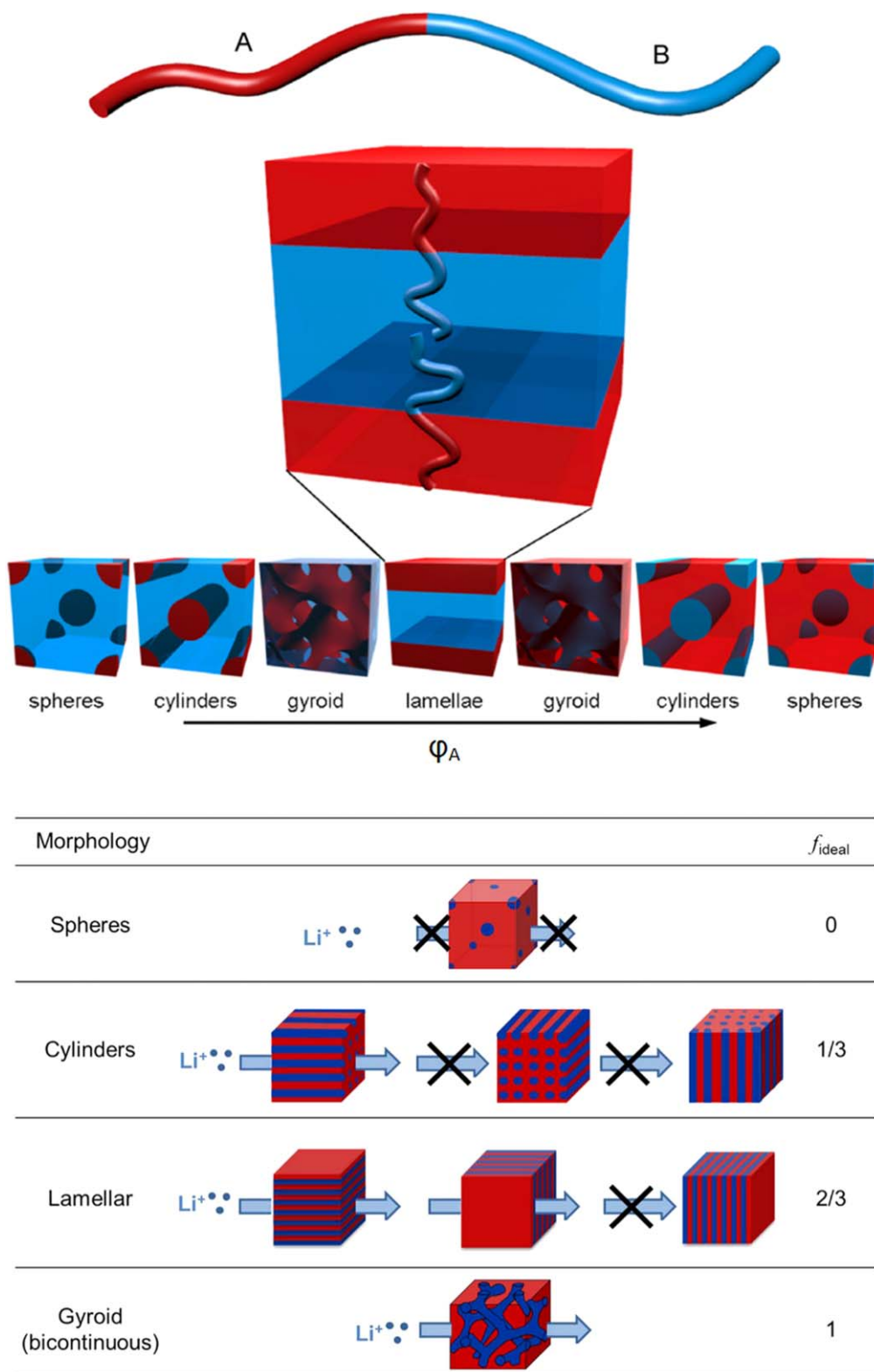


**Figure 2.** (a) Schematic illustration of the (potential) phase evolution of a di-BCP as a function of  $\phi_A$ . Reprinted with permission from [78]. Copyright 2007 Elsevier Ltd. All rights reserved. (b) Schematic overview of the ideal morphology factor  $f_{ideal}$  for the  $\text{Li}^+$  conductivity depending on the phase separated BCP nanostructure. The blue and red regions represent conducting and non-conducting microphases, respectively. Reprinted with permission from [85]. Copyright 2015 American Chemical Society.

often referred to as  $\chi_{\text{eff}}$ , which can be determined by the proportional correlation of  $d$  with  $\chi_{\text{eff}}$  ( $d \sim \chi_{\text{eff}}^{1/6}$ ) for a varying salt content within the strong segregation regime [72, 87]. Investigating a series of different lithium salts (i.e.  $\text{LiClO}_4$ ,  $\text{LiCF}_3\text{SO}_3$ , and  $\text{LiAsF}_6$ ), Young *et al* [87] found a linear relationship between  $\chi_{\text{eff}}$  and the salt concentration for the PS-PEO-based di-BCP. Additionally, they observed that the slope of this linear behaviour tends to increase with an increasing Lewis acidity of the anion. The investigation of the impact of the conducting salt is important, since the charge transport is eventually dependent on the nanostructure of the BCP when forming an ionic/ionophilic and a non-ionic/ionophobic phase upon the ODT, specifically the structure of the ionophilic phase within which the charge transport occurs [22, 88]. Consequently, the ionic conductivity of the BCP ( $\sigma_{\text{BCP}}$ ) can vary substantially depending on the phases formed and their spatial orientation hence this differs from the corresponding homopolymer. This can be described by equation (3):

$$\sigma_{\text{BCP}} = \alpha \cdot \phi_c \cdot \sigma_c, \quad (3)$$

where  $\phi_c$  is the volume fraction of the conducting phase,  $\sigma_c$  represents the intrinsic conductivity of the conducting phase (in a first approximation corresponding to the conductivity of the homopolymer) and  $\alpha$  is a tortuosity factor, which takes into account the morphology of the BCP and is related to the volume ratio of the different blocks, as discussed above.  $\alpha$  also considers the fraction of the ion conducting phase, which is capable of contributing to the effective conductivity. For instance, in the case of a BCP for which the conducting phase forms randomly oriented cylinders, approximately only one third of these cylinders are contributing to the charge transport between two opposite electrodes. In this case,  $\alpha$  would be  $1/3$ . For a lamellar system, it increases to  $2/3$  according to the 2D morphology and potential (effective) charge transport, while it increases to 1 for 3D gyroid structures and to 0 for spherical ion-conducting domains. As a result,  $\alpha$  is frequently referred to as an ideal morphology factor  $f_{\text{ideal}}$  (see figure 2(b) for the schematic overview [85]).

The practical use of these rather simplistic considerations has to be accounted for since they are based on the assumption that  $\sigma_{\text{BCP}} = \sigma_c$ , which might not be the case given potentially different conductivities in the bulk phase and at the interface with the non-conductive phase [56, 85].

### 3. Lithium salt-doped BCP electrolytes

#### 3.1. Brief overview and initial development

Following the seminal work of Wright and co-workers in 1973 [11] and Armand and co-workers starting from 1978 [12–14], research on polymer-based electrolytes has attracted the curiosity of scientists and engineers around the world, reflected by the evolution of scientific publications as well as patents in this field (depicted in figure 3). The number of related publications and patents increased initially until the late 1980s, before declining around 1990/1991 presumably related to the commercialization of LIBs [89, 90], which have

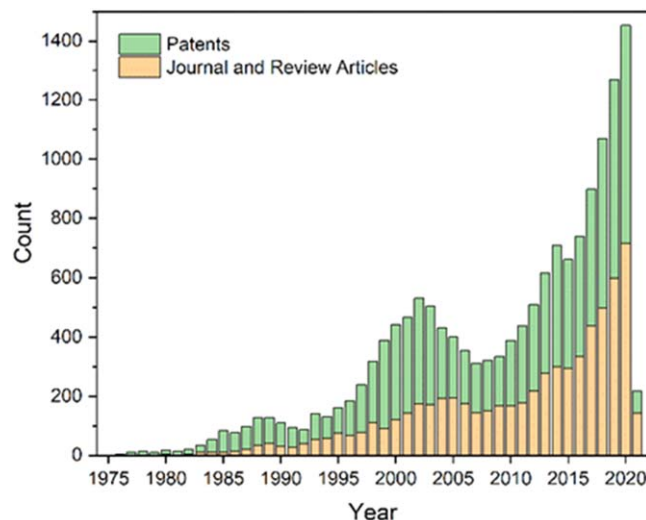


**Figure 3.** Publication trend from 1975 until today based on a bibliographic analysis using the key words ‘polymer electrolyte battery (concept)’ in SciFinder® (last update: February 24, 2021). Please, note that the data for the year 2021 cover only the first two months and that the count results provided by SciFinder® also include duplications, hence, the data is not directly equivalent to the number of publications and patents.

been and are still using liquid organic electrolytes. With the rising interest in battery research, the attention for polymer-based electrolytes steadily began to increase again until the mid-2000s. Subsequently, there was a slight decrease in published research output, which is potentially linked to the rapidly growing study of inorganic solid-state electrolytes, causing a slight shift in the main focus of battery research [91]. Nonetheless, since then the number of publications and patents has experienced a roughly exponential rise.

Initially, several polymers, BCPE systems and architectures were introduced although only a few played a pivotal role in ongoing research. For example, in 1987, Vincent and co-workers introduced an ABA tri-BCP with a comb-shaped structure [92]. The mid-block B was composed of PEO side chains covalently tethered to a poly(butadiene) backbone via a urethane linkage, and the two side blocks of A were made of PS. This conventional concept is repeatedly found in every BCPE, independent of its architecture or composition. While a hard segment in the BCPE provides mechanical rigidity due to its high  $T_g$ , the transport of ions is ensured in a soft ionophilic block with a low  $T_g$ , which can easily dissolve the conducting salt. A comb-shaped architecture effectively prevents the short PEO chains from crystallization favoring ion transport. Moreover, the chemical incompatibility of the different blocks, while still being covalently connected, commonly results in a microphase separation instead of a macrophase separation, as would be observed for polymer blends. The incorporation of lithium trifluoromethanesulfonate (Li triflate,  $\text{LiOTf}$ ,  $\text{LiTf}$  or  $\text{LiCF}_3\text{SO}_3$ ) into this early-generation BCPE led to ionic conductivity values of approximately  $10^5 \text{ S cm}^{-1}$  at ambient temperature and about  $10^{-3} \text{ S cm}^{-1}$  at elevated temperatures of up to  $90^\circ \text{C}$  with the choice of the casting solvent influencing the membrane preparation [92]. In a related study, the effect of

varying the conducting salt concentration as well as blending the BCP with either a PS or a PEO homopolymer was investigated [93]. The addition of homo-PS resulted in an increase of mechanical strength without any dramatic effect on the ionic conductivity. In contrast, the introduction of homo-PEO led to an increased ionic conductivity while simultaneously lowering the mechanical strength. In both cases, no macrophase separation was observed due to the solubility of the homopolymers in the respective blocks. A similar architecture was used by Smid and co-workers in 1989 [94], reporting an ABA tri-BCP with a PS mid-block and side-blocks composed of a poly(methacrylate) backbone with covalently tethered oligomeric ethylene oxide (EO; eight repeating units of EO in average). This comb-shaped BCPE was doped with different concentrations of LiClO<sub>4</sub>. The authors found that an increasing salt concentration initially led to an increase in ionic conductivity due to the increasing charge carrier density. At higher concentrations, a maximum was reached because of ion clustering and chain stiffening caused by the interaction of the lithium ions with the ether oxygen in the oligomeric PEO chains; both aspects being reflected by an increasing  $T_g$ . Moreover, an increase in polarity between the two blocks upon salt addition further facilitated the phase segregation and led to a higher  $T_g$  also for the PS phase due to the decreasing interpenetration by PEO chains in the vicinity of the interface. Further studies on ABA tri-BCPs were reported by Melchior *et al* [95], investigating poly(2,2-dimethyltrimethylene carbonate)-*b*-poly(ethylene oxide)-*b*-poly(2,2-dimethyltrimethylene carbonate), abbreviated as PDTC-*b*-PEO-*b*-PDTC. Doping with various alkali metal salts resulted in a suppression of crystallinity up to a certain amount, while a further increase in salt concentration triggered the formation of crystalline complexes of clustered salt molecules with a negative impact on the ionic conductivity, since the charge carriers became less mobile. XRD analysis revealed that the salt preferentially resided in the PEO domains and did not affect the crystallization behavior of the rigid PDTC phase. LiCF<sub>3</sub>SO<sub>3</sub>-doped samples (9.1 mol%) showed conductivities around 10<sup>4</sup> S cm<sup>-1</sup> at 60 °C and VTF behavior. In addition to the findings reported by Smid and co-workers [94], Melchior *et al* [95] observed a second increase in conductivity when adding very high salt concentrations exceeding 25 mol% and reaching up to 50 mol%. This was attributed to lithium ions not being attracted to the already saturated ether oxygen in the PEO chains, thus enhancing their mobility and providing an additional contribution to the charge transport. Saunier *et al* [96] presented a similar ABA triblock architecture with a PEO soft segment surrounded by two poly(methacrylonitrile) blocks (PMAN-*b*-PEO-*b*-PMAN), providing high  $T_g$  and enhanced electrochemical stability versus lithium metal in comparison to poly(acrylonitrile) due to the additional methyl group. The incorporation of high concentrations like (O + CN)/Li = 1 of lithium bis(trifluoromethanesulfonyl)imide (LiTFSI, Li[N(SO<sub>2</sub>CF<sub>3</sub>)<sub>2</sub>]) resulted in a maximum ionic conductivity of 3·10<sup>5</sup> S cm<sup>-1</sup> at 60 °C. Interestingly, the authors detected a certain solubility of the salt also in the PMAN block. Another early-stage ABA tri-BCP was reported by Jannasch [97], who synthesized a PE-*b*-PEOPO-*b*-PE BCPE, in which the hard

segment was formed by poly(ethylene) (PE), while the conducting phase consisted of a poly(ethylene oxide-*co*-propylene oxide) copolymer. Doping with LiTFSI yielded conductivities of around 10<sup>5</sup> S cm<sup>-1</sup> at 20 °C, accompanied by a thermo-plastic behavior of the resulting membrane. Hvilsted and co-workers [98] used poly(pentafluorostyrene) (PFS) as the rigid block in combination with either pure PEO or the aforementioned PEOPO copolymer as the conductive matrix for the ATRP-type synthesis of PFS-*b*-PEOPO-*b*-PFS and PFS-*b*-PEO-*b*-PFS, respectively. After doping with LiTFSI they also observed ionic conductivities of around 10<sup>5</sup> S cm<sup>-1</sup> at 20 °C, indicating that the variation of the different blocks did not have a significant effect on the charge transport. However, at 25 °C inferior conductivities in the range of 10<sup>6</sup> S cm<sup>-1</sup> and below were reported by Spiegel *et al* [99] for an AB-type poly(dimethylsiloxane)-*b*-poly(bisphenol A carbonate) (PDMS-*b*-PBPA) di-BCP doped with LiCF<sub>3</sub>SO<sub>3</sub> despite the addition of a plasticizer (triacetoxymethyl)silane, which the authors assigned to the very rigid nature of the aromatic PBPA block. Another interesting finding was reported by Armand and co-workers [100], who studied a poly(iminoethylene)-*b*-poly(ethylene oxide)-*b*-poly(iminoethylene) (PEI-*b*-PEO-*b*-PEI) ABA tri-BCP in order to investigate the behavior of the nitrogen analogue (i.e. PEI) of PEO. The authors showed that hard cations such as Li<sup>+</sup> (from LiTFSI) were preferentially located in the PEO domains, coordinating to the hard ether oxygen atom, while soft cations such as Cu<sup>2+</sup> (from Cu(TFSI)<sub>2</sub>) were coordinated by the soft nitrogen atoms within the PEI chains. With LiTFSI as conducting salt, ionic conductivities in the range of 10<sup>4</sup> S cm<sup>-1</sup> at 90 °C and ca. 10<sup>-6</sup> S cm<sup>-1</sup> at RT were observed. It was concluded that both the high crystallinity of the PEI domains and an insufficient percolation of the PEO domains hindered the Li<sup>+</sup> ion conduction.

While all these studies revealed very interesting findings for the variety of different BCPEs synthesized, also highlighting the richness of polymer chemistry, most of them remained restricted to thermal characterization techniques and the determination of the ionic conductivity.

An exception is the BCPE system reported by Mayes, Sadoway and co-workers [101–106], who reported a comprehensive set of BCPs including poly(lauryl methacrylate)-*b*-poly[oligo(oxyethylene) methacrylate] (PLMA-*b*-POEM, sometimes also abbreviated as poly(oligo(ethylene glycol) methacrylate), POEGMA) and for comparison PnBMA-*b*-POEM (poly(*n*-butyl methacrylate)) and PMMA-*b*-POEM (poly(methyl methacrylate)), all synthesized by anionic polymerization techniques. The chemical formulas are presented in figure 4(a). The premise was to investigate the impact of varying the length of the aliphatic side chain of the ionophobic block with the intention to create a fully rubber-like polymer with a  $T_g$  of the two blocks well below RT [101]. The initial variation of the content of the ionophilic POEM block resulted in quite low ionic conductivities, which the authors assigned to the formation of non-percolating (e.g. spherical) ionophilic domains, thus hindering the Li<sup>+</sup> ion transport [101]. The importance of the block architecture, was evidenced by a comparison with a random P(MMA-*r*-OEM) copolymer, which showed a relatively low conductivity in the

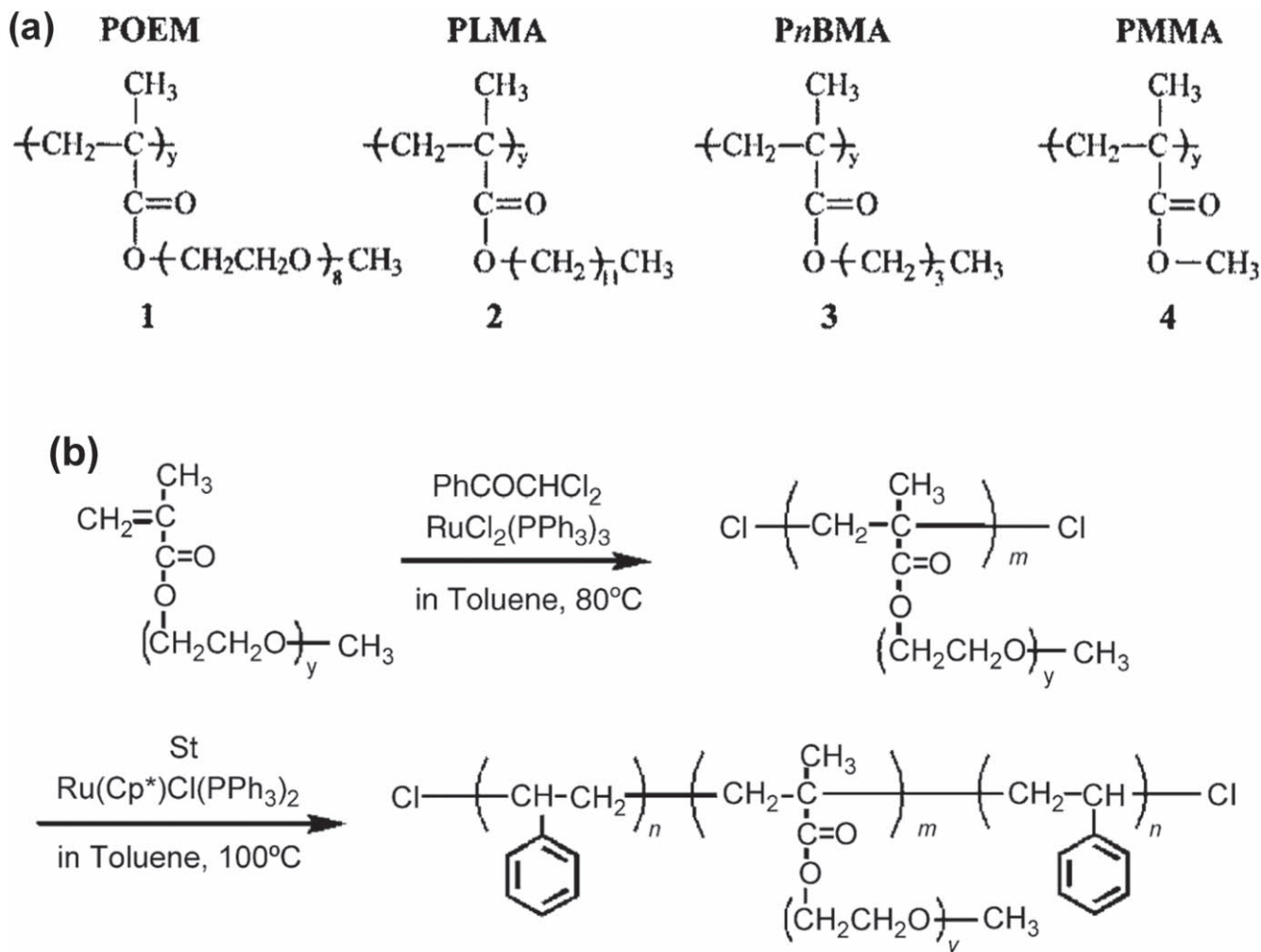


**Figure 4.** (a) Chemical structures of the different blocks for realizing BCPs by Mayes, Sadoway and co-workers [104]. Reprinted with permission. Copyright 2002 American Chemical Society. (b) Synthesis route for the BCPE reported by Kanamura and co-workers. Reprinted from [107], © 2005 Elsevier B.V. All rights reserved.

absence of microphase separation [101]. For the reference system, i.e. PLMA-*b*-POEM doped with LiCF<sub>3</sub>SO<sub>3</sub>, an ionic conductivity below 10<sup>-5</sup> S cm<sup>-1</sup> at ambient temperatures and approaching 10<sup>-4</sup> S cm<sup>-1</sup> at 90 °C was achieved, which was further enhanced to 2·10<sup>-4</sup> S cm<sup>-1</sup> at 90 °C by adding poly(ethylene glycol dimethyl ether) (PEGDME, i.e. low molecular weight PEO). An electrochemical stability window of more than 4 V was reported, which allowed a fairly stable short term cycling of Li|BCPE|LiAl<sub>0.25</sub>Mn<sub>0.75</sub>O<sub>2</sub> full-cells when setting the cut-off potentials to 2 and 4.4 V [101]. Reasonable cycling performance was also reported for thin-film Li|BCPE|VO<sub>x</sub> full-cells, employing PMMA-*b*-POEM doped with LiCF<sub>3</sub>SO<sub>3</sub> and PEGDME [102], synthesized by the less demanding ATRP-controlled radical polymerization technique [105]. While neat PMMA-*b*-POEM did not exhibit a distinct phase separation, the incorporation of LiCF<sub>3</sub>SO<sub>3</sub> triggered the segregation of the two blocks, accompanied by an increase of the ODT temperature. Accordingly, the doped PMMA-*b*-POEM was melt-processable at temperatures between 100 °C and 200 °C (depending on the salt concentration) thanks to its disordered state and provided the beneficial phase separation for the

charge transport at RT [103]. Based on their work, the authors identified four important parameters for the realization of potentially relevant BCPEs with respect to their application in batteries: (i) the molecular architecture, (ii) the composition of the different blocks, (iii), the block and overall chain length, as well as (iv) the concentration of the conducting salt.

Following a similar tactic for the polymer structure, Kanamura and co-workers [107–109] synthesized the ABA tri-BCP via radical polymerization, also based on POEM as the conducting block, but surrounded by two PS blocks (see figure 4(b)). Focusing on the impact of the PEO side chain length, the authors found that these formed a continuous PEO phase when having 13 or 23 repeating units. The resulting ionic conductivity of up to 2·10<sup>-4</sup> S cm<sup>-1</sup> at ambient temperature with LiClO<sub>4</sub> as conducting salt allowed for the realization of Li|BCPE|LiCoO<sub>2</sub> full-cells, providing stable cycling when limiting the anodic cut-off potential to 4.3 V. Superior cycling performance was reported for the AB-type PS-*b*-POEM di-BCP doped with LiClO<sub>4</sub> by Rolland *et al* [110] in Li|BCPE|LiFePO<sub>4</sub> full-cells thanks to the lower de-/lithiation potential of LiFePO<sub>4</sub> (LFP) compared to LiCoO<sub>2</sub> (LCO).

### 3.2. Impact of lithium salt doping on the BCP nanostructure

As (briefly) mentioned in the previous section, the incorporation of the conducting lithium salt and its eventual concentration tend to influence the BCP nanostructure due to its (diverse) interaction with the different blocks. A well investigated BCP is the AB di-BCP poly(isoprene)-*b*-poly(styrene) (PI-*b*-PS), for which all relevant nanostructures, i.e. spheres (S), cylinders (C), lamellae (L), HPL, and gyroidal (G; or bicontinuous) networks have been reported [111]. For the related ABA tri-BCP PS-*b*-PI-*b*-PS it was also proposed that the PS blocks form two interpenetrating 3D gyroidal networks embedded in a PI matrix [112]. Based on this fundamental work, e.g. Bates and co-workers investigated the impact of the block arrangement [113] and the effect of introducing LiClO<sub>4</sub> [114] for ABC tri-BCPs PI-*b*-PS-*b*-PEO (ISO) and PS-*b*-PI-*b*-PEO (SIO). The authors observed a frustration in microphase separation for SIO due to the very unfavorable interface between PI and PEO (i.e. I and O) [113]. Moreover, they found that the addition of the conducting salt led to a dramatic increase of the ODT temperature, triggered by a stronger phase segregation due to an intensified polarity between the salt-containing PEO domain and the other blocks [114]. This finding was confirmed by Epps and co-workers [115], using a PS-*b*-PEO model component. Doping with LiClO<sub>4</sub> or LiCF<sub>3</sub>SO<sub>3</sub> at high salt concentrations ([EO]:[Li] ratio of 3:1) resulted in an increased ODT temperature. In addition, the authors detected an OOT between two L phases with differing domain spacing. The extension to a broad concentration range ([EO]:[Li] ratio from 48:1 to 3:1) for a variety of lithium salts such as LiClO<sub>4</sub>, LiCF<sub>3</sub>SO<sub>3</sub>, and LiAsF<sub>6</sub> also provided evidence of an increasing domain spacing with an increasing salt content for the L nanostructures, which was assigned to the (additional) volume of the dissolved salt and the increasing segregation strength [87]. Moreover, a transition from hexagonally packed cylinders (HEX-C) to L with an increasing salt content confirmed the preferential residence of the lithium salt in the PEO domain thus the role of the anion on the morphology was elucidated. This proves that the effective interaction with the polymer blocks, i.e.  $\chi_{\text{eff}}$ , follows a linear relationship with the salt concentration for all three salts, but with a different slope. The AsF<sub>6</sub><sup>-</sup> anion caused the greatest increase in segregation strength, which the authors ascribed to the weaker Lewis basicity and hence a weaker interaction/stronger dissociation between AsF<sub>6</sub><sup>-</sup> and Li<sup>+</sup>, resulting in enhanced stretching of the PEO chains due to the stronger association between Li<sup>+</sup> and the PEO units [87]. Generally, a combination of two different salts, e.g. LiClO<sub>4</sub> and LiTFSI appeared beneficial for the ionic conductivity due to the suppression of crystalline phases in the PEO block. In fact, the conductivity was increased by one order of magnitude at RT compared to the single-salt BCPEs [116].

Of equal importance to the ionic conductivity is the BCP nanostructure, with 3D HPL or HEX-C phases providing superior conductivity compared to 2D L phases [117]. In a new study, this was shown for PS-*b*-POEM doped with LiCF<sub>3</sub>SO<sub>3</sub> and including a POEM homopolymer, providing

additional conducting pathways within the system [118]. Gunkel and Thurn-Albrecht presented similar results for PS-*b*-PEO and PS-*b*-poly(2-vinylpyridine) (PS-*b*-P2VPy), both doped with LiCF<sub>3</sub>SO<sub>3</sub> [86]. They found a strong increase in both ODT temperature and domain spacing upon salt addition. Resolving the latter observation indicated that small amounts of salt only contribute to the increasing domain spacing because of the natural volume uptake. However, the incorporation of higher salt concentrations introduced additional effects such as an increased segregation strength due to the uptake of the highly polar salt and chain stretching effects related to the interaction between the salt molecules and the polymer chains. Overall salt addition had a greater effect on PEO than P2VPy.

Another important feature of introducing a lithium salt was reported by Russell and co-workers, studying LiCl-doped PS-*b*-PMMA [119, 120]. The application of an electric field led to a lamellar alignment due to the lithium ion complexation by the carbonyl groups in the PMMA block, enhancing the dielectric constant therefore facilitating the alignment. Similarly, the complexation of lithium cations by ether oxygen in PEO blocks allowed for a modification of the orientation of the cylindrical domains formed in PS-*b*-PEO BCPEs, indicating that the BCPE nanostructure can be tailored to a certain extent by adjusting the lithium salt concentration [121].

Although great progress had been achieved in the 1990s until the mid-2000s, regarding both the design of new BCPEs and new insights concerning the factors which influence the nanostructure of these systems; a thorough understanding remains hampered, since the reported systems were hardly comparable due to the absence of a model system that was studied comprehensively.

### 3.3. PS-*b*-PEO (SEO) + LiTFSI as a model system for BCPEs

For the field of BCPEs, this model system is represented by PS-*b*-PEO (or SEO), which has been briefly mentioned in section 3.2. This section is dedicated to this essential model system, elucidating its evolution over almost fifteen years. Great efforts have been undertaken by Balsara and co-workers to present an in-depth and step-by-step analysis of the SEO system, usually doped with LiTFSI as the conducting salt, by a stepwise variation of a series of parameters and exploiting the limits of the current existing analytical methods. From the first publication in 2007 until today, the SEO system is synthesized by sequential living anionic polymerization, as introduced by Quirk and co-workers [122] as well as Hadjichristidis and co-workers [123], enabling a well-defined block length and molecular weight of the polymer and narrow molecular weight distributions accompanied by polydispersity indices close to unity.

Before describing the findings for this model system in detail, a few fundamental aspects must be mentioned. Firstly, almost all of the subsequently mentioned studies focused on temperatures between 90 °C and 120 °C, i.e. well above the melting point of PEO ( $T_m = 65$  °C). Secondly, the lithium salt concentration in such BCPEs is commonly referred to as

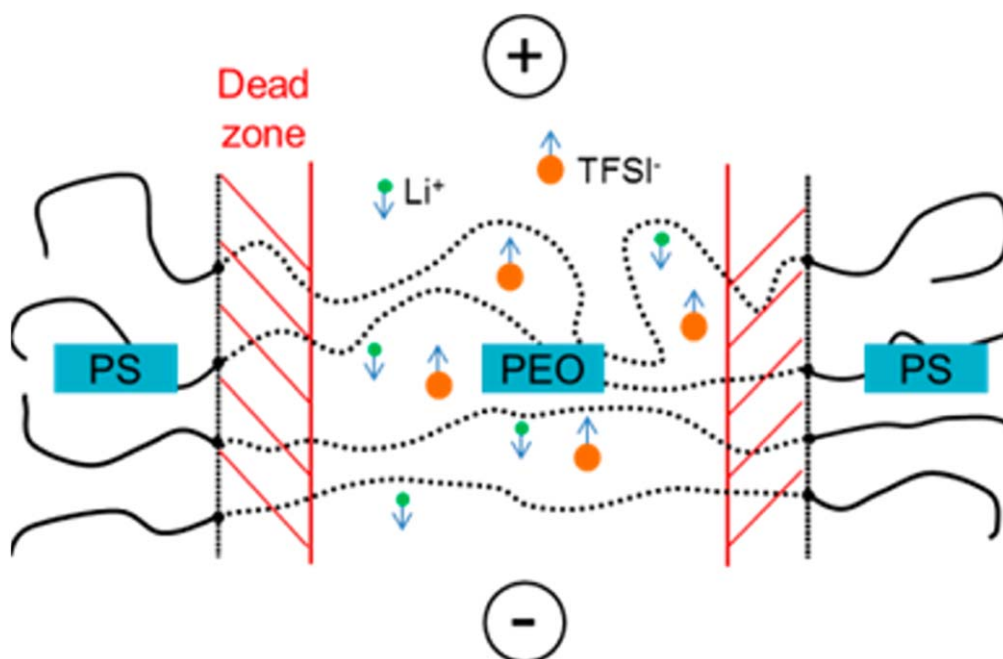


**Figure 5.** Schematic illustration of the ‘dead zone’ in the vicinity of the PEO-PS interface. Reprinted with permission from [127]. Copyright 2014 American Chemical Society.

the molar ratio between the lithium ions and the EO moieties  $[\text{Li}^+]:[\text{EO}]$  (or, more precisely, the strongly lithium coordinating ether oxygen). The latter is determined by SEC/GPC. For simplicity and brevity, we will refer to this as  $r = \frac{[\text{Li}^+]}{[\text{EO}]}$ . Typical values for  $r$  are in the range from 0.02 to 0.1, translating into one lithium ion for every fifty up to every ten EO moieties, respectively. However, higher lithium concentrations have also been reported and will be mentioned.

**3.3.1. Nanostructure, interfaces, and ionic conductivity.** In their first study on SEO, Balsara and co-workers detected L and HPL nanostructures via SAXS and TEM in the neat BCPE, depending on the volume fraction of PEO and PS [124]. The maximum ionic conductivity was obtained for a salt concentration of  $r = 0.067$  ( $3.6 \cdot 10^{-4} \text{ S cm}^{-1}$  at  $90^\circ \text{C}$ ). At higher salt concentrations, the conductivity decreased again, which the authors attributed to the transient crosslinking of the polymer chains by coordinating lithium ions, limiting their segmental motion, and the formation of (neutral) ion pairs/clusters. Interestingly, the authors observed an increase in conductivity with an increase in molecular weight, contrasting previous results reported for PEO homopolymer systems. In line with theoretical studies on the charge transport in such systems [125, 126], it was proposed that the interface between the two chemically incompatible domains, later denominated as the so-called ‘dead zone’ by Bouchet *et al* [127] (see figure 5), might play a role, i.e. a larger interface area results in lower conductivity. It was proposed that at such interfaces, the PEO chains have a reduced dielectric constant leading to a decreased salt dissociation [124], and/or that the chain mobility in the vicinity of the PS domains is restricted [127]. With an increasing molecular weight, the influence of these ‘dead

zones’ diminishes since the volume fraction of such zones decreases. EFTEM revealed that the lithium cations are exclusively found in the PEO lamellae and more precisely in the bulk of these lamellae, being in good agreement with the aforementioned excluded zones in the vicinity of the PS-PEO interface [128]. The PEO chains in these zones cannot provide the preferential setup of six ether oxygen atoms for coordinating one lithium cation due to chain stretching effects. Hence, they do not provide the ability to dissolve the lithium salt which leads to the accumulation in the unaffected bulk of the PEO lamellae. Shortly after this study evidence was found via principal component analysis of low-loss EFTEM data that small amounts of  $\text{NaPF}_6$  segregated towards the PS-PEO interface, creating a third phase in addition to the two polymer domains [129]. This finding suggests that the overall evidence is far more complex than initially predicted or that there are simply differences between lithium and sodium.

A subsequent study [130] provided further insights into the impact of the salt concentration and molecular weight on the ionic conductivity, identifying a combination of  $r = 0.085$  and  $M_{\text{PEO}} > 60\,000 \text{ g mol}^{-1}$  as ideal for the application in lithium batteries. Consequently, this  $r$  value served as the benchmark for many succeeding studies. Recently, the investigation of varying salt concentrations was extended to a wider range of  $0 \leq r \leq 0.55$  in combination with considerably high molecular weight SEO [131]. The resulting conductivity curve showed three maxima at  $r = 0.075$ ,  $0.275$ , and  $0.350$  (figure 6, right panel). The authors attributed this behavior to the partially stepwise increasing  $T_g$  when increasing the salt concentration (figure 6, middle panel) in combination with morphological changes, as detected by SAXS/WAXS and STEM (figure 6, left and

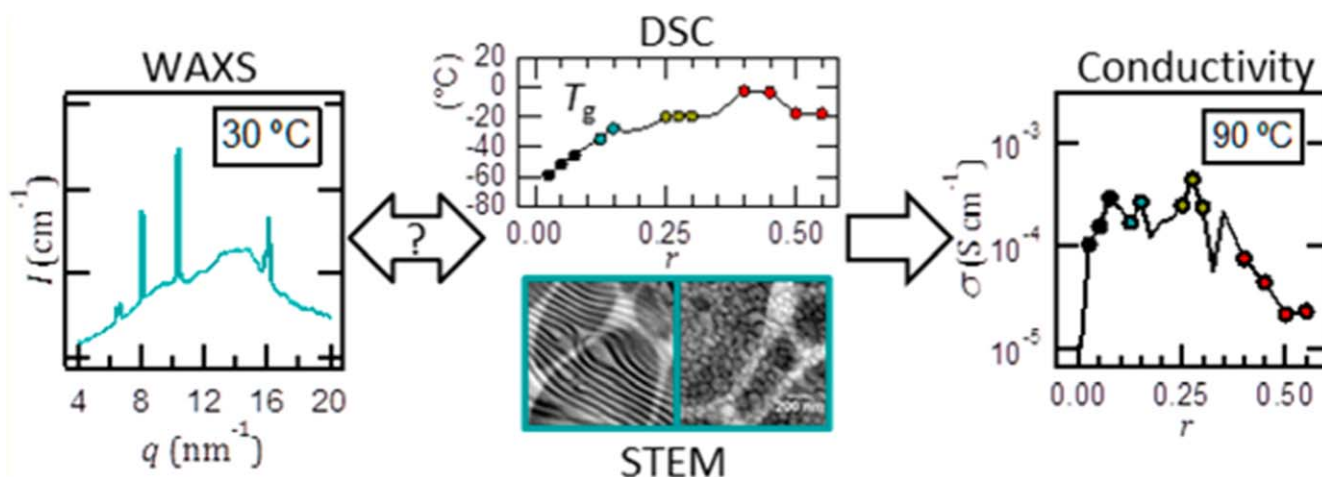


**Figure 6.** Right: Plot of the ionic conductivity,  $\sigma$ , versus the salt concentration,  $r$ , showing three distinct maxima. Middle: the corresponding DSC data (top) and STEM images (bottom) for an  $r$  value of 0.15 (different regions of the sample are showing lamellar and weakly ordered ellipsoidal morphologies). Left: The WAXS data for an  $r$  value of 0.15 showing distinct reflections related to a lamellar morphology. Reprinted with permission from [131]. Copyright 2018 American Chemical Society.

middle panel). Vanishing and newly evolving peaks in the SAXS/WAXS patterns support the theory of the formation of different PEO-LiTFSI complexes, such as  $C_6$  (i.e. one  $\text{Li}^+$  associated with six EO units),  $C_3$ , and  $C_2$  while increasing the salt concentration of the BCPE. Samples in the high salt concentration regime showed similar conductivities as reported for the PEO homopolymer despite the presence of the insulating PS block, which was assigned to the higher segmental mobility of the PEO chains in such BCPEs. For an improved understanding of the effect of the nature of the cation, Wanakule *et al* [132] compared SEO-based BCPEs comprising of either LiTFSI or (liquid) imidazolium TFSI (ImTFSI). The authors found negligible differences between the two systems, concluding that the thermodynamics of SEO-salt mixtures are predominantly influenced by the nature of the anion. Following the investigation of potential maxima for the molecular weight in the SEO-LiTFSI system [130], also potential minima were studied for BCPEs with an essentially equivalent chain length of the PS and PEO blocks, ranging from 2700 to 13 700  $\text{g mol}^{-1}$  [133]. One would usually expect an increasing ionic conductivity with a decreasing chain length, as known from PEO homopolymers (until the crystallization threshold; in the case of PEO ca.  $M_w$  7000  $\text{g mol}^{-1}$  [134, 135]), due to the facilitated segmental mobility [51] and the potential diffusion of the PEO molecules as a whole. Given the unique architecture, the latter effect is suppressed in SEO-based BCPEs, thus limiting it to the facilitated segmental motion. The results obtained for low molecular weights, i.e. from 2700 up to about 10 000  $\text{g mol}^{-1}$  depict the same trend: the conductivity is decreasing with an increasing molecular weight (figure 7), which was assigned to the decreasing mobility of the PEO segments and the increasing  $T_g$  of PS with an increase in molecular weight [133]. Nevertheless, at even higher molecular weights, the conductivity was found to increase, which was explained by the broadening of the PEO conducting channels and the diminishing effect of the interfacial ‘dead zones’ with a thickness of around 5 nm. Further studies on the low

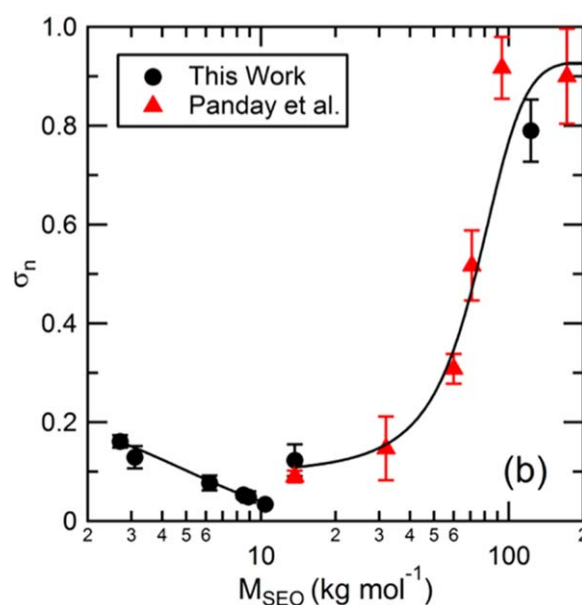


**Figure 7.** Plot of the normalized conductivity,  $\sigma_n$ , versus the total molecular weight  $M_{\text{SEO}}$  at 90 °C, displaying the data points reported in [133] (black circles) and the results reported in [130] (red triangles). The normalized conductivity is neglecting the influence of the segmental motion on the ionic conductivity by equalizing the correlation between temperature and segmental motion in homopolymers and block copolymers. Reprinted with permission from [133]. Copyright 2013 American Chemical Society.

molecular weight BCPEs and the influence of different salt concentrations led to comprehensive insights into the thermodynamics of the SEO system in this region [136]. While the interaction parameter of the neat BCP,  $\chi_0$ , was found to be a strong function of the chain length,  $N$ , the effective interaction parameter of the salt-containing BCPE,  $\chi_{\text{eff}}$ , appeared to be a nonlinear function of  $r$  (remember that  $\chi_{\text{eff}}$  describes the interaction between the salt-containing and the structural block of the BCPE, since the interaction parameter usually changes substantially upon salt addition;

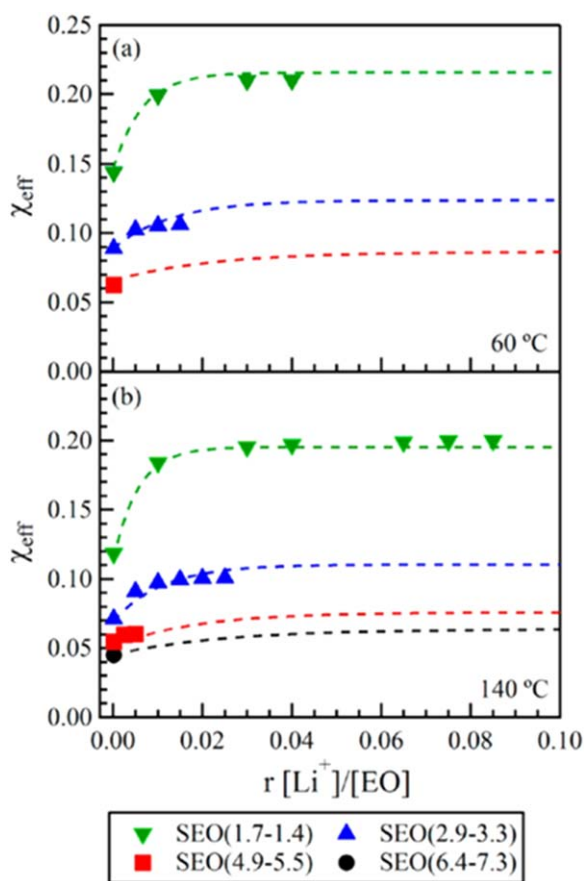


**Figure 8.** Plot of the effective interaction parameter,  $\chi_{\text{eff}}$ , versus the salt concentration,  $r$ , of symmetric diblock SEO copolymers at (a) 60 °C and (b) 140 °C, revealing the nonlinear relationship between these two parameters. Reprinted with permission from [136]. Copyright 2014 American Chemical Society.

see also figure 8). These results challenge the previous assumption that  $\chi_0$  and  $N$  were independent and that there was a linear relationship between  $\chi_{\text{eff}}$  and  $r$ , which Teran and Balsara [136] assigned to the limited range of samples investigated in those studies.

Among the first to study the impact of the nanostructure (including potential phase transitions) was Wanakule *et al* [137], focusing on the ODT and the OOT occurring in SEO-based BCPEs. As the names imply, ODTs refer to the transition from an ordered microphase-separated state to a disordered/homogeneously mixed state (DIS), as it is usually found at elevated temperatures when entropic factors overcompensate the repulsive forces between the two blocks. OOTs refer to the transition between two ordered states, such as LAM-to-HEX, triggered by either a change in temperature or salt concentration. Depending on the polymer composition and the salt concentration, three different transitions were found, i.e. HEX-C-to-DIS, L-to-DIS, and L-to-G [137]. Surprisingly, no differences in ionic conductivity were found upon these transitions, contrasting the results of other studies. However, further elaboration of this anomalous finding via *in situ* SAXS on a low molecular weight SEO revealed a coexistence region for the L and DIS phase at around  $114 \pm 4$  °C and a discontinuous change in ionic conductivity

over the L-to-DIS ODT, with a sudden discontinuous increase in conductivity by a factor of 1.8 when entering the DIS region (see also figure 9) [138]. Additional studies on the L-to-DIS ODT provided similar results concerning the coexistence window of about 11 °C in such BCPEs, which is different from the neat BCP exhibiting a sharp ODT [139, 140]. This coexistence is accompanied by a swelling of the L domains due to the partitioning of the lithium salt into the remaining lamellae instead of the DIS phase [139, 140]. It is important to recall at this point that the coherent order in BCPEs (e.g. in terms of lamellae) is commonly restricted to small, usually micro-sized regions (hereinafter referred to as grains) [141]; and depending on the spatial orientation of such grains towards each other, conducting and non-conducting grain boundaries are obtained (figure 10). Importantly, the grain size depends on the thermal history of the polymer. Annealing the BCPE at high temperatures beyond the  $T_g$  of the PS block results in a drastic increase in grain size and the cooling leads only to a small decrease in grain size. This behavior has been attributed to the healing of defects that had been introduced during the manufacturing process. Curiously, a decreasing conductivity was obtained for an increasing grain size most likely due to the formation of non-conducting grain boundaries, thus rendering BCPEs with poor long-range order more desirable (at least in the absence of almost only conducting grain boundaries). These results provide a potential explanation for earlier studies reporting an increasing conductivity for an increasing chain length/molecular weight, since the annihilation of defects and the formation of larger grains is reduced in such cases.

To obtain additional insights into the behavior of the grains, Wang *et al* [142] further investigated the ODT reported in [139] via depolarized light scattering and analyzed a series of samples which has been heated above the ODT followed by different quenching depths, i.e. 6 °C, 12 °C, and 24 °C. While the shallow quenching step ended up in the (earlier discussed) coexistence area, deeper quenching steps resulted in the formation of highly anisotropic prolate ellipsoid grains, followed by a reduction in aspect ratio converging to an almost isotropic shape with aspect ratios close to unity. In contrast, neat BCPEs with a sharp ODT exhibit a weak anisotropy regarding the grain formation. Considering the increasing complexity of potential phase transitions when moving from symmetric to highly asymmetric SEO BCPEs (see also figure 11) [143, 144], further studies are essential to comprehend the underlying phenomena.

**3.3.2. Insights into the charge transport mechanism.** For application in batteries, it is imperative to understand the diffusion processes in BCPEs beyond the commonly determined ‘simple’ ionic conductivity as the sum of all charge transport processes. A general and comprehensive overview on this topic can be found in the recent literature [51]. Specifically, for SEO it was found that the segmental relaxation processes as well as concentration effects play a detrimental role for charge transport and diffusion. A first

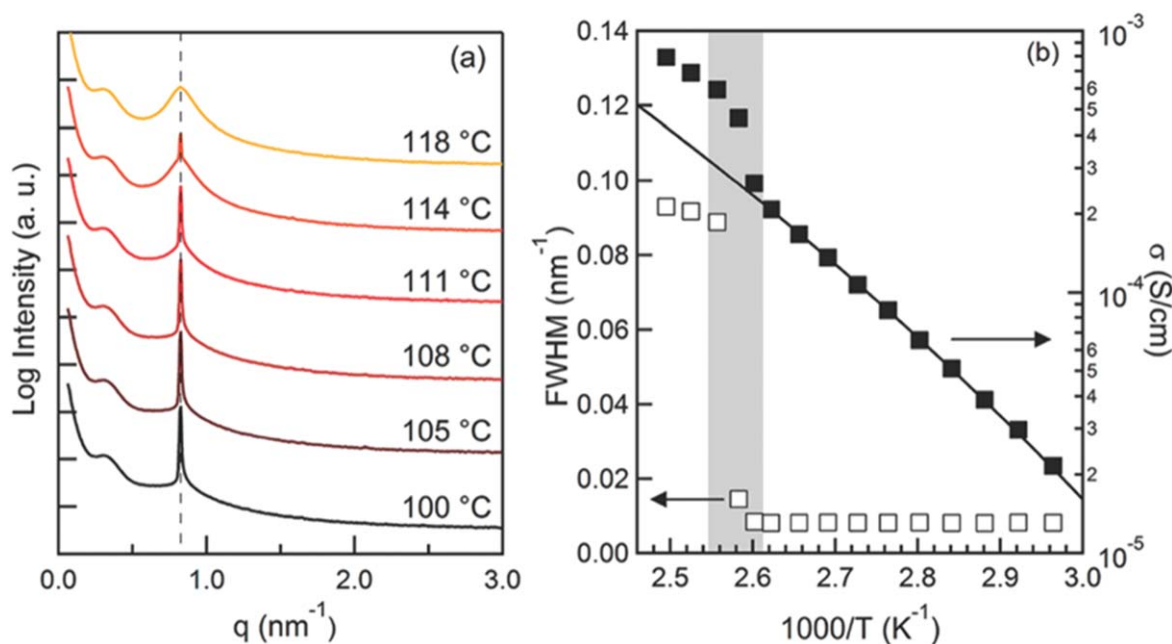


**Figure 9.** (a) SAXS patterns for a BCPE based on SEO (1.7 1.4; with ‘ $xx$   $yy$ ’ being the molecular weight of the PS ( $xx$ ) and PEO ( $yy$ ) block in  $\text{kg mol}^{-1}$ ) and LiTFSI with  $r = 0.085$  at selected temperatures, revealing the L-to-DIS ODT. (b) Plot of the full width at half maximum (FWHM) of the primary scattering peak (empty squares) and ionic conductivity (filled squares) versus the inverse temperature: the grey bar indicates the temperature region of the ODT and the solid black line represents the VTF fit of the conductivity data below the ODT temperature. Reprinted with permission from [138]. Copyright 2012 American Chemical Society.

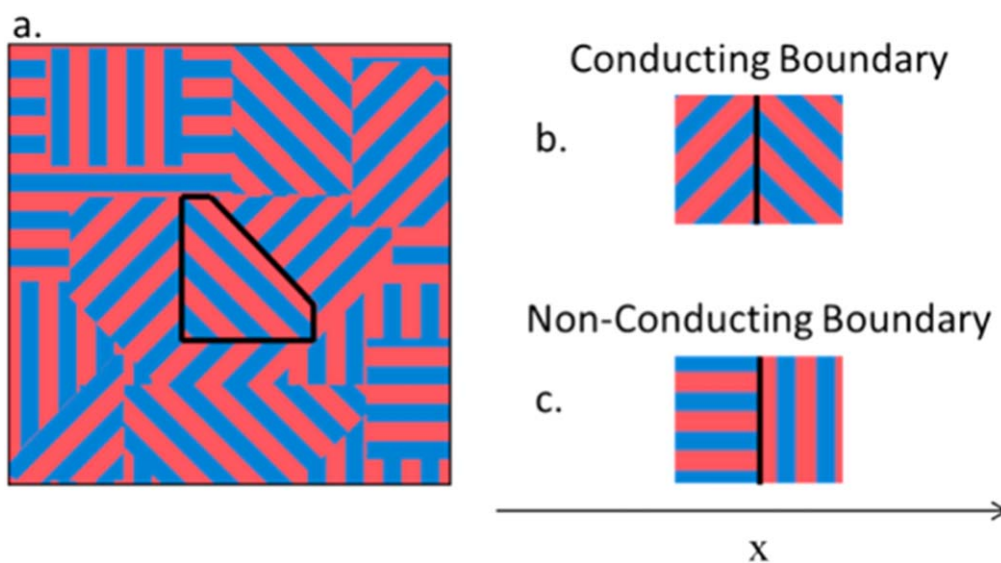


**Figure 10.** (a) Schematic illustration of grains of different size and orientation in a BCPE with lamellar morphology, conducting domains as well as non-conducting domains are highlighted in blue and red, respectively. Depending on the orientation of these domains in the vicinity to other grains, (b) conducting or (c) non-conducting grain boundaries are obtained; enabling, or blocking ion transport along a certain direction. Reprinted with permission from [141]. Copyright 2014 American Chemical Society.

attempt to measure the so-called mutual diffusion coefficient by analyzing the OCV with a Laplace inversion algorithm being directly applicable to cell modelling (also referred to as restricted diffusion method), in contrast to the self-diffusion coefficient measured by PFG-NMR, spectroscopy and other techniques was made in 2011 [145]. In line with the ionic conductivity measurements, the diffusion coefficient showed a plateau when exceeding a molecular weight of the PEO block of  $50\,000\text{ g mol}^{-1}$ . Timachova *et al* [146] reported a

complete continuum characterization of a SEO/LiTFSI mixture exhibiting lamellar morphology, including the determination of the ionic conductivity, the mutual salt diffusion coefficient, and the  $\text{Li}^+$  transference number  $t_{\text{Li}}^+$  via PFG-NMR spectroscopy. The authors found that the presence of defects influences the charge transport (in line with the previous findings). An additional important factor for the charge transport, though frequently overlooked, is the need for the polymer chains to fill the free volume remaining from

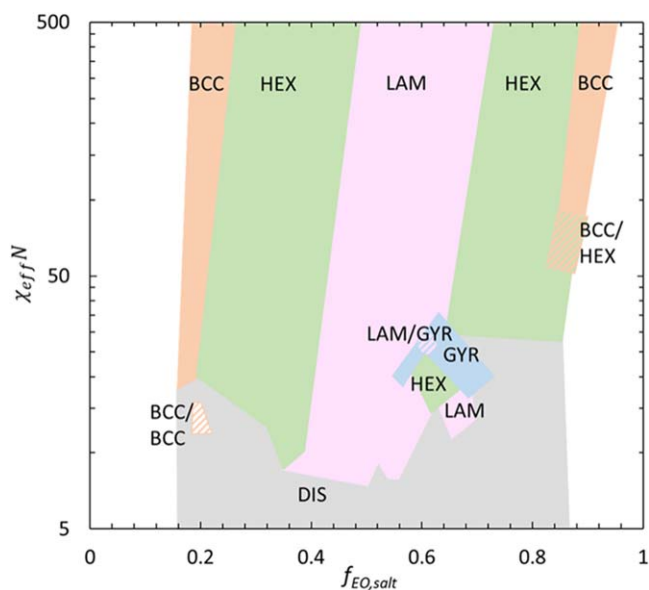


**Figure 11.** Overview of potential phases of SEO/LiTFSI BCPEs at 100 °C plotted as a function of  $\chi_{\text{eff}}N$  versus the volume fraction of the salt containing phase  $f_{\text{EO}/\text{salt}}$  (LAM: lamellar; HEX: hexagonal; BCC: body-centered cubic; GYR: gyroidal; DIS: disordered). Phase boundaries were drawn to bisect known morphologies where no window of coexistence was observed. Non-vertical phase boundaries are due to the addition of the lithium salt, and vertical phase boundaries refer to the neat BCPs. Coexistence regions are indicated by hatched regions. While the polymer composition is accounted for in the  $x$  axis, the molecular weight/chain length  $N$  as well as the salt concentration (via  $\chi_{\text{eff}} = \chi_0 + m \cdot r$ ;  $m$  = proportionality constant) is integrated by the product  $\chi_{\text{eff}}N$  on the  $y$  axis. Reprinted with permission from [144]. Copyright 2018 American Chemical Society.

the diffusion of the salt ions, i.e. their diffusion in the opposite direction of the charge flow, which has been highlighted by a fundamental investigation by Loo *et al* [147] using neutron spin echo spectroscopy and high current flows. In summary, charge transport in BCPEs is complex and while standard ionic conductivity measurements are certainly a necessity, they only provide a ‘global’ insight of the overall dynamics.

**3.3.3. PS-*b*-PEO (SEO) + LiTFSI BCPEs and lithium-metal electrodes.** One of the main motives to study and develop polymer electrolytes is their common compatibility with lithium-metal electrodes. The suppression of dendritic lithium growth (and deposition) is essential. According to Monroe and Newman in 2005 [38], dendrite formation can be suppressed if the polymer electrolyte has a shear modulus twice as high as the one of lithium metal. This would mean that the shear modulus has to be at least as high as 6 GPa, considering a shear modulus of 3.4 GPa for lithium metal at RT [148] (note that other publications have reported different values of 1.9–7.9 GPa [149] or 5–8 GPa [150], most likely due to a different sample preparation). Common SEO BCPEs provide shear moduli of about 0.02 GPa at 90 °C [148] and PEO homopolymers are characterized by even lower shear moduli of well below 1 MPa [151], rendering both of them theoretically incapable of effectively suppressing dendritic lithium growth. Moreover, a further increase in shear modulus

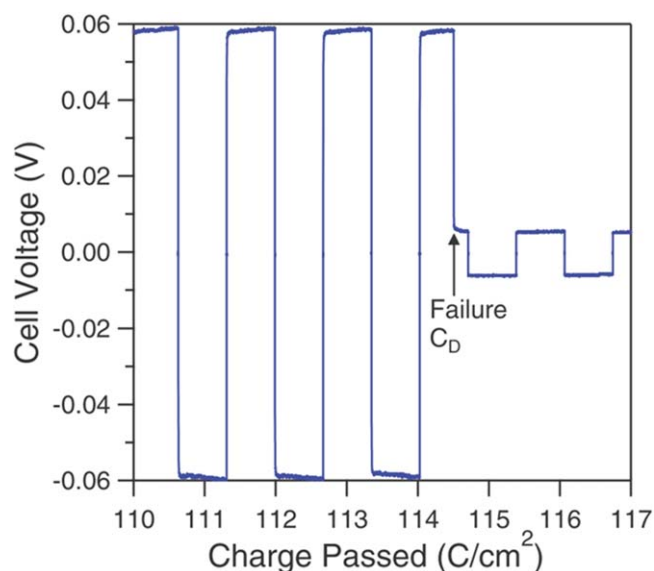


**Figure 12.** Exemplary illustration of a short circuit-induced failure of a symmetric Li|BCPE|Li cell cycled with lithium stripping/plating steps of 4 h at  $\pm 0.175 \text{ mA cm}^{-2}$ . Reproduced from [152]. © IOP Publishing Ltd. All rights reserved.

of SEO-type BCPEs by increasing the PS fraction appears unsuitable in relation to the resulting decrease in ionic conductivity, as discussed above, and negatively affects the realization of a smooth interface with the electrode surface due to the higher rigidity. The latter aspect is of particular importance in the case of lithium-metal electrodes, which are varying by several micrometers in thickness upon cycling. Additionally, it has been reported that lithium dendrites may have a substantially higher shear modulus than bulk lithium, which makes the approach to suppress dendrite growth by sufficiently strong polymer electrolytes very challenging [149].

In the following years, Balsara and co-workers systematically investigated different (potential) effects on the growth and structure of lithium dendrites, including the ambient temperature, the applied current density, the polymer composition, and the salt concentration. A comparative analysis of SEO/LiTFSI systems and PEO/LiTFSI revealed that the former allows for the application of higher currents prior to the occurrence of a short circuit [39]. No delamination at the electrode/electrolyte interface could be detected, which was attributed to the stabilizing effect of the lamellar nanostructure. The bulk electrolyte appears to behave like a solid, consisting of randomly oriented grains according to modulus measurements, therefore being capable of dendrite suppression, while the lamellae in the vicinity of the interface exhibit perpendicular orientation and thus, liquid-like behavior, which guarantees good adhesion properties. Furthermore, it was found that thicker electrolyte membranes provide superior dendrite suppression than thinner ones and that the investigation of symmetric Li|BCPE|Li cells is more efficient for such studies than the characterization of Li|BCPE|LFP cells, as dendrite formation (or cell fading) is delayed in the latter case [152]. Figure 12 displays a typical behavior of a

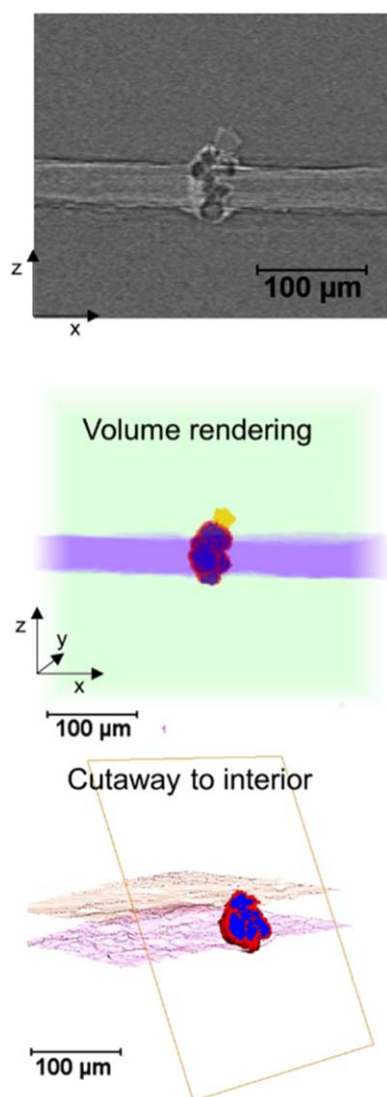


**Figure 13.** Top: Representative digital cross-section of an x-ray microtomography image of a multiglobular lithium structure that is short-circuiting a symmetric Li|BCPE|Li cell (the BCPE is in the middle between the two lithium electrodes). Middle: The corresponding volume rendering. Bottom: A slice through the volume rendering of the multiglobular structure, revealing the internal network of globular lithium surrounded by the BCPE electrolyte. Reprinted with permission from [157]. Copyright 2019 American Chemical Society.

short-circuited Li|BCPE|Li cell. For the investigation of delamination effects it was found that Li|BCPE|LFP cells are more suitable, since there is (theoretically) no volume change in symmetric Li|BCPE|Li cells when lithium is shuttled between the two electrodes [153] or an increase in volume when the deposited lithium is less dense than the original foil. In any case, the importance of the mechanical properties became particularly apparent again when cycling the cells at temperatures between 90 °C and 120 °C, i.e. temperatures which are approaching or exceeding the  $T_g$  of the PS block, as rapid failure was observed when the ambient temperature was beyond the  $T_g$  of PS [154]. Dendritic lithium growth (more precisely referred to as ‘multiglobular structures’ by the authors) was observed inside the electrolyte layer, as depicted

in figure 13. Differently, at lower temperatures, it was found by x-ray microtomography that short circuiting of symmetric Li|BCPE|Li cells originated from subsurface globular structures in the bulk of the lithium electrode [151, 155]. Accordingly, prior to the occurrence of a short circuit most of the dendritic volume was located beneath the surface of the lithium-metal electrode, before eventually protruding into the BCPE. Interestingly, these dendritic subsurface structures appeared to arise from impurities in the bulk lithium such as (crystalline)  $\text{Li}_2\text{O}$ ,  $\text{LiOH}$ , or  $\text{Li}_3\text{N}$  [156], which could be avoided by electrochemically plating lithium on a suitable substrate, resulting in a substantially extended cycle life, providing a potential method for intrinsically safer lithium-metal electrodes [157]. Nonetheless, the application of high current densities [148] and high salt concentrations [158] still led to a decreased cycle life. A modeling study by Ganser *et al* [159] indicates that the overall ‘picture’ may be more complicated than earlier proposed by Monroe and Newman [38]. Following an extension of a mechanical model by electrochemistry, they found that the required mechanical stiffness is decreasing with an increasing ionic conductivity,  $\text{Li}^+$  transference number, and interface conductivity as well as a decreased charging rate. Hence, any specific value for the shear modulus needed to suppress any kind of dendritic lithium growth must be carefully reconsidered in light of all (physicochemical, mechanical, and electrochemical) properties of the polymer electrolyte system.

#### 3.4. Other PS-*b*-PEO-based BCPEs and triblock PS-*b*-PEO-*b*-PS

Park and co-workers investigated the SEO system doped with  $\text{LiClO}_4$  and PEO as dry polymer doped with either dimethyl phthalate or 1-ethyl-3-methylimidazolium tetrafluoroborate ( $\text{EMImBF}_4$ ) and a non-ionic and ionic additive, respectively [160]. In the latter case, a good ionic conductivity of almost  $10^{-3} \text{ S cm}^{-1}$  was obtained at 80 °C. The same group also showed that the modification of the end group of the polymer chains is a powerful tool for tailoring the morphology of such microphase-separated BCPEs [161] and modifying the segregation strength [162].

Bouchet and co-workers focused on the triblock analog PS-*b*-PEO-*b*-PS and studied the impact of different BCPE compositions, using LiTFSI as conducting salt [163]. In accordance with the findings of the Balsara group, the appearance of a ‘dead zone’ (see figure 5) at the PEO-PS interface was proposed, but the negative impact on the ionic conductivity turned negligible when the PEO content was increased to an extent that the 4–5 PEO units in the confining layer became less relevant. After, Bouchet and co-workers synthesized a wide variety of diblock, triblock, and comb-shaped BCPEs, always using PEO (doped with LiTFSI) as the conductive block/side chain and PS as the structural block [164]. No substantial differences were detected between the diblock and triblock architectures. The comb-shaped BCPE manifested inferior electrochemical behavior, particularly the electrochemical stability and cycling behavior. The linear architectures revealed high conductivities of  $2.55 \cdot 10^{-4} \text{ S cm}^{-1}$

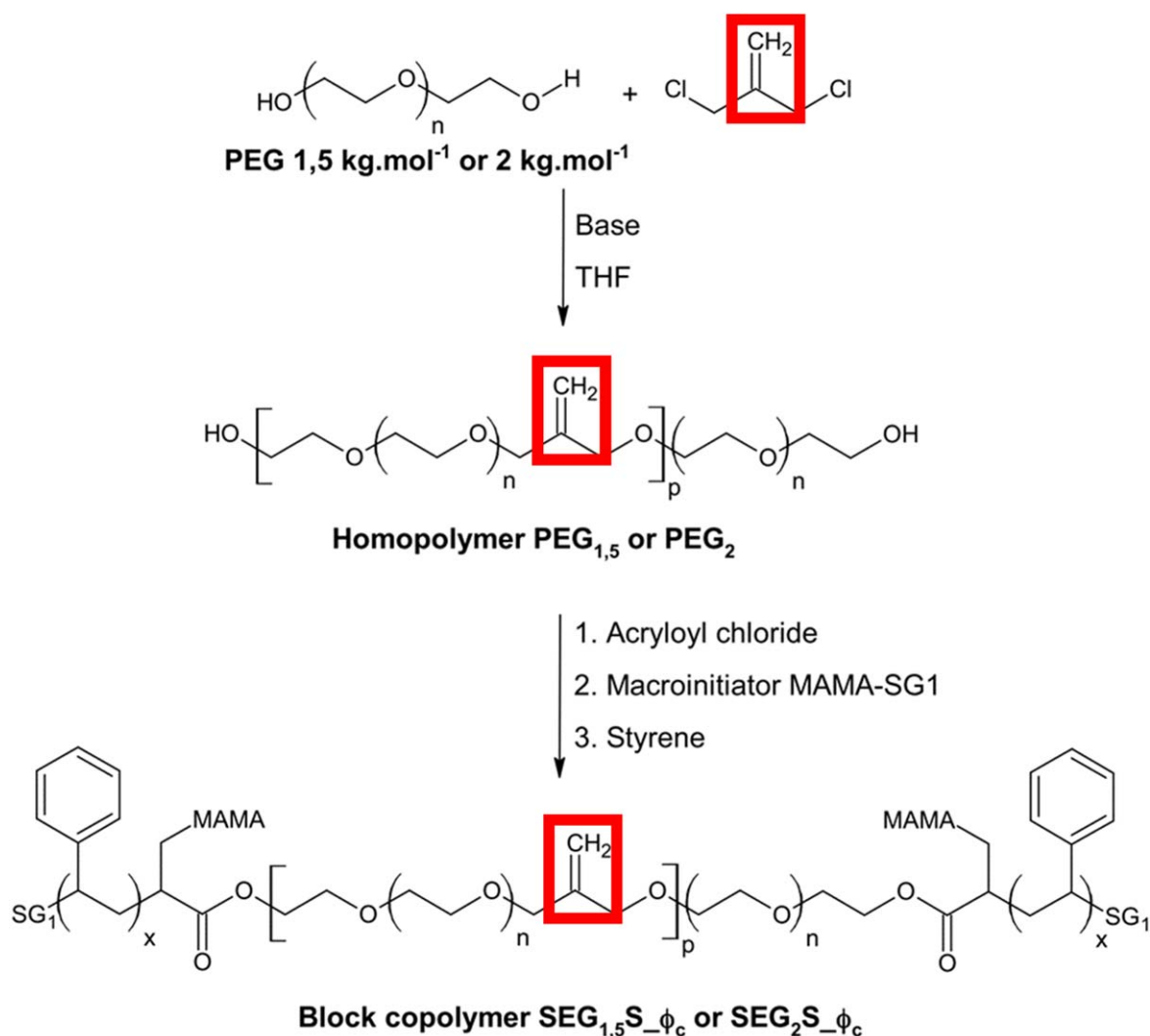


**Figure 14.** Synthesis scheme of the PS-*b*-PEO-*b*-PS BCPE modified by the introduction of methallyl dichloride as a ‘chemical defect’ into the PEO block (highlighted by a red frame) to disturb the high stereoregularity of PEO therefore preventing crystallization. Reprinted with permission from [165]. Copyright 2017 Elsevier Ltd. All rights reserved.

at 60 °C, accompanied by a  $t_{Li}^+$  of about 0.15 and a reasonable stability towards oxidation of 3.8 V versus Li<sup>+</sup>/Li. As a result, Li||LFP cells comprising such linear BCPEs provided a good cycling stability for more than 600 cycles at 50 °C and moderate dis-/charge rate without any evidence of lithium dendrite formation. A significant increase in ionic conductivity to 10<sup>-4</sup> S cm<sup>-1</sup> at 40 °C could be obtained by introducing methallyl dichloride (3-chloro-2-chloromethyl-1-propene) as a ‘chemical defect’ between the EO repeating units (see figure 14), leading to a drop in melting temperature  $T_m$  by suppressing crystallization of the PEO chains due to a disturbed stereoregularity [165]. Remarkably, the electrochemical stability and  $t_{Li}^+$  remained unaffected.

Zhang *et al* [166] followed the triblock PS-*b*-PEO-*b*-PS (incl. LiTFSI) BCPE method and reported a comprehensive electrochemical, thermal, and morphological characterization. With short PS blocks, conductivities beyond 10<sup>-4</sup> S cm<sup>-1</sup> at 30 °C and 10<sup>-3</sup> S cm<sup>-1</sup> at 70 °C were achieved at the expense

of mechanical stability. In fact, with such short PS blocks the authors did not obtain self-standing membranes due to the waxy behavior. When increasing the PS fraction, this issue could be fixed, but the conductivity dropped by an order of magnitude. In addition, the authors reported an average  $t_{Li}^+$  of 0.17 and a stability towards oxidation of 4.5 V versus Li<sup>+</sup>/Li. Nonetheless, stable cycling was only acquired for Li||LFP cells, while the Li||NCM<sub>532</sub> (LiNi<sub>x</sub>Co<sub>y</sub>Mn<sub>z</sub>O<sub>2</sub>, lithium nickel cobalt manganese oxide) cells cycled at 70 °C showed a significant fading, accompanied by a low Coulombic efficiency of well below 100% over the 20 cycles presented.

Another way to enhance the mechanical properties of BCPEs (just as for common polymer electrolytes) is the incorporation of nanoparticles such as TiO<sub>2</sub> or SiO<sub>2</sub> or even hydrogen-bond donating materials like Au-OH-type species [167, 168]. The addition of these nanoparticles can trigger a phase separation into structures which are otherwise difficult or even impossible to achieve, while also enabling the control

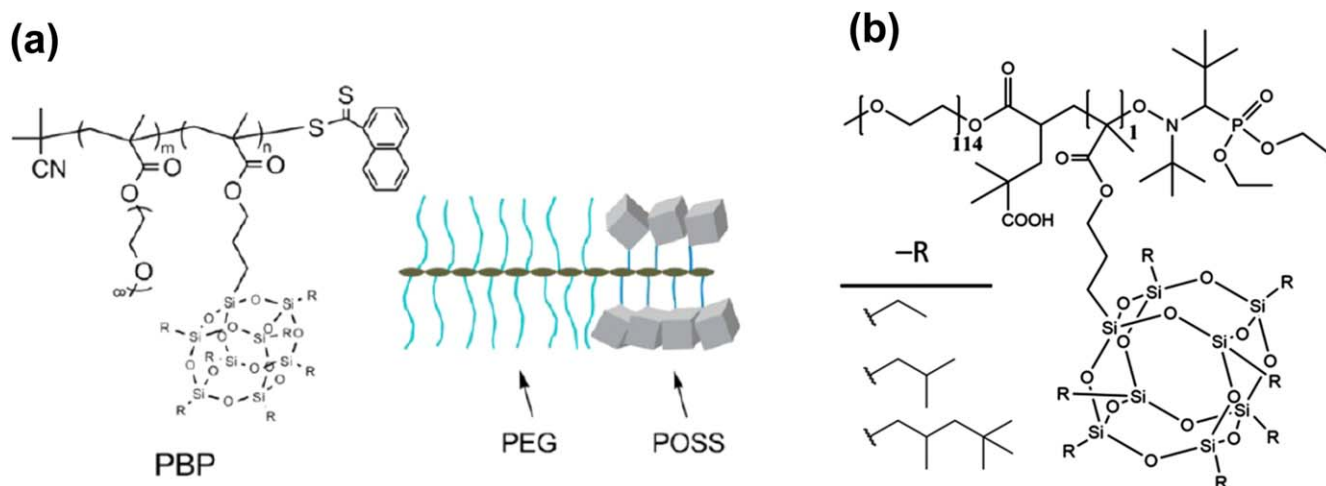


**Figure 15.** (a) Chemical structure and schematic illustration of the comb-shaped organic-inorganic hybrid BCPEs reported by Kim *et al* (R = isobutyl). Reprinted with permission from [170]. Copyright 2012 American Chemical Society. (b) Chemical structure of the linear PEO-*b*-POSS BCPE reported by Balsara *et al*. Reprinted with permission from [173] John Wiley & Sons. © 2020 Wiley Periodicals, Inc.

of the domain size of the segregated regimes [168]. However, a quite large fraction of nanoparticles ( $\gg 10$  wt%) is usually required to apply enough force on the polymer system.

One example is the incorporation of specifically surface-modified TiO<sub>2</sub> nanoparticles into SEO + LiTFSI as reported by Gurevitch *et al* [169]. The ionic conductivity decreased by a factor of three, i.e. from  $\sim 5 \cdot 10^{-4}$  S cm<sup>-1</sup> without any TiO<sub>2</sub> to  $\sim 2 \cdot 10^{-5}$  S cm<sup>-1</sup> with about 28 wt% TiO<sub>2</sub> at 90 °C, while the shear modulus and tensile strength increased. Simultaneously, the nanostructure changed from a lamellar phase to a homogeneous mixture at high TiO<sub>2</sub> loadings, indicating that the presence of the latter limited the nanophase separation. Even so, at an optimum TiO<sub>2</sub> content of 24 wt% substantially higher currents could be passed through the cell (by a factor of 4.7), highlighting the suitability for hindering dendrite formation. Similarly, though with a different outcome, Villaluenga *et al* [85] introduced POSS (polyhedral oligomeric silsesquioxane) nanoparticles, which had been surface-functionalized with short PEO chains, into SEO/LiTFSI BCPEs. When adding 2 wt% of such nanoparticles, the ionic conductivity increased to almost  $10^3$  S cm<sup>-1</sup> at temperatures beyond 100 °C due to the introduction of a phase transition from L to G with 3D conducting pathways. The direct integration of POSS together with short poly(ethylene glycol) (PEG) chains into the polymer, in this case poly(methacrylate), was reported by Kim *et al* [170] (figure 15(a)). This organic-inorganic hybrid comb-shaped BCPE revealed an ionic conductivity of around  $2 \cdot 10^5$  S cm<sup>-1</sup> at 30 °C. The introduction of POSS did not significantly affect the ionic conductivity compared to a reference system but enhanced the dimensional stability of the polymer membrane. Sethi *et al* [171] extended this concept using a linear PEO chain covalently joined with the poly(acryloisobutyl polyhedral oligomeric silsesquioxane) block (see figure 15(b)). In the salt-free state a regular L-to-DIS ODT was observed, but after adding LiTFSI an unconventional DIS-to-L disorder-to-order transition was found. This was attributed to the solubility of LiTFSI in both domains due to interactions of the Li salt with

PEO and POSS domains (not just with the PEO segments as usually observed), leading to the mixing of otherwise incompatible phases. Nevertheless, at elevated temperatures, the entropic contribution surpasses these interactions, resulting in a phase separation, as stated by the authors. Besides, the resulting BCPE showed superior ionic conductivity ( $\sim 5 \cdot 10^4$  S cm<sup>-1</sup> at 90 °C) compared to regular SEO/LiTFSI BCPEs. To further investigate this DIS-to-L transition, Timachova *et al* [172] performed a comprehensive study via PFG-NMR spectroscopy (<sup>7</sup>Li and <sup>19</sup>F). Their findings revealed isotropic diffusion of Li<sup>+</sup> and TFSI<sup>-</sup> in the disordered state and anisotropic diffusion when transitioning to the lamellar phase due to the increasing segregation strength of the two blocks, favoring ion transport parallel to the PEO lamellae, whereas the transport perpendicular to the lamellae was blocked by non-conducting POSS lamellae. In a subsequent study, Gao *et al* [173] evaluated the impact of the alkyl substituents at the silica cage, adding either ethyl, isobutyl, or isooctyl alkyl chains. A decrease in ionic conductivity was observed for an increasing alkyl chain length, which the authors assigned to a certain solubility of LiTFSI in the non-conducting block. Balsara and co-workers reported a reversible change in grain size therefore also in ionic conductivity for a lamellar POSS-PEO-POSS/LiTFSI BCPE upon annealing, which is in strong contrast to the commonly irreversible grain size changes under such conditions [174]. This effect was attributed to the crystallization of the non-conducting POSS-rich microphase and clearly highlights the importance of understanding the grain structure of BCPEs to further enhance their charge transport properties.

### 3.5. Recent BCPE systems beyond SEO

As a potential alternative for the PS block in SEO, Young *et al* [175] investigated an ABA triblock copolymer PP-*b*-PEO-*b*-PP (PEOP), using azide-alkyne click chemistry for the incorporation of a semi-crystalline syndiotactic poly(propylene) (PP) block with superior mechanical and chemical

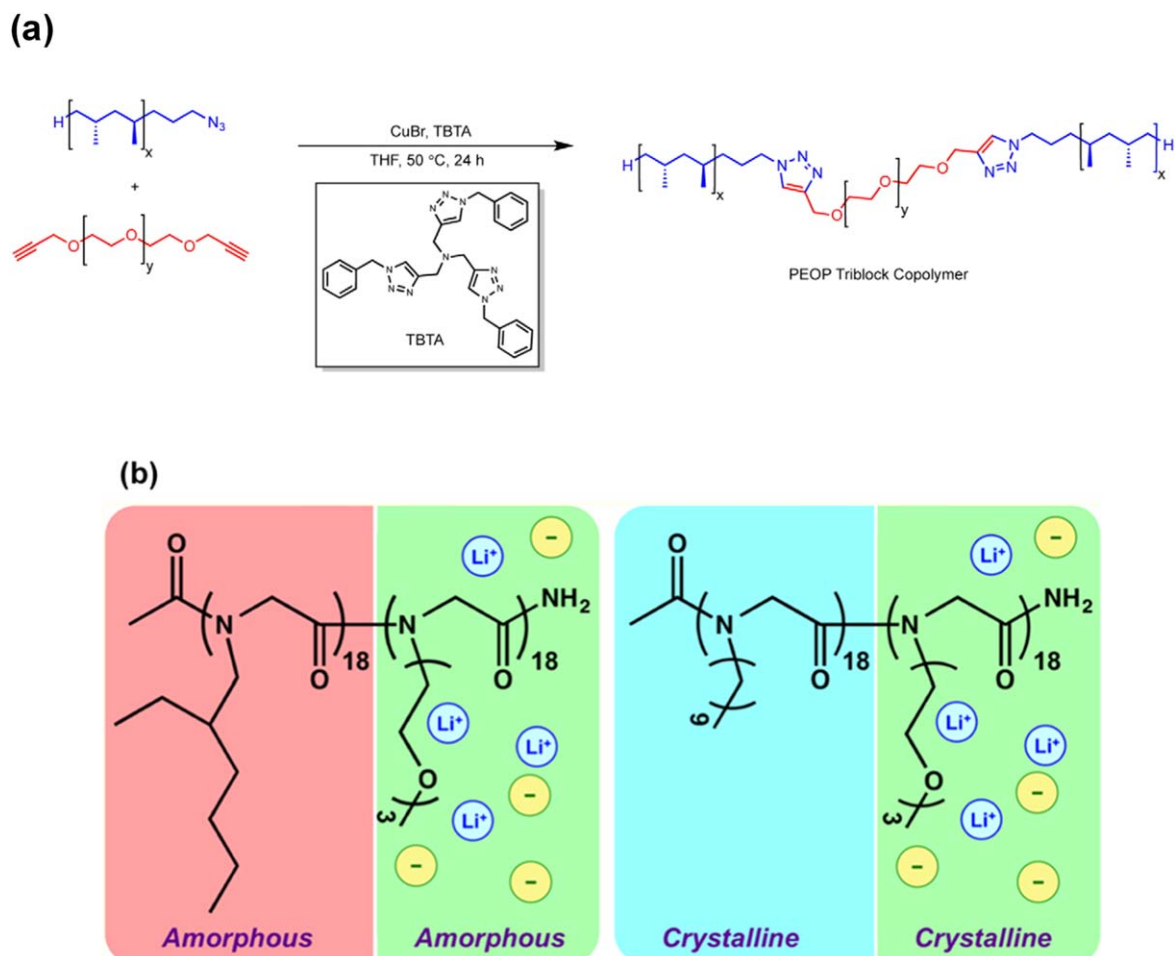


**Figure 16.** (a) Synthesis route of syndiotactic poly(propylene)-*b*-poly(ethylene oxide)-*b*-syndiotactic poly(propylene) (PEOP) ABA triblock copolymers. Reprinted from [175], © 2014 Elsevier Ltd. All rights reserved. (b) Chemical structures of amorphous (left) and crystalline (right) AB diblock copolypeptoids. Reprinted with permission from [176]. Copyright 2014 American Chemical Society.

stability (figure 16(a)). While LiTFSI was still preferentially dissolved in the PEO domains, the conductivity appeared to be influenced by the molecular weight of the structural PP block in contrast to the SEO system. When normalizing the conductivity, a maximum was found for PEOP with a molecular weight of  $20\,000\text{ g mol}^{-1}$  along with a strong phase separation, the authors recorded an ionic conductivity close to  $10^{-3}\text{ S cm}^{-1}$  at  $120\text{ }^{\circ}\text{C}$ . A superior method of yielding a new (LiTFSI-containing) BCPE was presented by Sun *et al* [176], yielding monodisperse diblock copolypeptoids synthesized via solid-phase sub-monomer synthesis (figure 16(b)). Depending on the branching of the side chain located in the structural block, amorphous or crystalline lamellae were obtained. Surprisingly, both materials showed similar ionic conductivities (reaching  $10^{-5}\text{ S cm}^{-1}$  at around  $80\text{ }^{\circ}\text{C}$ ), indicating that crystalline structures might not be completely discarded when searching for advanced polymer electrolytes.

Targeting the replacement of the PEO block, Bergfelt *et al* [177] reported the synthesis of poly(styrene)-*b*-poly( $\epsilon$ -caprolactone) and poly(styrene)-*b*-poly( $\epsilon$ -caprolactone-*r*-trimethylene carbonate) (PS-*b*-PCL and PS-*b*-[PCL-*r*-TMC] respectively; see figure 17(a) for the latter one). The PCL homopolymer, studied as a reference system, showed a pronounced tendency to

crystallize at temperatures below  $60\text{ }^{\circ}\text{C}$ . Also, it decomposed when getting in contact with lithium metal, which was assigned to the presence of the ester groups. When incorporated into PS-*b*-PCL, the interfacial stability increased and the resulting Li|BCPE|LFP cells revealed stable cycling for several hundred cycles. The additional introduction of TMC led to further improved performance as well as a slightly increased ionic conductivity due to the reduced crystallization. Bergfelt *et al* [178] replaced the PS block by poly(benzyl methacrylate), yielding poly(benzyl methacrylate)-*b*-poly( $\epsilon$ -caprolactone-*r*-trimethylene carbonate) (figure 17(b)), which is characterized by a comparable mechanical stability. Adding LiTFSI resulted in a fully amorphous BCPE already at ambient temperature. With an ionic conductivity of about  $10^{-5}\text{ S cm}^{-1}$  and a high  $\text{Li}^{+}$  transference number of ca. 0.64, this electrolyte permitted the stable cycling of Li|BCPE|LFP cells. A completely amorphous BCPE was also reported by Armand and co-workers [179], with a different structural motif, employing PS and PPO/PEO (Jeffamine<sup>®</sup>-type) moieties covalently tethered as side chains to a poly(ethylene-*alt*-maleic anhydride) backbone (see figure 17(c)). The amorphicity of the BCPE originates from the PS side chains preventing the crystallization of the PPO and PEO side chains, resulting in an ionic conductivity of  $5 \cdot 10^{-4}\text{ S cm}^{-1}$  at  $70\text{ }^{\circ}\text{C}$  for an optimized salt

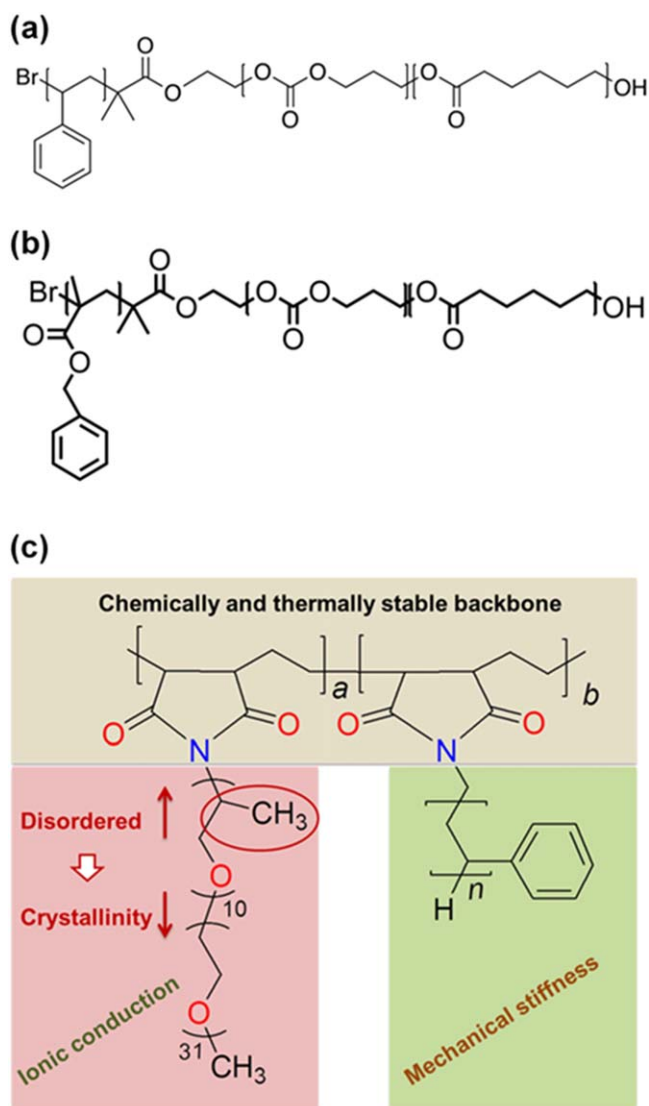


**Figure 17.** (a) Chemical structure of poly(styrene)-*b*-poly( $\epsilon$ -caprolactone-*r*-trimethylene carbonate), also abbreviated as PS-*b*-[PCL-*r*-TMC]. Reproduced from [177]. CC BY 3.0. (b) Replacement of the PS block in (a) by poly(benzyl methacrylate) yields poly(benzyl methacrylate)-*b*-poly( $\epsilon$ -caprolactone-*r*-trimethylene carbonate). Reprinted with permission from [178]. Copyright 2020 American Chemical Society. (c) Chemical structure of the poly(ethylene-*alt*-maleic anhydride) backbone with covalently attached PS and PPO/PEO (Jeffamine<sup>®</sup>-type) side chains (including the functionality of each part of the BCP). Reprinted with permission from [179]. Copyright 2018 Wiley-VCH GmbH.

concentration and stable cycling of the corresponding Li|BCPE|LFP cells.

Dörr *et al* [180] suppressed crystallization in poly(isoprene)-*b*-poly(styrene)-*b*-poly(ethylene oxide) (ISO), which had been reported earlier by Epps *et al* [114], by incorporating a short PEO block. When introducing a very large amount of LiTFSI, i.e. up to  $r = 5$ , which corresponds to 5 Li<sup>+</sup> per EO moiety, the authors observed an exceptionally high ionic conductivity of  $1.4 \cdot 10^{-3} \text{ S cm}^{-1}$  at 20 °C; notably, without losing suitable mechanical properties. The possibility of adding such a high amount of the lithium salt was attributed to the fact

that some tetrahydrofuran (THF), which had been used as casting solvent, remained in the polymer membrane, since it could not be completely removed (neither by applying elevated temperatures nor by subjecting the membranes to a vacuum treatment). The additional coordination sites for the lithium cations in combination with the high mobility of the THF molecules also contributed to the high ionic conductivity [181], while the high Li<sup>+</sup> transference number of 0.7 [180] indicated that the very high salt concentration also led to modified lithium transport mechanism, similarly to the polymer-in-salt method [51]. Additional insights into this BCPE system were reported by Sutton *et al* [182], who observed that the interface between the electrode and the electrolyte plays a crucial role for the determination of the ionic conductivity; potentially an even more important one than the bulk conductivity, (including the types of electrodes used and the temperature history of the polymer membrane). The authors demonstrated that the use of PEO-functionalized electrode surfaces, allowing for a good contact with the BCPE and an accumulation of the PEO block at the interface, led to much higher conductivities than the use of polar (untreated) stainless steel electrodes, which favored the segregation of the PS block towards the interface, acting as an insulating layer. Coote *et al* [183] also showed for a PS-*b*-PIL-based BCPE poly(ionic liquid) (PIL) that the orientation of nanostructured BCPEs impacts the determination of the ionic conductivity. Highly oriented lamellae were observed at the electrode|electrolyte interface due to preferential surface wetting, while the bulk material consisted of randomly oriented lamellae. This resulted in a 20 times higher in-plane conductivity compared to the values obtained by through-plane measurements.

Using ROMP as a novel synthetic technique to realize BCPs, Bullock and Kofinas [184, 185], prepared a new set of diblock and triblock copolymers (see figure 18(a)). For the diblock copolymer-based electrolyte comprising LiTFSI, they obtained ionic conductivities of  $2 \cdot 10^{-6} \text{ S cm}^{-1}$  at RT and around  $10^{-4} \text{ S cm}^{-1}$  at 60 °C. The ABC triblock copolymer was designed in an even more sophisticated manner to achieve a self-contained nanoscale battery, with one block providing the ‘negative electrode’ and another one the ‘positive electrode’, both being separated by a PEO-type electrolyte block. Of late, an AB diblock architecture with an imidazolium-functionalized norbornene block and a benzene-functionalized norbornene block was reported by He and co-workers (figure 18(b)) [186]. The benzene functionalization ensured a strong phase separation in combination with the norbornene backbone, and high mechanical stability; the latter could be further increased by adding silica nanoparticles. After doping with LiTFSI conductivity values of around  $7.5 \cdot 10^{-5} \text{ S cm}^{-1}$  at 25 °C and  $1.3 \cdot 10^{-3} \text{ S cm}^{-1}$  at 100 °C were attained, along with an electrochemical stability of up to 4.2 V at 30 °C. An elevated ionic conductivity of  $1.58 \cdot 10^{-3} \text{ S cm}^{-1}$  at an even higher temperature of 200 °C was reported by Ping *et al* [187] for a (LiTFSI-doped) poly(norbornene) derivative backbone modified with PEO and poly {2, 5-bis [(4-methoxyphenyl)-oxy-carbonyl]styrene} (PMPCS) side chains (figure 18(c)). PMPCS

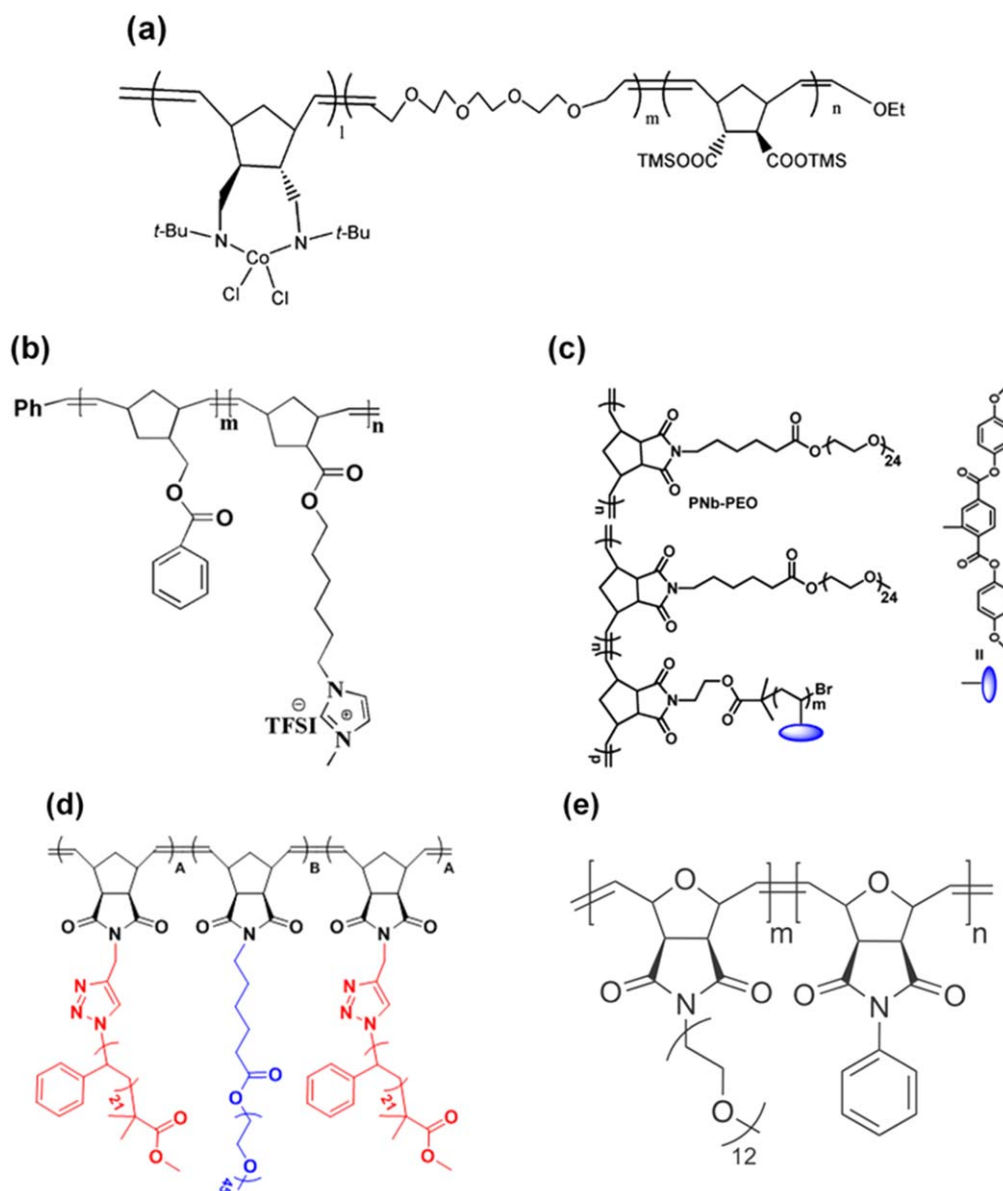


**Figure 18.** Examples for ROMP-derived BCPs: (a) chemical structure of a representative ABC triblock copolymer serving as nanoscale battery and consisting of a ‘negative electrode’ block with an organo-cobalt species attached to the polymer backbone, a PEO-type electrolyte block in the center, and a ‘positive electrode’ block with binding abilities for metal salts. Reprinted with permission from [185]. Copyright 2004 American Chemical Society. (b) Chemical structure of a norbornene-based AB diblock BCP with one of the blocks containing an ionic imidazolium function and the other block a phase separation inducing benzene function. Reprinted with permission from [186] John Wiley & Sons. © 2017 Wiley Periodicals, Inc. (c) Structural motif of a poly(norbornene) backbone derivative modified with PEO and liquid-crystalline poly{2,5-bis[(4-methoxyphenyl)-oxycarbonyl]styrene} (PMPCS) side chains. Reprinted with permission from [187]. Copyright 2017 American Chemical Society. (d) Chemical structure of the ABA triblock copolymer based on a poly(norbornene) derivative backbone with PEO side chains located in the mid-block surrounded by two blocks with PS-based side chains. Reprinted with permission from [188]. Copyright 2015 American Chemical Society. (e) BCP based on the same oxanorbornene dicarboximide backbone with alternating PEO-type and phenyl-type side chains. Reprinted with permission from [189], © 2018 Elsevier Ltd. All rights reserved.

is a so-called mesogen-jacketed liquid crystalline polymer that provides, together with the rigid norbornene backbone, excellent temperature stability. Therefore, the lamellar nanostructure was maintained beyond 200 °C, producing a system suitable for high-temperature applications. A more common BCP architecture was developed by Grubbs and co-workers [188] grafting PEO and PS moieties to a poly(norbornene) derivative backbone, yielding a ABA triblock copolymer with the PEO side chains located in the mid-block surrounded by two blocks

with PS-based side chains (figure 18(d)). The PS component formed hexagonally packed cylinders and the incorporation of LiTFSI led to ionic conductivities as high as  $10^{-3}$  S  $\text{cm}^{-1}$  at 105 °C though, at the expense of a very low mechanical stability. Longstaff *et al* [189] used the same oxanorbornene dicarboximide backbone for the synthesis of another BCPE via ROMP. Sidechains of oligomeric PEO (doped with LiTFSI) served as the ionophilic part and phenyl groups directly attached to the backbone guaranteed the mechanical rigidity of

**Table 1.** Summary of the main characteristics of selected BCPEs discussed in section 3.5 and the findings reported, including the polymerization technique used for the synthesis, the ionic conductivity, the conducting lithium salt added, and the cell setup used for cycling tests (if provided).

Name	Figure	Polymerization technique	Ionic conductivity $\sigma/S\text{ cm}^{-1}$	Conducting salt	Cell setup	Reference
PP- <i>b</i> -PEO- <i>b</i> -PP (PEOP)	16(a)	Azide-alkyne click chemistry	$\sim 10^{-5}$ (30 °C) $\sim 10^{-3}$ (120 °C)	LiTFSI		[175]
Monodisperse diblock copolypeptoids	16(b)	Solid-phase sub-monomer synthesis	$< 10^{-6}$ (40 °C) $\sim 10^{-5}$ (80 °C)	LiTFSI		[176]
Poly(styrene)- <i>b</i> -poly( $\epsilon$ -caprolactone- <i>r</i> -trimethylene carbonate) (PS- <i>b</i> -[PCL- <i>r</i> -TMC])	17(a)	Anionic ring-opening polymerization	$< 10^{-5}$ (30 °C) $\sim 10^{-4}$ (90 °C)	LiTFSI	Li BCPE LFP	[177]
Poly(benzyl methacrylate)- <i>b</i> -poly( $\epsilon$ -caprolactone- <i>r</i> -trimethylene carbonate)	17(b)	Anionic ring-opening polymerization	$\sim 10^{-5}$ (30 °C) $\sim 10^{-4}$ (90 °C)	LiTFSI	Li BCPE LFP	[178]
Poly(ethylene- <i>alt</i> -maleic anhydride) backbone, PS and Jeffamine <sup>®</sup> -type side chains	17(c)	Addition of sidechains	$\sim 10^{-5}$ (30 °C) $\sim 10^{-3}$ (100 °C)	LiTFSI	Li BCPE LFP	[179]
Poly(isoprene)- <i>b</i> -poly(styrene)- <i>b</i> -poly(ethylene oxide)		Living anionic polymerization	$1.4 \cdot 10^{-3}$ (20 °C), THF remaining	LiTFSI		[180, 181]
[NORCo] <sub>80</sub> /[TOCD] <sub>150</sub> /[NORCOOTMS] <sub>150</sub>	18(a)	ROMP	$2.22 \cdot 10^{-6}$ (20 °C) $1.05 \cdot 10^{-4}$ (60 °C)	LiTFSI	Li BCPE LiMn <sub>2</sub> O <sub>4</sub>	[184, 185]
[P(NPh- <i>b</i> -NIm-TFSI)]	18(b)	ROMP	$7.5 \cdot 10^{-5}$ (25 °C) $1.3 \cdot 10^{-3}$ (100 °C)	LiTFSI		[186]
<i>g</i> PEO- <i>b</i> - <i>g</i> PMPCS	18(c)	ROMP	$\sim 10^{-5}$ (25 °C) $1.6 \cdot 10^{-3}$ (200 °C)	LiTFSI		[187]
<i>g</i> PS- <i>g</i> PEO- <i>g</i> PS (PS and PEO side chains grafted to poly(norbornene) backbone)	18(d)	ROMP	$\sim 10^{-3}$ (105 °C)	LiTFSI		[188]
Oxanorbornene dicarboximide backbone with PEO and phenyl side chains	18(e)	ROMP	$\sim 10^{-6}$ (20 °C) $\sim 10^{-4}$ (80 °C)	LiTFSI		[189]

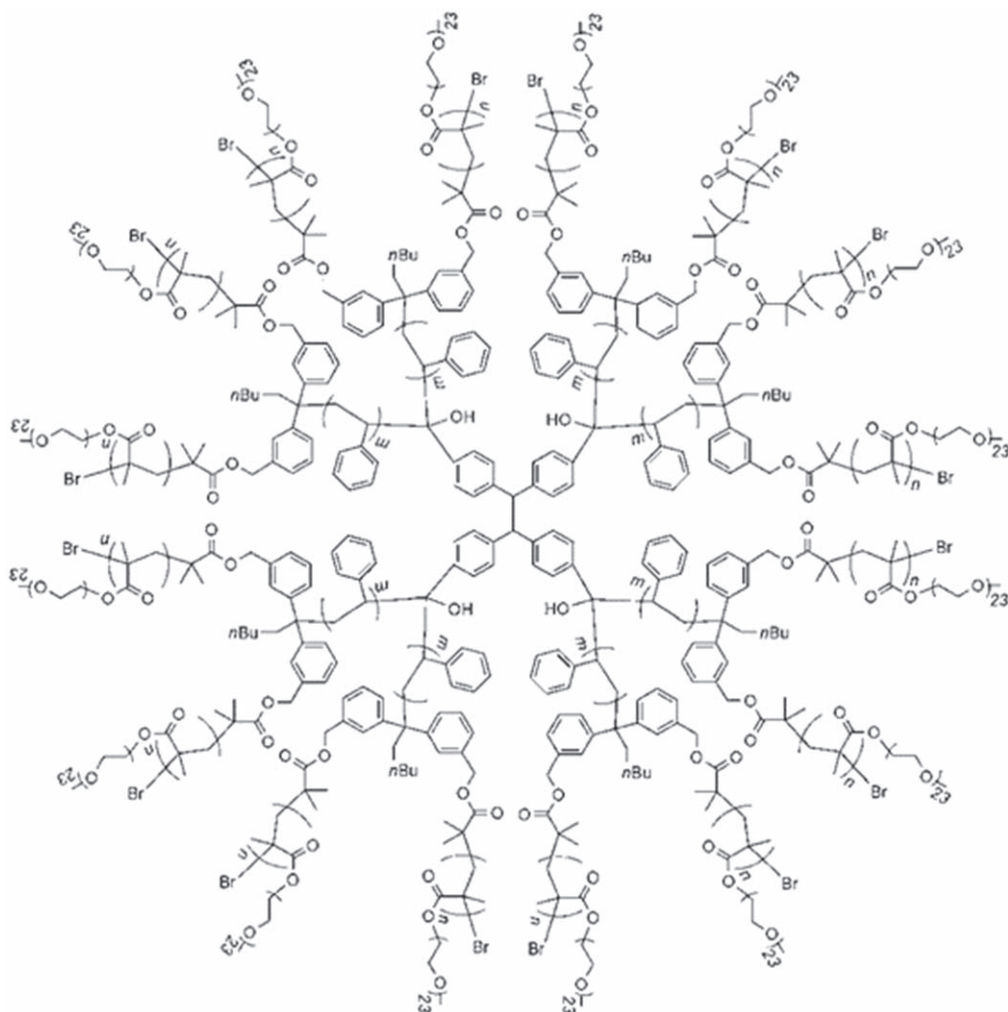


**Figure 19.** Chemical structure of a star-shaped BCP, synthesized via a combination of living anionic polymerization and metal-catalyzed living radical polymerization for the attachment of the PS and POEM segments. Reproduced from [191]. © IOP Publishing Ltd. All rights reserved.

the system via their high  $T_g$  (figure 18(e)). Despite the interesting finding of lamellar and cylindrical nanostructures, the ionic conductivity remained low at 25 °C (in the range of  $10^{-6}$  S cm $^{-1}$ ).

Table 1 presents an overview including the most important characteristics of several BCPEs discussed in this section.

### 3.6. Star-shaped BCPEs

Reports on star-shaped BCPEs are less frequent than linear and comb-type BCPEs. However, they possess unique features making them (potentially) interesting alternatives. Most strikingly the outer parts of such star-shaped structures can move more freely due to the greater accessible space, while the segments close to the core (as well as the core itself) are usually less mobile as a result of the dense packing. This can be exploited, e.g. by using a very rigid core, providing mechanical stability owing to the dense packing, supplemented by a flexible polymer chain in the outer area to promote charge transport. Already in 1989, Xie *et al* [190] reported the synthesis of a four-armed, star-shaped BCP with

two arms consisting of PS and another two of PEO, accompanied by various graft copolymers. Lately, Niitani *et al* [191] transferred the widely investigated PS-*b*-POEM motif into a star-shaped system (figure 19). The essentially amorphous morphology for the BCPE comprising, e.g. LiTFSI led to ionic conductivities in the range from  $10^{-5}$  to  $10^{-4}$  S cm $^{-1}$  at ambient temperature. The Li|BCPE|LCO full-cells cycled at 30 °C with an upper cut-off voltage of 4.3 V showed no significant fading over (the rather limited number of) 10 cycles. In a successive study, Tong *et al* [192] reported a four-armed ABC triblock copolymer consisting of a PS block as the core, surrounded by a POEM-like, comb-shaped block and finally completed by a cyanobiphenyl end-cap. The latter function acts as a mesogen, leading to a liquid-like state, which promotes the arrangement of a micro-phase separated morphology that favors ionic conductivity. Nonetheless, the conductive domains remained amorphous in itself as indicated by the VTF-type conductivity behavior with a maximum at around  $10^{-4}$  S cm $^{-1}$  at RT. Guan *et al* [193] synthesized and investigated a two-armed star brush BCP consisting of PEO side chains grafted to a poly(methacrylate)

backbone, followed by a PS block. While the conductivity was high with about  $2.1 \cdot 10^{-4} \text{ S cm}^{-1}$  at  $28 \text{ }^\circ\text{C}$ , the incorporation of a large amount of short-chained PEG-based plasticizer (in addition to fumed  $\text{SiO}_2$ ) means a direct comparison with the previous systems is difficult.

### 3.7. BCPEs incorporating ionic liquids

Doping BCPEs with ionic liquids (ILs) provides a promising route to maintain the advantageous properties of BCPEs such as low flammability and separation of the ionophilic and ionophobic domains, while simultaneously allowing for increased ionic conductivities. These advantages are commonly related to the preferential swelling of the ionic domains, as shown, for instance, by Elabd and co-workers [88] for a PS-*b*-PMMA-based BCPE and 1-ethyl-3-methylimidazolium TFSI (EMIm-TFSI), in which the rigid PS block was capable of compensating the plasticizing effect of the IL. The group then reported the synthesis of a BCPE comprising a PMMA block and a PIL block using the RAFT polymerization technique and doped this with EMIm-TFSI and LiTFSI [194]. The resulting high ionic conductivity of  $10^{-3} \text{ S cm}^{-1}$  at ambient temperature up to  $10^{-2} \text{ S cm}^{-1}$  at  $105 \text{ }^\circ\text{C}$ , were accompanied by a low electrochemical stability. Zardalidis *et al* [195] investigated poly(isoprene-*b*-ethylene oxide) AB diblock copolymers doped with either LiTf or EMIm-Tf. Higher conductivities were observed for the IL-doped BCPE due to the plasticizing effect and the higher mobility of the IL compared to the salt. Similarly, Metwalli *et al* [196] reported a high ionic conductivity of  $10^{-3} \text{ S cm}^{-1}$  at RT for the SEO system doped with LiTf and EMIm-Tf.

It should be recalled that any 'simple' ionic conductivity value always considers the contribution of the highly mobile IL. As a result, care must be taken when comparing these conductivity values with IL-free BCPE systems, especially when evaluating their potential application in lithium batteries, for which the mobility of the  $\text{Li}^+$  cation is of importance.

### 3.8. BCPEs with mixed ionic and electronic conductivity

Targeting a mixed ionic and electronic conductivity, Balsara and co-workers investigated diblock poly(3-hexylthiophene)-*b*-poly(ethylene oxide) (P3HT-*b*-PEO), which was synthesized via a Grignard metathesis polymerization [197–199]. While they found that the ionic conductivity was lower when adding LiTFSI than the PEO homopolymer reference system, the electronic conductivity of the BCPE, arising from the conjugated P3HT block, was surprisingly higher compared to the P3HT homopolymer. Such a simultaneous ionic and electronic conductivity makes this BCPE suitable for incorporation into the electrode composite, potentially replacing the polymer binder and the conductive carbon (while an electronically insulating polymer electrolyte layer with a separator function would also be required). It should be noted that the use of such P3HT-*b*-PEO-based BCPE is essentially limited to the positive electrode, since the semiconducting P3HT block must be electrochemically oxidized to achieve a

suitable electronic conductivity. The successful cycling of Li||LFP cells, comprising the P3HT-*b*-PEO-based BCPE in the positive electrode, with cut-off voltages of 3.8 and 2.5 V was enabled by the fact that the electrochemical oxidation of the P3HT block has its onset at 3.1 V during charge. Upon discharge, the electronic conductivity severely drops below 3.3 V due to the loss of electronic conductivity of the P3HT block under such conditions, which may effectively prevent an accidental over-discharge.

## 4. Single-ion conducting BCPEs

### 4.1. General considerations

An important parameter for the evaluation of BCPEs (and electrolytes in general) is the  $\text{Li}^+$  transference number,  $t_{\text{Li}^+}$ , i.e. the contribution of  $\text{Li}^+$  cations to the overall conductivity. Most BCPEs are characterized by a  $t_{\text{Li}^+}$  in the range from 0.1 to 0.3, comparable with common liquid organic electrolytes [52]. However, such low transference numbers are potentially causing strong concentration gradients and reversed cell polarization, particularly when applying elevated current densities. These detrimental effects have a negative impact on the overall performance and safety of the cell, as they limit the lifetime and favor dendritic lithium deposition [41, 43]. A potential strategy to overcome such issues is the realization of single-ion conductors (SICs) [45]. Kim and Srinivasan [200] reported that the ionic conductivity that is required for EV applications is substantially lower for SICs (ca.  $4 \cdot 10^{-4} \text{ S cm}^{-1}$ ) compared to electrolyte systems with a low transference number of about 0.2 (ca.  $5 \cdot 10^{-3} \text{ S cm}^{-1}$ ). Such SICs are commonly obtained by covalently tethering the anionic function to the polymer backbone, making the  $\text{Li}^+$  cation the only mobile species in the polymer electrolyte.

### 4.2. 'Dry' SIC-BCPEs

An early study on SIC-BCPEs was presented by Sadoway *et al* in 2001 [201], who randomly copolymerized tert-butyl methacrylate monomers with lauryl methacrylate to form the non-conducting block, followed by the attachment of a regular POEM block as the conductive part. In the next step, tert-butyl methacrylate repeating units were quantitatively converted into methacrylic acid by hydrolysis, and further lithiated using an organic lithium base in order to eventually obtain poly(lauryl methacrylate-*r*-lithium methacrylate)-*b*-poly(oligooxyethylene methacrylate), abbreviated as P(LMA-*r*-LiMA)-*b*-POEM with a virtual salt concentration of  $r \approx 0.1$ . The authors compared this system with a SIC-BCPE in which they introduced the lithiated repeating units into the POEM block and found inferior ionic conductivity for the latter independent of the addition of PEGDME as plasticizer. The better performing system bearing the LiMA group in the non-conducting block provided an ionic conductivity of about  $3 \cdot 10^{-7} \text{ S cm}^{-1}$  at ambient temperature in the dry state and around  $6 \cdot 10^{-6} \text{ S cm}^{-1}$  in the PEGDME-doped state. Besides low ionic conductivity, the authors reported a  $\text{Li}^+$  transference number of 0.9 in combination with high electrochemical stability beyond 4 V determined from

CV measurements. In a follow-up study, Ryu *et al* [202] compared these two systems using anionic copolymerization techniques, i.e. P(LMA-*r*-LiMA)-*b*-POEM and PLMA-*b*-P(LiMA-*r*-OEM), with a triblock copolymer architecture: PLMA-*b*-PLiMA-*b*-POEM. The comparative determination of the ionic conductivity confirmed the detrimental impact of introducing the lithiated segment into the ion conductive block. The authors concluded that this inferior conductivity originates from the impeded dissociation of the R-COO<sup>-</sup> Li<sup>+</sup> ion pairs in the POEM block, while the phase separation occurring in the other two SIC-BCPE systems permits the spatial separation of the anionic functions due to the migration of the Li<sup>+</sup> ions into the POEM conductive block. The incorporation of the Lewis acid BF<sub>3</sub> (introduced as a BF<sub>3</sub>-THF complex using methanol as a solvent) led to a decreased charge density at the anion due to the strong association with the carboxylate function, resulting in increased conductivities. Rolland *et al* [203] focused on the synthesis of a related ABC triblock copolymer architecture, comprising a PS block, a lithiated poly(methacrylic acid) block, and a conventional POEM block (see figure 20(a)). Due to the strongly coordinating nature of the carboxylic moiety low ionic conductivities were obtained, but the addition of BF<sub>3</sub> led to an increase in conductivity, eventually achieving around 10<sup>5</sup> S cm<sup>-1</sup> at 20 °C. Kofinas and co-workers [204] extended their work on PEO-*b*-PMMA BCPs comprising lithium bis(oxalato)borate (LiBOB) by partially hydrolyzing PMMA and the lithiation of the resulting poly(acrylic acid) functionalities producing PEO-*b*-(PMMA-*r*-PMAALi), as depicted in figure 20(b). With surplus lithium (in addition to LiBOB) ionic conductivities of around 10<sup>5</sup> S cm<sup>-1</sup> were obtained at ambient temperature. The Li<sup>+</sup> transference number was reported to be about 0.9 for such a ‘hybrid’ system [205]. When completely hydrolyzing and lithiating the PMMA block (i.e. PEO-*b*-PMAALi), the ionic conductivity was further enhanced to 10<sup>4</sup> S cm<sup>-1</sup> at RT and almost 10<sup>3</sup> S cm<sup>-1</sup> at 65 °C [206].

Based on the earlier findings regarding the advantageous separation of the ionic and the conducting phase, Bouchet *et al* [207] developed a BAB triblock copolymer with a conventional PEO mid-block (dissolving and conducting the Li<sup>+</sup> cations [217, 218]) surrounded by two lithiated poly(styrene sulfonyl(trifluoromethanesulfonyl)imide) (P(STFSILi)) blocks, as shown in figure 20(c). A NMPT using the end-group modified PEO block as a macro-initiator was applied to yield the desired polymer structure. Thanks to the rigid PS-type blocks, a sufficient mechanical stability was obtained, along with an electrochemical stability exceeding 4 V, a  $t_{Li}^+$  beyond 0.85, and an ionic conductivity of more than 10<sup>5</sup> S cm<sup>-1</sup> at 60 °C. This high ionic conductivity in the absence of a plasticizer was achieved due to the high dissociation of the TFSI-type anionic function, characterized by a highly delocalized negative charge. The authors also reported stable cycling of Li|SIC-BCPE|LFP cells at 60 °C, applying C rates up to 0.5C. For a similar system with an AB diblock architecture, Balsara and co-workers [218] observed an excellent morphology-conductivity relationship due to an ODT between 50 °C and 55 °C, related to the energetically

favorable interaction between the Li<sup>+</sup> cations and the EO moieties. In the lamellar state, the SIC-BCPE exhibits an inferior ionic conductivity due to the formation of ion clusters trapped in the glassy PS block. However, a rapid increase in conductivity was detected as soon as the polymer turned into the mixed/disordered state, facilitating an increased mobility of the Li<sup>+</sup> ions, as depicted in figures 21(a), (b). Therefore, the superior ionic conductivity was assigned to the homogeneous mixing of the different blocks, facilitating the migration of the Li<sup>+</sup> cations into the PEO-rich domains. In a related study, Balsara and co-workers [219] varied the volume fraction of the P(STFSILi) block and the lithium concentration, while the PEO volume fraction was kept constant. In line with the previous findings, the presence of the disordered morphology was revealed to be crucial for obtaining suitable ionic conductivities. The samples with a higher lithium concentration exhibited a fully disordered nanostructure already at RT resulting in a high VTF-type ionic conductivity along the investigated temperature range, while the SIC-BCPEs with a lower lithium concentration displayed a sudden drop in conductivity below the ODT. A slightly modified ABCA-type BCPE architecture was reported by Long and co-workers [208], who combined the STFSILi monomer with PS and POEM blocks by using a RAFT polymerization technique; the latter one containing a short, i.e. dimeric, side chain (figure 20(d)). Comparable ionic conductivities were reported. Müller-Buschbaum and co-workers [209] further modified the BCPE architecture by attaching a PEO-type unit to the PS function applying the NMPT method (figure 20(e)). While this SIC-BCPE showed suitable performance at 0.7 °C and 90 °C in Li|SIC-BCPE|LFP cells, the focus had been on the investigation via operando SANS (for which part of the BCPE was deuterated to increase the contrast), revealing no dendritic lithium deposition and a noticeable increase in size of the conductive pathways attributed to a high ionic current creating enough ‘pressure’ to deform the polymer nanostructure. In a slightly different approach, Aissou *et al* [220] blended PS-*b*-PSTFSILi with a PEO homopolymer and a comparison with the PSTFSILi homopolymer revealed superior performance for the micro/nanostructured SIC-BCPEs. Using the same ionic group, Villaluenga *et al* [210] attached short chains of P(STFSILi) to silsesquioxane cores via NMPT (figure 20(f)) and utilized these nanoparticles for doping conventional (salt-free) SEO. The nanoparticles were preferentially located in the PEO domains due to the miscibility of the surface-modified nanoparticles with this phase. The ionic conductivity remained around 10<sup>5</sup> S cm<sup>-1</sup> at 90 °C, well below the conductivities reported for regular SEO/LiTFSI BCPEs and SIC-BCPEs with the ion containing block directly integrated in the chain. This inferior conductivity was attributed to the need for Li<sup>+</sup> cations to hop from one fixed anionic site to another and from one POSS nanoparticle to another. Though the Li<sup>+</sup> transference number was almost unity (0.98) and the nanostructure changed from lamellar to cylindrical when adding the nanoparticles, this suggests that the charge transport was affected in several ways.

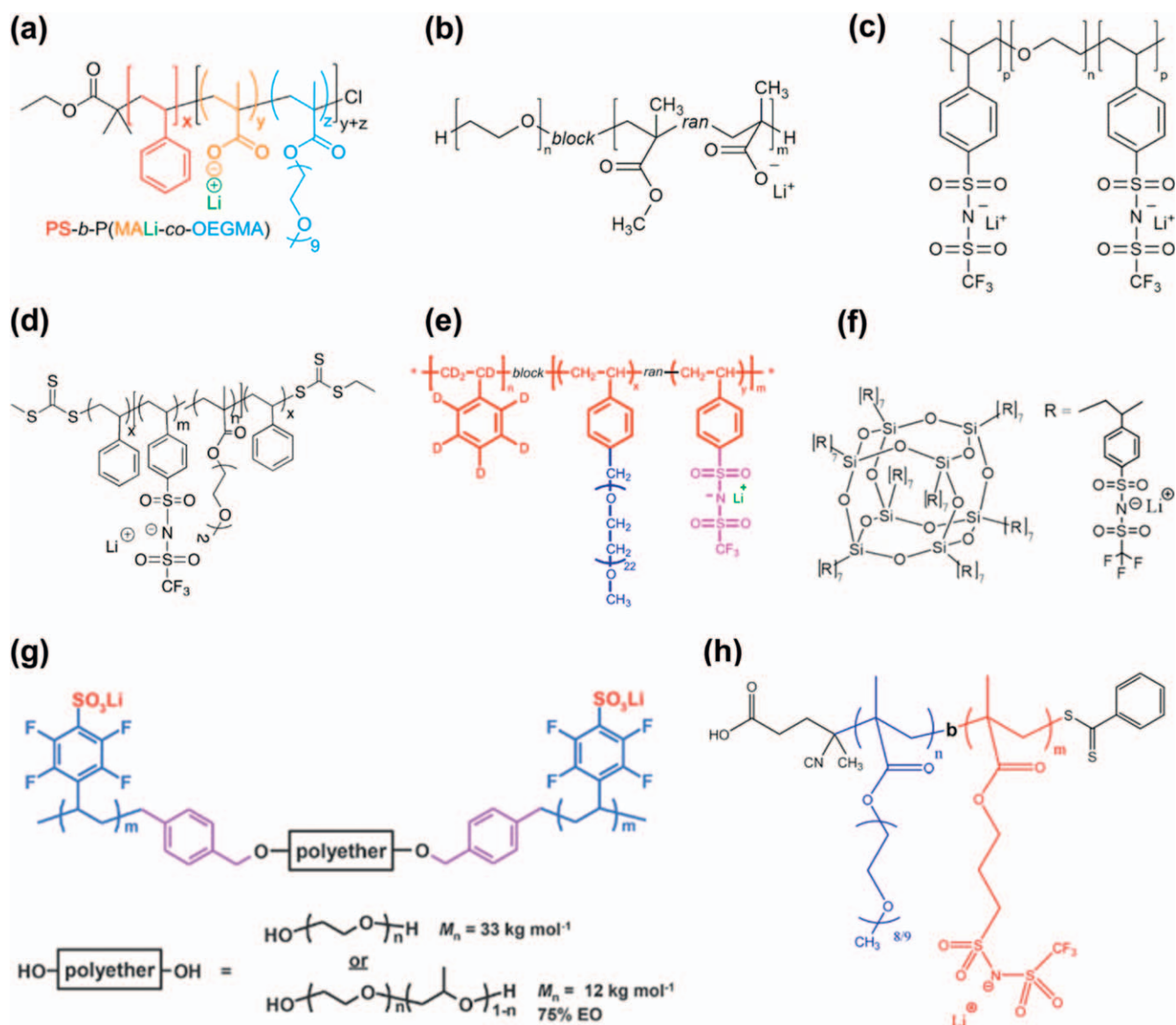


**Figure 20a.** Overview of SIC-BCPEs reported in literature: (a) ABC-type SIC-BCPE based on a PS block, a lithiated poly(methacrylic acid) block, and a POEM block. Reprinted with permission from [203], Copyright © 2015 Elsevier Ltd. All rights reserved. (b) Partially hydrolyzed and subsequently lithiated PEO-*b*-PMMA, i.e. PEO-*b*-(PMMA-*r*-PMAALi), as reported by Kofinas and co-workers [204]. (c) BAB-type SIC-BCPE architecture based on a conventional PEO-block surrounded by ionic P(STFSILi) blocks, as developed by Bouchet *et al* [207]. (d) ABCA-type BCPE obtained by RAFT polymerization, containing a P(STFSILi) block surrounded by PS and PEO blocks. Reprinted with permission from [208]. Copyright 2015 American Chemical Society. (e) Randomly copolymerized BCPE system consisting of P(STFSILi) and PEO-modified PS units as well as deuterated PS. Reprinted with permission from [209]. Copyright 2018 American Chemical Society. (f) Silsesquioxane cage with attached short chains of P(STFSILi), which had been used as ‘lithium salt’ in SEO-type BCPs, enabling a very high Li<sup>+</sup> transference number of 0.98. Reprinted with permission from [210]. Copyright 2017 American Chemical Society. (g) ABA triblock copolymer with a polyether mid-block flanked by two blocks of perfluorinated PS modified with a lithium sulfonate function. Reproduced from [211] with permission of The Royal Society of Chemistry. (h) SIC-BCPE architecture based on a POEM block and a block containing LiTFSI moieties covalently connected to a poly(methacrylate) backbone P(MTFSILi), i.e. POEM-*b*-P(MTFSILi). Reprinted with permission from [212]. Copyright 2016 American Chemical Society. (i) Copolymerization of a lithiated poly(arylene ether) monomer with PEO chains, yielding a linear SIC-BCPE with the ionic function integrated in the polymer chain. Reprinted with permission from [213], © 2018 Elsevier B.V. All rights reserved. (j) Chemical structure of poly(ethylene)-*b*-poly(acrylic lithium (fluoro sulfonyl) imide) as SIC-BCPE with self-healing properties. (k) SIC-BCPE based on PEO blocks and lithium disulfonyl imide moieties as ionic function. Reproduced from [214] with permission of The Royal Society of Chemistry. (l) Ionic BCPE based on two partially lithiated blocks of poly(acrylic acid) flanking a PMMA mid-block to which an IL was added. Reprinted from [215], © 2017 Elsevier B.V. All rights reserved. (m) Multiblock copolymer consisting of poly(arylene ether) blocks with TFSI-like side chains attached to the polymer backbone and partially perfluorinated structural blocks. Reproduced from [216] with permission of The Royal Society of Chemistry.

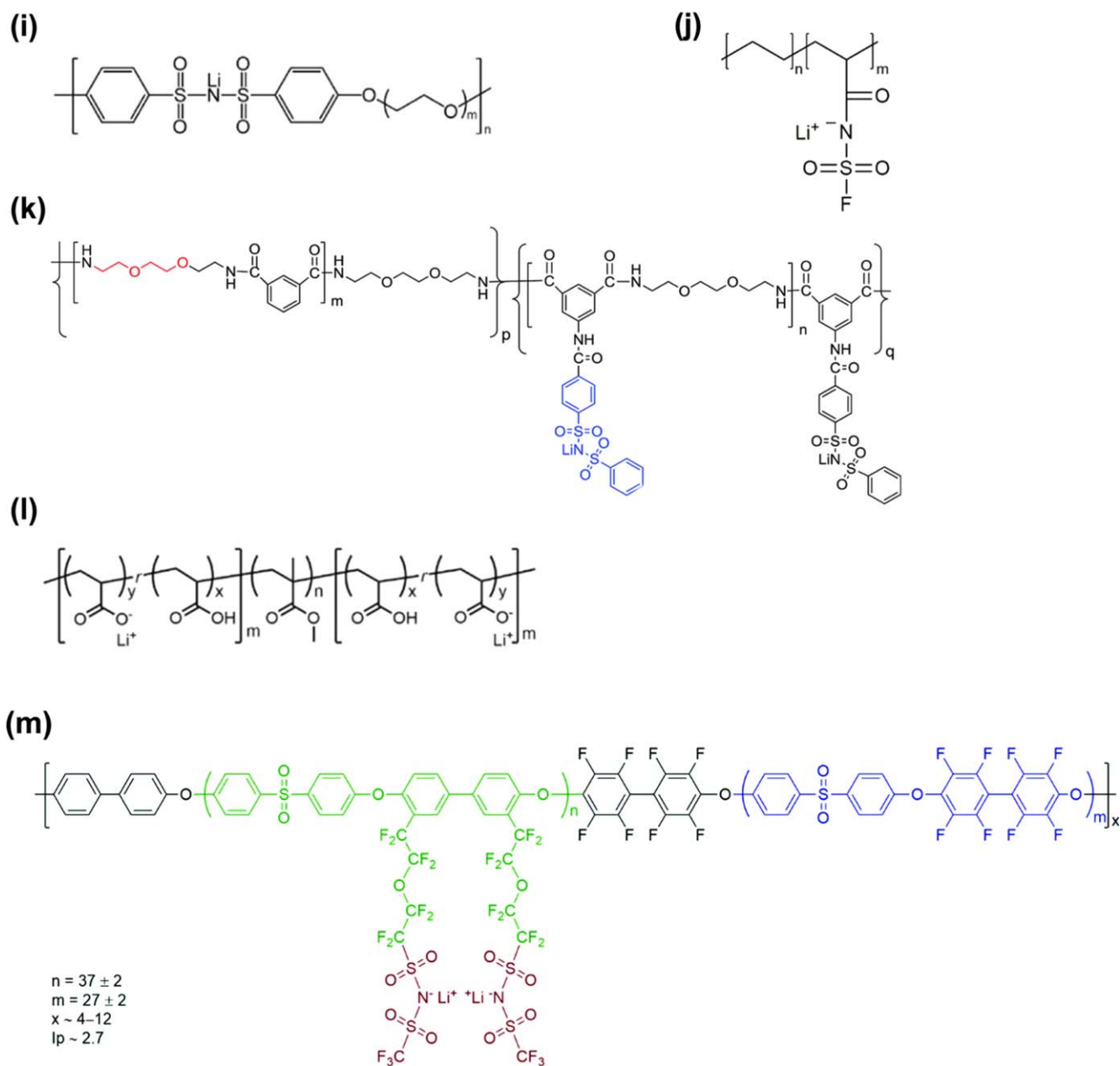
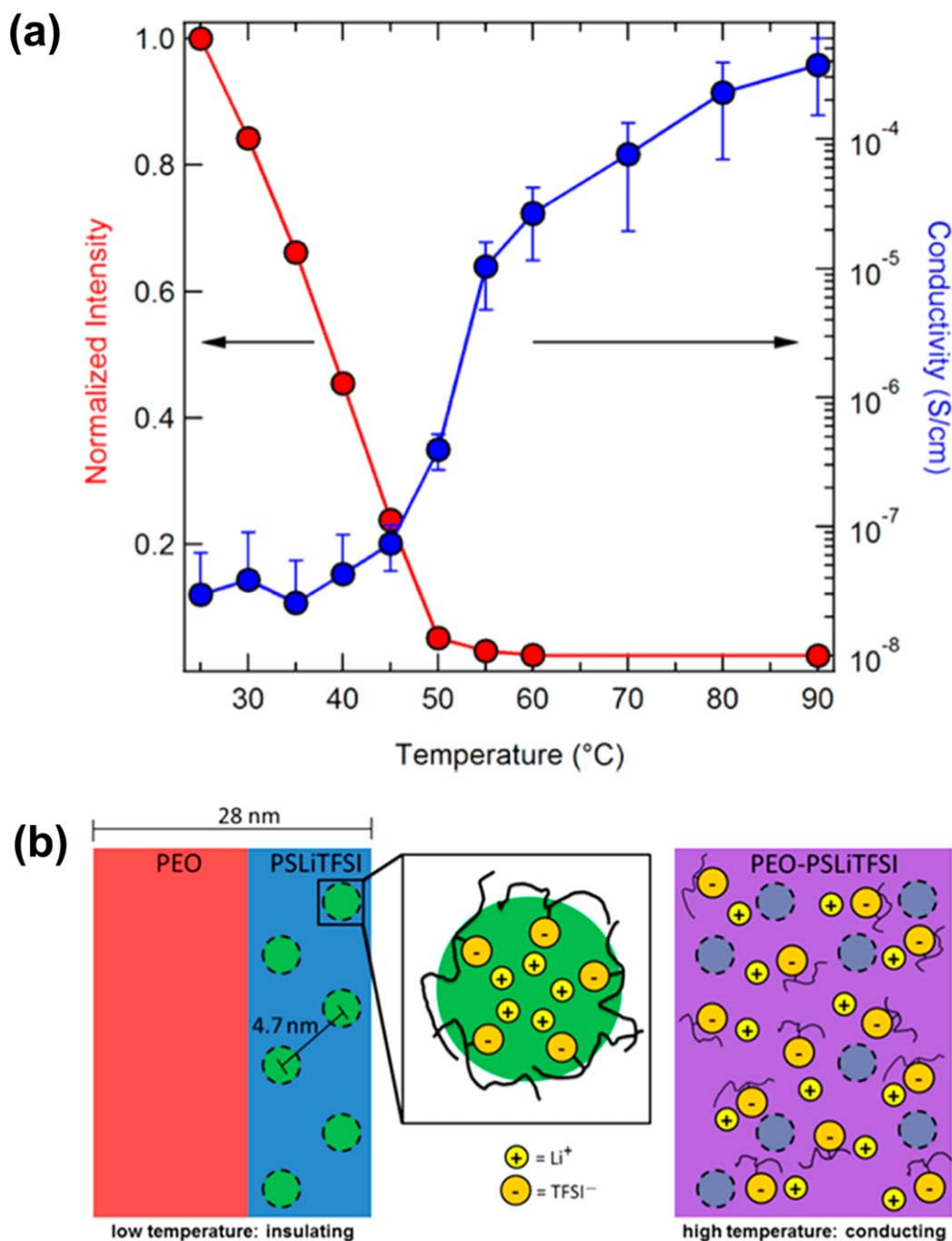


Figure 20b. (Continued.)

Shao and Jannasch [211] reported a sulfonate-type ionic moiety for the synthesis of a BAB-type triblock copolymer employing the ATRP method, which was composed of a PEO or PEO-co-PPO mid-block surrounded by two blocks of poly(lithium 2, 3, 5, 6-tetrafluorostyrene-4-sulfonate) (PPFSLi) (see figure 20(g)). Their investigation displayed a similar morphology-conductivity relationship, as proposed earlier by Balsara and co-workers [219] and the recorded ionic conductivity values were in good agreement with earlier reports on SIC-BCPEs employing a TFSI-type ionic function. This finding is noteworthy given the commonly lower dissociation of the sulfonate group but might be related to the electron withdrawing effect of the fluorine substituents at the attached phenyl ring. Additionally, the authors observed that the PEO mid-block was advantageous for

the ionic conductivity at elevated temperatures (i.e. at 50 °C and beyond), while the PEO-co-PPO mid-block was beneficial at lower temperatures due to the suppressed crystallization.

In 2016, Porcarelli *et al* [212] introduced a new SIC-BCPE architecture using a controlled radical polymerization technique (RAFT) and comprising the well-established POEM block and a block containing LiTFSI moieties covalently connected to a poly(methacrylate) backbone (P(MTFSILi), i.e. lithiated poly(3-sulfonyl (trifluoromethanesulfonyl)imide propyl methacrylate)), also abbreviated as POEM-*b*-P(MTFSILi) (figure 20(h)). Following the correlation of ionic conductivity and  $T_g$ , the authors observed a maximum conductivity of  $2.3 \cdot 10^6 \text{ S cm}^{-1}$  at ambient temperatures (and  $\sim 10^5 \text{ S cm}^{-1}$  at 55 °C) for the sample with the lowest volume fraction of P(MTFSILi) in relation to the constant



**Figure 21.** (a) Plot of the SAXS intensity at  $q = 0.228 \text{ nm}^{-1}$  (in red) and ionic conductivity (in blue) of the PEO-*b*-P(STFSiLi) electrolyte versus temperature ( $r = 0.088$ ). The intensity at each temperature was normalized by the measured value at 25 °C. (b) Schematic illustration of the PEO-*b*-P(STFSiLi) SIC-BCPE at low (left) and high (right) temperatures. At low temperatures, the PEO (red) and P(STFSiLi) (blue) blocks are microphase-separated and the ions are clustering (green circles) in the P(STFSiLi) domain. At high temperatures, the PEO and P(STFSiLi) blocks are mixed (purple). Consequently, the clusters are essentially dissolved (indicated by grey circles with the dashed surrounding) and the lithium cations are more mobile. Reprinted with permission from [218]. Copyright 2014 American Chemical Society.

POEM fraction with the lowest  $T_g$ . The  $t_{Li}^+$  at 0.83, suggesting that there was still a significant mobility of anionic groups. In a subsequent work, Porcarelli *et al* [221] refined the previously developed SIC-BCPE by replacing the POEM block with a PEO block, yielding ABA-type P(MTFSiLi)-*b*-PEO-*b*-P(MTFSiLi). The ionic conductivity was substantially increased to around  $10^{-4} \text{ S cm}^{-1}$  at 70 °C, and so was  $t_{Li}^+$  with 0.91. Additionally, the SIC-

BCPE allowed for the stable cycling of Li||LFP cells with C rates up to 0.5 °C.

In 2018, Devaux *et al* [222] published a direct comparison of the two ionic blocks, i.e. P(STFSiLi) and the P(MTFSiLi), in combination with a PEO block polymerized via NMPT. Using water as an environmentally friendly processing solvent, both P(STFSiLi)-*b*-PEO-*b*-P(STFSiLi) and

**Table 2.** Summary of the main characteristics of selected BCPEs discussed in section 4 and the findings reported, including the polymerization technique used for the synthesis, the ionic conductivity, additives such as salts or solvents, and the cell setup used for cycling tests (if provided).

Name	Figure	Polymerization technique	Ionic conductivity $\sigma/S\text{ cm}^{-1}$	Additive(s)	Cell setup	Reference
P(OEGMA- <i>co</i> -tBMA)- <i>b</i> -PS	20(a)	ATRP	$\sim 10^{-5}$ (20 °C)	BF <sub>3</sub>		[203]
PEO- <i>b</i> -(PMMA- <i>r</i> -PMAALi)	20(b)	Partial or full hydrolysis	$\sim 10^{-4}$ (20 °C) $\sim 10^{-3}$ (60 °C)	LiBOB		[204 206]
Lithiated poly(styrene sulfonyl(trifluoro methanesulfonyl)imide) (P(STFSiLi))	20(c)	NMP	$> 10^{-5}$ (60 °C)		Li BCPE LFP	[207, 217, 218]
PS- <i>b</i> -P(STFSiLi)- <i>b</i> -POEM- <i>b</i> -PS	20(d)	RAFT	$\sim 10^{-5}$ (20 °C)			[208]
PS(d)- <i>b</i> -P(SPEG- <i>co</i> -STFSiLi)	20(e)	NMP			Li BCPE LFP	[209]
PPFSLi- <i>b</i> -(PEO- <i>co</i> -PPO)-PPFSLi	20(g)	ATRP	$\sim 10^{-6}$ (20 °C) $\sim 10^{-5}$ (90 °C)			[211]
POEM- <i>b</i> -P(MTFSiLi)	20(h)	RAFT	$\sim 10^{-6}$ (25 °C) $> 10^{-5}$ (80 °C)		Li BCPE LFP	[212]
P(MTFSiLi)- <i>b</i> -PEO- <i>b</i> -P(MTFSiLi)		RAFT	$\ll 10^{-7}$ (25 °C) $> 10^{-4}$ (80 °C)		Li BCPE LFP	[221]
Lithium-4, 4'-difluoro bis(benzene sulfonyl) imide- <i>b</i> -PEO $> 10^{-4}$ (100 °C)	20(i)	polycondensation	$\ll 10^{-5}$ (30 °C)			
	Glass fiber reinforcement	Li BCPE LFP	[213]			
Poly(ethylene)- <i>b</i> -poly(acrylic lithium (fluoro sulfonyl) imide)	20(j)	Only side chain modification	$5.84 \cdot 10^{-4}$ (20 °C) $2.20 \cdot 10^{-3}$ (80 °C)		Li BCPE LFP	[223]
Polyamide backbone functionalized with lithium disulfonyl imide moieties	20(k)	polycondensation	$3.39 \cdot 10^{-4}$ (25 °C) $1.16 \cdot 10^{-3}$ (80 °C)	PVdF-HFP EC/PC	Li BCPE LFP	[214]
(PAA- <i>r</i> -PAALi)- <i>b</i> -PMMA- <i>b</i> -(PAA- <i>r</i> -PAAALi)	20(l)	ATRP	$> 10^{-3}$ (20 °C) (20% polymer content)	ionic liquid		[215]
Poly(arylene ether sulfone) backbone with covalently attached TFSI-like side chains	20(m)	polycondensation	$\sim 10^{-3}$ (20 °C) (65 wt% EC)	EC	Li BCPE NCM <sub>811</sub>	[216]

P(MTFSiLi)-*b*-PEO-*b*-P(MTFSiLi) revealed a lamellar morphology and the expected ODT when exceeding the melting point of the PEO domain,  $T_{m,PEO}$ , between 50 °C and 65 °C (depending on the polymer composition). Based on this observation, the authors suggested that the crystallization of the PEO block plays a decisive role in the evolution of the SIC-BCPE nanostructure. Both SIC-BCPEs showed a similar  $t_{Li}^+$  of  $0.88 \pm 0.03$  for P(STFSiLi) and  $0.84 \pm 0.03$  for P(MTFSiLi) with conductivity behavior due to the presence of the ODT, yet the conductivity of the copolymer comprising P(MTFSiLi) was higher by at least a factor of two. Interestingly, the electrochemical stability of the P(STFSiLi) containing polymer was about 0.5 V higher than the stability of the P(MTFSiLi)-based SIC-BCPE due to a lower fraction of PEO at the electrode|electrolyte interface.

Chen *et al* [213] reported a poly(arylene ether) based AB-type alternating diblock copolymer with the ionic function (lithium 4,4'-difluoro bis(benzene sulfonyl)imide) being integrated in the PEO chain (figure 20(i)). The alternating polymer architecture was intended to suppress the aggregation of the ionic groups and the EO moieties by spatially separating them, hindering the crystallization of the latter. The eventually amorphous SIC-BCPE provided an ionic conductivity of  $6.6 \cdot 10^{-6} \text{ S cm}^{-1}$  at 30 °C and  $2.2 \cdot 10^{-4} \text{ S cm}^{-1}$  at 100 °C. Nevertheless, the authors had to reinforce the polymer by including glass fibers to achieve suitable mechanical properties for the preparation of self-standing membranes; and while the electrochemical stability decreased with an increasing chain length of the PEO segment from 5.2 to 4.4 V, Li||LFP cells displayed stable cycling for 200 cycles at 0.1 °C and 40 °C with about 100 mAh  $g^{-1}$ .

A substantial increase in conductivity was reported by Ahmed *et al* [223] for a polyolefin-backbone SIC-BCPE with an FSI-like ionic function, i.e. poly(ethylene)-*b*-poly(acrylic lithium (fluoro sulfonyl) imide), as depicted in figure 20(j). After pressing the electrolyte at 90 °C, they obtained an ionic conductivity of  $5.8 \cdot 10^{-4} \text{ S cm}^{-1}$  at 25 °C. Additionally, they observed self-healing properties of their SIC-BCPE and the  $Li^+$  transference number was 0.91. Usually, such an 'ether-free' polymer backbone is considered advantageous for the electrochemical stability towards oxidation, although the authors used LFP as cathode material.

#### 4.3. SIC-BCPEs containing small molecules

Given the improved ionic conductivities of 'dry' SIC-BCPEs at ambient temperatures (and pressure), which are in part also related to the relatively low charge carrier concentration in order to maintain suitable mechanical properties, several groups introduced small (liquid) molecules into such electrolyte systems. This additional phase potentially provides different effects, such as serving as a plasticizer and/or a molecular transporter by facilitating the hopping from one anionic coordination site to another [51]. Zhang *et al* [214], for instance, achieved an ionic conductivity of  $3.4 \cdot 10^{-4} \text{ S cm}^{-1}$  at ambient temperature with a sophisticated poly (amide)-type SIC-BCPE based on the polycondensation of end-group modified PEO blocks and lithium disulfonyl imide

moieties (figure 20(k)), comprising 141 wt% of a 1:1 mixture of ethylene carbonate (EC) or propylene carbonate (PC). While a high  $t_{Li}^+$  of 0.9 was maintained in this case, the mechanical properties had to be reinforced by introducing a significant amount of poly(vinylidene difluoride-*co*-hexafluoropropylene) (PVdF-HFP). Following a different approach, Watanabe and co-workers [215] incorporated a hydrophobic IL into an ABA-type triblock BCPE (up to 30 wt% in the ion gel) based on a conventional PMMA mid-block flanked by two ion-containing blocks of partially lithiated poly(acrylic acid) (figure 20(l)) synthesized by the ATRP technique. The authors reported an excellent ionic conductivity of more than  $10^{-3} \text{ S cm}^{-1}$  at RT (in the case of a polymer content of 20 wt%). Notwithstanding, this conductivity value also includes a (presumably significant) contribution of the IL with an assumed transference number of 0.5 transferred from another electrolyte system with similar properties [224].

On the other hand, Ngyuen *et al* [216] presented a multi-block SIC-BCPE based on a poly(arylene ether sulfone) backbone synthesized by a one-pot polycondensation reaction with covalently attached TFSI-like side chains (figure 20(m)) comprising of a low amount of EC (45–65 wt% of the total membrane weight), which enabled the realization of self-standing membranes without the addition of a second (lithium-free) polymer; not least, since the EC molecules remain highly confined to the ionic domains up to a threshold of about 50 wt%. Remarkably, the increase in ionic conductivity also reflected this threshold. Up to about 50 wt% the increase is steep, then it is reduced, suggesting that the highly confined EC molecules facilitate charge transport by serving as a kind of molecular transporter or additional coordination site, while the additional 'free' EC has a more plasticizing effect. Whereas, for the highest amount of EC, an ionic conductivity of more than  $10^{-3} \text{ S cm}^{-1}$  was reported at 30 °C and the casting solvent (as a result the degree of nanophase separation) turns out to have a vital contribution to the conductivity and overpotential when cycling symmetric Li||Li cells: the more pronounced the nanostructuration, the higher the conductivity and the lower the overpotential. Due to the careful chemical design of the SIC-BCPE, the authors attained very stable cycling for Li||NCM<sub>111</sub> cells. In later studies, the possibility to cycle Li||NCM<sub>622</sub> cells [225] and Li||NCM<sub>811</sub> cells [226] with a stable capacity for several hundred cycles at different anodic cut-off voltages and temperatures even at 0 °C was shown.

An overview including the most important properties of the single-ion conducting polymer electrolytes reviewed in section 4 is provided in table 2.

## 5. Conclusions and perspective

Great progress has been achieved towards the fundamental understanding of the characteristics and thermodynamics of BCPs and BCPEs, including the incorporation of the conducting lithium salt having a key effect on the nanostructure and the phase transitions. These advancements stem from the

promising properties of this class of materials due to the potential combination of highly functional BCP components, with advantageous mechanical, chemical, and electrochemical properties. The in-depth investigation of suitable model compounds like SEO has led to insights to acquire a thorough understanding of such systems such as that (i) the Li salt is preferably dissolved in the PEO domains, (ii) the influence of the salt concentration, block composition, and molecular weight of the BCPE on phase transitions, ionic conductivity and morphology, (iii) the behavior and stability of lithium metal in contact with the BCPEs, (iv) the diffusion processes in BCPEs, and (v) the potential advantages of hybrid BCPEs. This may also be extended to single-ion conducting electrolyte systems, including suitable small molecules to enhance the Li<sup>+</sup> transport along with an improved comprehension of these systems particularly the charge transport mechanisms.

For further exploration it is of utmost importance to choose suitable model compounds, investigating these in detail physicochemically, electrochemically, and in battery cells, while the approach for the new developments is essentially the opposite, i.e. the design of new structural, conducting and/or ionic blocks, providing enhanced mechanical and electrochemical properties—especially an improved charge transport and stability towards state-of-the-art active materials. In fact, several studies have already shown that the richness of organic and polymer chemistry still provides avenues for further improvements to develop polymer-based electrolytes that satisfy all the requirements for their successful exploitation in next-generation lithium batteries. An important component lies in the design of mixed electronic and ionic conductors, which may serve as a binding and conducting matrix, e.g. in positive electrodes, while a pure ion conductor serves as the separator and protection layer for the lithium-metal electrode. Such ‘on-the-spot design’ of specific components may offer a successful strategy to address the demanding requirements of the battery industry.

Below we detail a few research guidelines that should be considered in the future study of (SIC-)BCPEs:

- The effective Li<sup>+</sup> conductivity is the sum of the local scale mobility and the long-range transport across the whole thickness of the electrolyte membrane. The target should adhere to the following criteria (i) to enhance the dissociation from the anionic function, e.g. by delocalizing the negative charge as much as possible, weakening the bonding strength, introducing ‘transporting vehicles’, and/or providing additional coordination sites for the Li<sup>+</sup> cations to move forward and (ii) to facilitate the long-range transport by, e.g. limiting/suppressing the presence of grain boundaries (especially the blocking ones) within the bulk electrolyte and/or by realizing advantageous nanostructures, such as gyroid-type 3D ionic domains (see also the work from Lin and co-workers [227] and Shen *et al* [228]). One may also keep in mind which ionic species might contribute to the overall conductivity.
- The electrochemical stability of the polymer is a critical factor. Considering the potential combination of two polymers (which will have to provide a very low or ideally negligible charge transfer resistance between each other), the polymer may not have to be stable across the entire voltage range but should be sufficiently stable towards reduction or oxidation. This might be attained by considering the polymer as a whole or by ensuring a specific orientation of one of the blocks at the given interface. We also state that the determination of the electrochemical stability with blocking electrodes such as platinum is important to ascertain the degree of maximum stability. However, claiming stabilities of up to 5 V, while observing electrolyte decomposition in, e.g. Li||NCM cells and/or achieving stable cycling solely for Li||LFP cells should be reevaluated.
- The experimental setup should be carefully considered when studying specific properties of the electrolyte: While symmetric Li||Li cells appear to be suitable for the investigation of dendritic lithium morphologies (keeping in mind also the amount of lithium being cycled), Li||LFP cells, for instance, turned out to be more effective for analyzing potential contact losses at the electrode||electrolyte interface.
- Finally, in addition to the development, exploration, and optimization of new and existing BCPEs, researchers may critically evaluate the potential scale-up and commercial use of their electrolyte systems once a certain technology readiness level has been reached. This includes also the potential recycling of the electrolyte itself and its impact on the recycling of the battery cell as a whole. In fact, such information is of utmost importance for the industry and will help to bring these systems to the market.

This is not an exhaustive list of aspects that may be acknowledged for future research studies, but we hope that they may serve as a reference point to accompany researchers and scientists on their search for enhanced (SIC-)BCPEs.

## Acknowledgments

The authors would like to thank the Federal Ministry for Education and Research (BMBF) for financial support within the FestBatt (03XP0175B) and the LISI (03XP0224D) projects. The financial support from the Helmholtz Association is also kindly acknowledged.

## Data availability statement

The data generated and/or analysed during the current study are not publicly available for legal/ethical reasons but are available from the corresponding author on reasonable request.

## ORCID iDs

Alexander Mayer  <https://orcid.org/0000-0001-9670-5053>  
Dominik Steinle  <https://orcid.org/0000-0001-8137-9646>  
Stefano Passerini  <https://orcid.org/0000-0002-6606-5304>  
Dominic Bresser  <https://orcid.org/0000-0001-6429-6048>

## References

- [1] Tarascon J M and Armand M 2010 Issues and challenges facing rechargeable lithium batteries *Materials for Sustainable Energy: A Collection of Peer-Reviewed Research and Review Articles from Nature Publishing Group* (Singapore: World Scientific) pp 171–9
- [2] Scrosati B, Hassoun J and Sun Y K 2011 Lithium-ion batteries. a look into the future *Energy Environ. Sci.* **4** 3287–95
- [3] Bresser D, Hosoi K, Howell D, Li H, Zeisel H, Amine K and Passerini S 2018 Perspectives of automotive battery R&D in China, Germany, Japan, and the USA *J. Power Sources* **382** 176–8
- [4] Armand M *et al* 2020 Lithium-ion batteries – Current state of the art and anticipated developments *J. Power Sources* **479** 228708
- [5] Cheng X-B, Zhang R, Zhao C-Z and Zhang Q 2017 Toward safe lithium metal anode in rechargeable batteries: a review *Chem. Rev.* **117** 10403–73
- [6] Lin D, Liu Y and Cui Y 2017 Reviving the lithium metal anode for high-energy batteries *Nat. Nanotechnol.* **12** 194–206
- [7] Xu K 2004 Nonaqueous liquid electrolytes for lithium-based rechargeable batteries *Chem. Rev.* **104** 4303–418
- [8] Hammami A, Raymond N and Armand M 2003 Runaway risk of forming toxic compounds *Nature* **424** 635–6
- [9] Kalhoff J, Eshetu G G, Bresser D and Passerini S 2015 Safer electrolytes for lithium-ion batteries: state of the art and perspectives *ChemSusChem* **8** 2154–75
- [10] Scrosati B and Vincent C A 2000 Polymer electrolytes: the key to lithium polymer batteries *MRS Bull.* **25** 28–30
- [11] Fenton D E, Parker J M and Wright P V 1973 Complexes of alkali metal ions with poly(ethylene oxide) *Polymer* **14** 589
- [12] Armand M, Chabagno J M and Duclot M 1978 Polymeric solid electrolytes *Extended Abstract of the 2nd Int. Meeting on Solid Electrolytes (St Andrews, Scotland)*
- [13] Armand M, Chabagno J M and Duclot M 1979 Poly-ethers as solid electrolytes ed P Vashitshta *et al Fast ion transport in Solids. Electrodes and Electrolytes* (Amsterdam: North Holland Publ.)
- [14] Mauger A, Julien C M, Goodenough J B and Zanghi K 2020 Tribute to Michel Armand: from rocking chair Li-ion to solid-state lithium batteries *J. Electrochem. Soc.* **167** 070507
- [15] Wright P V 1998 Polymer electrolytes – the early days *Electrochim. Acta* **43** 1137–43
- [16] Di Noto V, Lavina S, Giffin G A, Negro E and Scrosati B 2011 Polymer electrolytes: present, past and future *Electrochim. Acta* **57** 4–13
- [17] Ratner M A and Shriver D F 1988 Ion transport in solvent-free polymers *Chem. Rev.* **88** 109–24
- [18] Ratner M A, Johansson P and Shriver D F 2000 Polymer electrolytes: ionic transport mechanisms and relaxation coupling *MRS Bull.* **25** 31–7
- [19] Armand M 1990 Polymers with Ionic Conductivity *Adv. Mater.* **2** 278–86
- [20] Henderson W A and Passerini S 2003 Ionic conductivity in crystalline-amorphous polymer electrolytes - P(EO)<sub>6</sub>:LiX phases *Electrochem. Commun.* **5** 575–8
- [21] Owen J 1989 Ionic conductivity *Comprehensive Polymer Science and Supplements* vol 1 (Amsterdam: Elsevier) pp 669–86
- [22] Sax J and Ottino J M 1983 Modeling of transport of small molecules in polymer blends: application of effective medium theory *Polym. Eng. Sci.* **23** 165–76
- [23] Quartarone E and Mustarelli P 2011 Electrolytes for solid-state lithium rechargeable batteries: recent advances and perspectives *Chem. Soc. Rev.* **40** 2525
- [24] Vogel H 1921 Das Temperaturabhängigkeitsgesetz der Viskosität von Flüssigkeiten *Phys. Z.* **22** 645–6
- [25] Tamman G and Hesse W 1926 Die abhängigkeit der Viskosität von der temperatur bei unterkühlten flüssigkeiten *Z. Anorg. Allg. Chem.* **156** 245–57
- [26] Fulcher G S 1925 Analysis of recent measurements of the viscosity of glasses *J. Am. Ceram. Soc.* **8** 339–55
- [27] Armand M 1983 Polymer solid electrolytes-an overview *Solid State Ion.* **9–10** 745–54
- [28] Long L, Wang S, Xiao M and Meng Y 2016 Polymer electrolytes for lithium polymer batteries *J. Mater. Chem. A* **4** 10038–69
- [29] Stephan A M 2006 Review on gel polymer electrolytes for lithium batteries *Eur. Polym. J.* **42** 21–42
- [30] Croce F, Appetecchi G B, Persi L and Scrosati B 1998 Nanocomposite polymer electrolytes for lithium batteries *Nature* **394** 456–8
- [31] Ganapathibhotla L V N R and Maranas J K 2014 Interplay of surface chemistry and ion content in nanoparticle-filled solid polymer electrolytes *Macromolecules* **47** 3625–34
- [32] Wang W and Alexandridis P 2016 Composite polymer electrolytes: nanoparticles affect structure and properties *Polymers* **8** 387
- [33] Walker C W and Salomon M 2019 Improvement of ionic conductivity in plasticized PEO-based solid polymer electrolytes *J. Electrochem. Soc.* **140** 3409–12
- [34] Kim Y T and Smotkin E S 2002 The effect of plasticizers on transport and electrochemical properties of PEO-based electrolytes for lithium rechargeable batteries *Solid State Ion.* **149** 29–37
- [35] Shin J H, Henderson W A and Passerini S 2005 An elegant fix for polymer electrolytes *Electrochem. Solid-State Lett.* **8** A125
- [36] Kim G T, Appetecchi G B, Alessandrini F and Passerini S 2007 Solvent-free, PYR1ATFSI ionic liquid-based ternary polymer electrolyte systems: I. Electrochemical characterization *J. Power Sources* **171** 861–9
- [37] Kim G T, Appetecchi G B, Carewska M, Joost M, Balducci A, Winter M and Passerini S 2010 UV cross-linked, lithium-conducting ternary polymer electrolytes containing ionic liquids *J. Power Sources* **195** 6130–7
- [38] Monroe C and Newman J 2005 The impact of elastic deformation on deposition kinetics at lithium/polymer interfaces *J. Electrochem. Soc.* **152** A396
- [39] Stone G M, Mullin S A, Teran A A, Hallinan D T, Minor A M, Hexemer A and Balsara N P 2012 Resolution of the modulus versus adhesion dilemma in solid polymer electrolytes for rechargeable lithium metal batteries *J. Electrochem. Soc.* **159** A222–7
- [40] Thomas K E, Sloop S E, Kerr J B and Newman J 2000 Comparison of lithium-polymer cell performance with unity and nonunity transference numbers *J. Power Sources* **89** 132–8
- [41] Chazalviel J-N 1990 Electrochemical aspects of the generation of ramified metallic electrodeposits *Phys. Rev. A* **42** 7355–67
- [42] Brissot C, Rosso M, Chazalviel J-N, Baudry P and Lascaud S 1998 *In situ* study of dendritic growth in lithium/PEO-salt/lithium cells *Electrochim. Acta* **43** 1569–74
- [43] Brissot C, Rosso M, Chazalviel J-N and Lascaud S 1999 Dendritic growth mechanisms in lithium/polymer cells *J. Power Sources* **81–82** 925–9

- [44] Bai P, Li J, Brushett F R and Bazant M Z 2016 Transition of lithium growth mechanisms in liquid electrolytes *Energy Environ. Sci.* **9** 3221 9
- [45] Zhang H, Li C, Piszcz M, Coya E, Rojo T, Rodriguez-Martinez L M, Armand M and Zhou Z 2017 Single lithium-ion conducting solid polymer electrolytes: advances and perspectives *Chem. Soc. Rev.* **46** 797 815
- [46] Strauss E, Menkin S and Golodnitsky D 2017 On the way to high-conductivity single lithium-ion conductors *J. Solid State Electrochem.* **21** 1879 905
- [47] Park M J, Choi I, Hong J and Kim O 2013 Polymer electrolytes integrated with ionic liquids for future electrochemical devices *J. Appl. Polym. Sci.* **129** 2363 76
- [48] Liu T and Liu G 2019 Block copolymers for supercapacitors, dielectric capacitors and batteries *J. Phys. Condens. Matter* **31** 1 27
- [49] Mauger A, Julien C M, Paoletta A, Armand M and Zaghbi K 2019 Building better batteries in the solid state: a review *Materials* **12** 1 86
- [50] Choo Y, Halat D M, Villaluenga I, Timachova K and Balsara N P 2020 Diffusion and migration in polymer electrolytes *Prog. Polym. Sci.* **103** 101220
- [51] Bresser D, Lyonard S, Iojoiu C, Picard L and Passerini S 2019 Decoupling segmental relaxation and ionic conductivity for lithium-ion polymer electrolytes *Mol. Syst. Des. Eng.* **4** 779 92
- [52] Bocharova V and Sokolov A P 2020 Perspectives for polymer electrolytes: a view from fundamentals of ionic conductivity *Macromolecules* **53** 4141 57
- [53] Mong A L, Shi Q X, Jeon H, Ye Y S, Xie X L and Kim D 2021 Tough and flexible, super ion-conductive electrolyte membranes for lithium-based secondary battery applications *Adv. Funct. Mater.* **31** 1 47
- [54] Wang J, Li S, Zhao Q, Song C and Xue Z 2021 Structure code for advanced polymer electrolyte in lithium-ion batteries *Adv. Funct. Mater.* **31** 1 35
- [55] Xi G, Xiao M, Wang S, Han D, Li Y and Meng Y 2021 Polymer-based solid electrolytes: material selection, design, and application *Adv. Funct. Mater.* **31** 1 28
- [56] Hallinan D T and Balsara N P 2013 Polymer electrolytes *Annu. Rev. Mater. Res.* **43** 503 25
- [57] Young W S, Kuan W F and Epps T H 2014 Block copolymer electrolytes for rechargeable lithium batteries *J. Polym. Sci. B* **52** 1 16
- [58] Xue Z, He D and Xie X 2015 Poly(ethylene oxide)-based electrolytes for lithium-ion batteries *J. Mater. Chem. A* **3** 19218 53
- [59] Zhang Q, Liu K, Ding F and Liu X 2017 Recent advances in solid polymer electrolytes for lithium batteries *Nano Res.* **10** 4139 74
- [60] Mindemark J, Lacey M J, Bowden T and Brandell D 2018 Beyond PEO alternative host materials for Li<sup>+</sup> conducting solid polymer electrolytes *Prog. Polym. Sci.* **81** 114 43
- [61] Phan T N T, Issa S and Gigmes D 2019 Poly(ethylene oxide)-based block copolymer electrolytes for lithium metal batteries *Polym. Int.* **68** 7 13
- [62] Hallinan D T, Villaluenga I and Balsara N P 2018 Polymer and composite electrolytes *MRS Bull.* **43** 775 81
- [63] Tieke B 2014 *Makromolekulare Chemie* (Weinheim: Wiley-VCH)
- [64] Feng H, Lu X, Wang W, Kang N-G and Mays J 2017 Block copolymers: synthesis, self-assembly, and applications *Polymers* **9** 494
- [65] Koltzenburg S, Maskos M and Nuyken O 2014 *Polymere* (Berlin: Springer)
- [66] Stevens M P 1999 *Polymer Chemistry An Introduction* 3rd edn (Oxford: Oxford University Press)
- [67] Flory P J 1942 Thermodynamics of high polymer solutions *J. Chem. Phys.* **10** 51 61
- [68] Huggins M L 1942 Some properties of solutions of long-chain compounds *J. Phys. Chem.* **46** 151 8
- [69] Huggins M L 1942 Theory of solutions of high polymers I *J. Am. Chem. Soc.* **64** 1712 9
- [70] Manias E and Utracki L A 2014 *Polymer Blends Handbook* ed L A Utracki and C A Wilkie (Dordrecht: Springer Netherlands)
- [71] Bates F S 1991 Polymer-polymer phase behavior *Science* **252** 898 905
- [72] Bates F S and Fredrickson G H 1990 Block copolymer thermodynamics: theory and experiment *Annu. Rev. Phys. Chem.* **41** 525 57
- [73] Leibler L 1980 Theory of microphase separation in block copolymers *Macromolecules* **13** 1602 17
- [74] Fredrickson G H and Helfand E 1987 Fluctuation effects in the theory of microphase separation in block copolymers *J. Chem. Phys.* **87** 697 705
- [75] Bates F S and Fredrickson G H 1999 Block copolymers designer soft materials *Phys. Today* **52** 32 8
- [76] Matsen M W and Schick M 1994 Stable and unstable phases of a diblock copolymer melt *Phys. Rev. Lett.* **72** 2660 3
- [77] Matsen M W 2012 Effect of architecture on the phase behavior of AB-type block copolymer melts *Macromolecules* **45** 2161 5
- [78] Darling S B 2007 Directing the self-assembly of block copolymers *Prog. Polym. Sci.* **32** 1152 204
- [79] Matsen M W and Schick M 1994 Microphase separation in starblock copolymer melts *Macromolecules* **27** 6761 7
- [80] Tyler C A, Qin J, Bates F S and Morse D C 2007 SCFT study of nonfrustrated ABC triblock copolymer melts *Macromolecules* **40** 4654 68
- [81] Rasmussen K O, Lookman T, Kober E M and Saxena A 2003 Morphology and bridging properties of (AB)<sub>n</sub> multiblock copolymers *J. Polym. Sci. B: Polym. Phys.* **41** 104 11
- [82] Matsen M W and Schick M 1994 Stable and unstable phases of a linear multiblock copolymer melt *Macromolecules* **27** 7157 63
- [83] Kavassalis T A and Whitmore M D 1991 On the theory of linear multiblock copolymers *Macromolecules* **24** 5340 5
- [84] Spontak R J and Smith S D 2001 Perfectly-alternating linear (AB)<sub>n</sub> multiblock copolymers: effect of molecular design on morphology and properties *J. Polym. Sci. B* **39** 947 55
- [85] Villaluenga I, Chen X C, Devaux D, Hallinan D T and Balsara N P 2015 Nanoparticle-driven assembly of highly conducting hybrid block copolymer electrolytes *Macromolecules* **48** 358 64
- [86] Gunkel I and Thurn-Albrecht T 2012 Thermodynamic and structural changes in ion-containing symmetric diblock copolymers: a small-angle x-ray scattering study *Macromolecules* **45** 283 91
- [87] Young W S and Epps T H 2009 Salt doping in PEO-containing block copolymers: counterion and concentration effects *Macromolecules* **42** 2672 8
- [88] Gwee L, Choi J H, Winey K I and Elabd Y A 2010 Block copolymer/ionic liquid films: the effect of ionic liquid composition on morphology and ion conduction *Polymer* **51** 5516 24
- [89] Nishi Y 2000 Lithium ion secondary battery technologies, present and future *Macromol. Symp.* **156** 187 94
- [90] Scrosati B 2011 History of lithium batteries *J. Solid State Electrochem.* **15** 1623 30
- [91] Wagner R, Preschitschek N, Passerini S, Leker J and Winter M 2013 Current research trends and prospects among the various materials and designs used in lithium-based batteries *J. Appl. Electrochem.* **43** 481 96

- [92] Giles J R M, Gray F M, MacCallum J R and Vincent C A 1987 Synthesis and characterization of ABA block copolymer-based polymer electrolytes *Polymer* **28** 1977 81
- [93] Gray F M, MacCallum J R, Vincent C A and Giles J R M 1988 Novel polymer electrolytes based on ABA block copolymers *Macromolecules* **21** 392 7
- [94] Khan I, Fish D, Delaviz Y and Smid J 1989 ABA triblock comb copolymers with oligo(oxyethylene) side chains as matrix for ion transport *Makromol. Chem.* **190** 1069 78
- [95] Melchioris M, Keul H and Höcker H 1996 Preparation and properties of solid electrolytes on the basis of alkali metal salts and poly(2, 2-dimethyltrimethylene carbonate)-block-poly(ethylene oxide)-block-poly(2, 2-dimethyltrimethylene carbonate) *Polymer* **37** 1519 27
- [96] Saunier J, Alloin F and Sanchez J Y 2000 Electrochemical and spectroscopic studies of polymethacrylonitrile based electrolytes *Electrochim. Acta* **45** 1255 63
- [97] Jannasch P 2002 Ionic conductivity in physical networks of polyethylene-polyether-polyethylene triblock copolymers *Chem. Mater.* **14** 2718 24
- [98] Jankova K, Jannasch P and Hvilsted S 2004 Ion conducting solid polymer electrolytes based on polypentafluorostyrene-b-polyether-b-polypentafluorostyrene prepared by atom transfer radical polymerization *J. Mater. Chem.* **14** 2902 8
- [99] Spiegel E F, Adamic K J, Williams B D and Sammells A F 2000 Solvation of lithium salts within single-phase dimethyl siloxane bisphenol-a carbonate block copolymer *Polymer* **41** 3365 9
- [100] Ionescu-Vasii L L, Garcia B and Armand M 2006 Conductivities of electrolytes based on PEI-b-PEO-b-PEI triblock copolymers with lithium and copper TFSI salts *Solid State Ion.* **177** 885 92
- [101] Soo P P, Huang B, Jang Y I I, Chiang Y M, Sadoway D R and Mayes A M 1999 Rubbery block copolymer electrolytes for solid-state rechargeable lithium batteries *J. Electrochem. Soc.* **146** 32 7
- [102] Huang B, Cook C C, Mui S, Soo P P, Staelin D H, Mayes A M and Sadoway D R 2001 High energy density, thin-film, rechargeable lithium batteries for marine field operations *J. Power Sources* **97-98** 674 6
- [103] Ruzette A-V G, Soo P P, Sadoway D R and Mayes A M 2001 Melt-formable block copolymer electrolytes for lithium rechargeable batteries *J. Electrochem. Soc.* **148** A537
- [104] Harris D J, Bonagamba T J, Schmidt-Rohr K, Soo P P, Sadoway D R and Mayes A M 2002 Solid-state NMR investigation of block copolymer electrolyte dynamics *Macromolecules* **35** 3772 4
- [105] Trapa P E, Huang B, Won Y Y, Sadoway D R and Mayes A M 2002 Block copolymer electrolytes synthesized by atom transfer radical polymerization for solid-state, thin-film lithium batteries *Electrochem. Solid-State Lett.* **5** A85
- [106] Mui S C *et al* 2002 Block copolymer-templated nanocomposite electrodes for rechargeable lithium batteries *J. Electrochem. Soc.* **149** A1610
- [107] Niitani T, Shimada M, Kawamura K and Kanamura K 2005 Characteristics of new-type solid polymer electrolyte controlling nano-structure *J. Power Sources* **146** 386 90
- [108] Niitani T, Shimada M, Kawamura K, Dokko K, Rho Y-H and Kanamura K 2005 Synthesis of Li<sup>+</sup> ion conductive PEO-PS block copolymer electrolyte with microphase separation structure *Electrochem. Solid-State Lett.* **8** A385 8
- [109] Nakano H, Dokko K, Sugaya J Ichi, Yasukawa T, Matsue T and Kanamura K 2007 All-solid-state micro lithium-ion batteries fabricated by using dry polymer electrolyte with micro-phase separation structure *Electrochem. Commun.* **9** 2013 7
- [110] Rolland J, Brassine J, Bourgeois J P, Poggi E, Vlad A and Gohy J F 2014 Chemically anchored liquid-PEO based block copolymer electrolytes for solid-state lithium-ion batteries *J. Mater. Chem. A* **2** 11839 46
- [111] Khandpur A K, Förster S, Bates F S, Hamley I W, Ryan A J, Bras W, Almdal K and Mortensen K 1995 Polyisoprene-polystyrene diblock copolymer phase diagram near the order-disorder transition *Macromolecules* **28** 8796 806
- [112] Dair B J, Honeker c.c., Alward D B, Avgeropoulos A, Hadjichristidis N, Fetters L J, Capel M and Thomas E L 1999 Mechanical properties and deformation behavior of the double gyroid phase in unoriented thermoplastic elastomers *Macromolecules* **32** 8145 52
- [113] Cochran E W, Morse D C and Bates F S 2003 Design of ABC triblock copolymers near the ODT with the random phase approximation *Macromolecules* **36** 782 92
- [114] Epps T H, Bailey T S, Waletzko R and Bates F S 2003 Phase behavior and block sequence effects in lithium perchlorate-doped poly(isoprene-b-styrene-b-ethylene oxide) and poly(styrene-b-isoprene-b-ethylene oxide) triblock copolymers *Macromolecules* **36** 2873 81
- [115] Young W S, Brigandi P J and Epps T H 2008 Crystallization-induced lamellar-to-lamellar thermal transition in salt-containing block copolymer electrolytes *Macromolecules* **41** 6276 9
- [116] Young W S, Albert J N L, Schantz A B and Epps T H 2011 Mixed-salt effects on the ionic conductivity of lithium-doped PEO-containing block copolymers *Macromolecules* **44** 8116 23
- [117] Young W S and Epps T H 2012 Ionic conductivities of block copolymer electrolytes with various conducting pathways: Sample preparation and processing considerations *Macromolecules* **45** 4689 97
- [118] Morris M A, Sung S H, Ketkar P M, Dura J A, Nieuwendaal R C and Epps T H 2019 Enhanced conductivity via homopolymer-rich pathways in block polymer-blended electrolytes *Macromolecules* **52** 9682 92
- [119] Wang J Y, Xu T, Leiston-Belanger J M, Gupta S and Russell T P 2006 Ion complexation: a route to enhanced block copolymer alignment with electric fields *Phys. Rev. Lett.* **96** 1 4
- [120] Wang J Y, Chen W and Russell T P 2008 Ion-complexation-induced changes in the interaction parameter and the chain conformation of PS-b-PMMA copolymers *Macromolecules* **41** 4904 7
- [121] Kim S H, Misner M J, Yang L, Gang O, Ocko B M and Russell T P 2006 Salt complexation in block copolymer thin films *Macromolecules* **39** 8473 9
- [122] Quirk R P, Kim J, Kausch C and Chun M 1996 Butyllithium-initiated anionic synthesis of well-defined poly(styrene-block-ethylene oxide) block copolymers with potassium salt additives *Polym. Int.* **39** 3 10
- [123] Hadjichristidis N, Iatrou H, Pispas S and Pitsikalis M 2000 Anionic polymerization: high vacuum techniques *J. Polym. Sci. A* **38** 3211 34
- [124] Singh M *et al* 2007 Effect of molecular weight on the mechanical and electrical properties of block copolymer electrolytes *Macromolecules* **40** 4578 85
- [125] Ganesan V, Pyramitsyn V, Bertoni C and Shah M 2012 Mechanisms underlying ion transport in lamellar block copolymer membranes *ACS Macro Lett.* **1** 513 8
- [126] Sethuraman V, Mogurampelly S and Ganesan V 2017 Ion transport mechanisms in lamellar phases of salt-doped PS-PEO block copolymer electrolytes *Soft Matter* **13** 7793 803
- [127] Bouchet R, Phan T N T, Beaudoin E, Devaux D, Davidson P, Bertin D and Denoyel R 2014 Charge transport in nanostructured PS-PEO-PS triblock copolymer electrolytes *Macromolecules* **47** 2659 65
- [128] Gomez E D *et al* 2009 Effect of ion distribution on conductivity of block copolymer electrolytes *Nano Lett.* **9** 1212 6

- [129] Allen F I, Watanabe M, Lee Z, Balsara N P and Minor A M 2011 Chemical mapping of a block copolymer electrolyte by low-loss EFTEM spectrum-imaging and principal component analysis *Ultramicroscopy* **111** 239 44
- [130] Panday A, Mullin S, Gomez E D, Wanakule N, Chen V L, Hexemer A, Pople J and Balsara N P 2009 Effect of molecular weight and salt concentration on conductivity of block copolymer electrolytes *Macromolecules* **42** 4632 7
- [131] Thelen J L, Wang A A, Chen X C, Jiang X, Schaible E and Balsara N P 2018 Correlations between salt-induced crystallization, morphology, segmental dynamics, and conductivity in amorphous block copolymer electrolytes *Macromolecules* **51** 1733 40
- [132] Wanakule N S, Virgili J M, Teran A A, Wang Z G and Balsara N P 2010 Thermodynamic properties of block copolymer electrolytes containing imidazolium and lithium salts *Macromolecules* **43** 8282 9
- [133] Yuan R, Teran A A, Gurevitch I, Mullin S A, Wanakule N S and Balsara N P 2013 Ionic conductivity of low molecular weight block copolymer electrolytes *Macromolecules* **46** 914 21
- [134] Godovsky Y K, Slonimsky G L and Garbar N M 1972 Effect of molecular weight on the crystallization and morphology of poly(ethylene oxide) fractions *J. Polym. Sci. C* **38** 1 21
- [135] Cheng S Z D, Bu H S and Wunderlich B 1988 Double lamellae of low-molecular-mass fractions of poly(ethylene oxide) crystallized from the melt *Polymer* **29** 579 83
- [136] Teran A A and Balsara N P 2014 Thermodynamics of block copolymers with and without salt *J. Phys. Chem. B* **118** 4 17
- [137] Wanakule N S, Panday A, Mullin S A, Gann E, Hexemer A and Balsara N P 2009 Ionic conductivity of block copolymer electrolytes in the vicinity of order-disorder and order-order transitions *Macromolecules* **42** 5642 51
- [138] Teran A A, Mullin S A, Hallinan D T and Balsara N P 2012 Discontinuous changes in ionic conductivity of a block copolymer electrolyte through an order-disorder transition *ACS Macro Lett.* **1** 305 9
- [139] Thelen J L, Teran A A, Wang X, Garetz B A, Nakamura I, Wang Z G and Balsara N P 2014 Phase behavior of a block copolymer/salt mixture through the order-to-disorder transition *Macromolecules* **47** 2666 73
- [140] Nakamura I, Balsara N P and Wang Z G 2013 First-order disordered-to-lamellar phase transition in lithium salt-doped block copolymers *ACS Macro Lett.* **2** 478 81
- [141] Chintapalli M, Chen X C, Thelen J L, Teran A A, Wang X, Garetz B A and Balsara N P 2014 Effect of grain size on the ionic conductivity of a block copolymer electrolyte *Macromolecules* **47** 5424 31
- [142] Wang X, Thelen J L, Teran A A, Chintapalli M, Nakamura I, Wang Z G, Newstein M C, Balsara N P and Garetz B A 2014 Evolution of grain structure during disorder-to-order transitions in a block copolymer/salt mixture studied by depolarized light scattering *Macromolecules* **47** 5784 92
- [143] Loo W S, Jiang X, Maslyn J A, Oh H J, Zhu C, Downing K H and Balsara N P 2018 Reentrant phase behavior and coexistence in asymmetric block copolymer electrolytes *Soft Matter* **14** 2789 95
- [144] Loo W S *et al* 2018 Phase Behavior of mixtures of block copolymers and a lithium salt *J. Phys. Chem. B* **122** 8065 74
- [145] Mullin S A, Stone G M, Panday A and Balsara N P 2011 Salt diffusion coefficients in block copolymer electrolytes *J. Electrochem. Soc.* **158** A619
- [146] Timachova K, Villaluenga I, Cirrincione L, Gobet M, Bhattacharya R, Jiang X, Newman J, Madsen L A, Greenbaum S G and Balsara N P 2018 Anisotropic ion diffusion and electrochemically driven transport in nanostructured block copolymer electrolytes *J. Phys. Chem. B* **122** 1537 44
- [147] Loo W S, Faraone A, Grundy L S, Gao K W and Balsara N P 2020 Polymer dynamics in block copolymer electrolytes detected by neutron spin echo *ACS Macro Lett.* **9** 639 45
- [148] Maslyn J A, Loo W S, McEntush K D, Oh H J, Harry K J, Parkinson D Y and Balsara N P 2018 Growth of lithium dendrites and globules through a solid block copolymer electrolyte as a function of current density *J. Phys. Chem. C* **122** 26797 804
- [149] Xu C, Ahmad Z, Aryanfar A, Viswanathan V and Greer J R 2017 Enhanced strength and temperature dependence of mechanical properties of Li at small scales and its implications for Li metal anodes *Proc. Natl. Acad. Sci. USA* **114** 57 61
- [150] Herbert E G, Hackney S A, Dudney N J and Sudharshan Phani P 2018 Nanoindentation of high-purity vapor deposited lithium films: The elastic modulus *J. Mater. Res.* **33** 1335 46
- [151] Harry K J, Higa K, Srinivasan V and Balsara N P 2016 Influence of electrolyte modulus on the local current density at a dendrite tip on a lithium metal electrode *J. Electrochem. Soc.* **163** A2216 24
- [152] Hallinan D T, Mullin S A, Stone G M and Balsara N P 2013 Lithium metal stability in batteries with block copolymer electrolytes *J. Electrochem. Soc.* **160** A464 70
- [153] Devaux D, Harry K J, Parkinson D Y, Yuan R, Hallinan D T, MacDowell A A and Balsara N P 2015 Failure mode of lithium metal batteries with a block copolymer electrolyte analyzed by x-ray microtomography *J. Electrochem. Soc.* **162** A1301 9
- [154] Schausser N S, Harry K J, Parkinson D Y, Watanabe H and Balsara N P 2015 Lithium dendrite growth in glassy and rubbery nanostructured block copolymer electrolytes *J. Electrochem. Soc.* **162** A398 405
- [155] Harry K J, Hallinan D T, Parkinson D Y, MacDowell A A and Balsara N P 2014 Detection of subsurface structures underneath dendrites formed on cycled lithium metal electrodes *Nat. Mater.* **13** 69 73
- [156] Harry K J, Liao X, Parkinson D Y, Minor A M and Balsara N P 2015 Electrochemical deposition and stripping behavior of lithium metal across a rigid block copolymer electrolyte membrane *J. Electrochem. Soc.* **162** A2699 706
- [157] Maslyn J A, Frenck L, Loo W S, Parkinson D Y and Balsara N P 2019 Extended cycling through rigid block copolymer electrolytes enabled by reducing impurities in lithium metal electrodes *ACS Appl. Energy Mater.* **2** 8197 206
- [158] Frenck L, Maslyn J A, Loo W S, Parkinson D Y and Balsara N P 2019 Impact of salt concentration on nonuniform lithium electrodeposition through rigid block copolymer electrolytes *ACS Appl. Mater. Interfaces* **11** 47878 85
- [159] Ganser M, Hildebrand F E, McMeeking R M and Kamlah M 2020 Stiffer is not necessarily better: requirements analysis for binary solid polymer electrolytes that ensure stable lithium metal electrodes *J. Electrochem. Soc.* **167** 130525
- [160] Choi I, Ahn H and Park M J 2011 Enhanced performance in lithium-polymer batteries using surface-functionalized Si nanoparticle anodes and self-assembled block copolymer electrolytes *Macromolecules* **44** 7327 34
- [161] Jo G, Ahn H and Park M J 2013 Simple route for tuning the morphology and conductivity of polymer electrolytes: One end functional group is enough *ACS Macro Lett.* **2** 990 5
- [162] Jo G, Kim O, Kim H, Hyeok Choi U, Lee S B and Jeong Park M 2016 End-functionalized block copolymer electrolytes: Effect of segregation strength on ion transport efficiency *Polym. J.* **48** 465 72

- [163] Beaudoin E, Phan T N T, Robinet M, Denoyel R, Davidson P, Bertin D and Bouchet R 2013 Effect of interfaces on the melting of PEO confined in triblock PS-b-PEO-b-PS copolymers *Langmuir* **29** 10874–80
- [164] Devaux D, Glé D, Phan T N T, Gignes D, Giroud E, Deschamps M, Denoyel R and Bouchet R 2015 Optimization of block copolymer electrolytes for lithium metal batteries *Chem. Mater.* **27** 4682–92
- [165] Lassagne A, Beaudoin E, Ferrand A, Phan T N T, Davidson P, Iojoiu C and Bouchet R 2017 New approach to design solid block copolymer electrolytes for 40 °C lithium metal battery operation *Electrochim. Acta* **238** 21–9
- [166] Zhang B *et al* 2019 Synthesis and interface stability of polystyrene-poly(ethylene glycol)-polystyrene triblock copolymer as solid-state electrolyte for lithium-metal batteries *J. Power Sources* **428** 93–104
- [167] Warren S C, DiSalvo F J and Wiesner U 2007 Nanoparticle-tuned assembly and disassembly of mesostructured silica hybrids *Nat. Mater.* **6** 156–61
- [168] Lin Y, Daga V K, Anderson E R, Gido S P and Watkins J J 2011 Nanoparticle-driven assembly of block copolymers: a simple route to ordered hybrid materials *J. Am. Chem. Soc.* **133** 6513–6
- [169] Gurevitch I, Buonsanti R, Teran A A, Gludovatz B, Ritchie R O, Cabana J and Balsara N P 2013 Nanocomposites of titanium dioxide and polystyrene-poly(ethylene oxide) block copolymer as solid-state electrolytes for lithium metal batteries *J. Electrochem. Soc.* **160** A1611–7
- [170] Kim S K, Kim D G, Lee A, Sohn H S, Wie J J, Nguyen N A, MacKay M E and Lee J C 2012 Organic/inorganic hybrid block copolymer electrolytes with nanoscale ion-conducting channels for lithium ion batteries *Macromolecules* **45** 9347–56
- [171] Sethi G K, Jiang X, Chakraborty R, Loo W S, Villaluenga I and Balsara N P 2018 Anomalous Self-Assembly and Ion Transport in Nanostructured Organic-Inorganic Solid Electrolytes *ACS Macro Lett.* **7** 1056–61
- [172] Timachova K, Sethi G K, Bhattacharya R, Villaluenga I and Balsara N P 2019 Ion diffusion across a disorder-to-order phase transition in a poly(ethylene oxide)-b-poly(silsesquioxane) block copolymer electrolyte *Mol. Syst. Des. Eng.* **4** 357–64
- [173] Gao K W, Jiang X, Hoffman Z J, Sethi G K, Chakraborty S, Villaluenga I and Balsara N P 2020 Optimizing the monomer structure of polyhedral oligomeric silsesquioxane for ion transport in hybrid organic inorganic block copolymers *J. Polym. Sci.* **58** 363–71
- [174] Chakraborty S, Jiang X, Ho Z J, Sethi G K, Zhu C and Balsara N P 2020 Reversible changes in the grain structure and conductivity in a block copolymer electrolyte *Macromolecules* **53** 5455–64
- [175] Young N P, Devaux D, Khurana R, Coates G W and Balsara N P 2014 Investigating polypropylene-poly(ethylene oxide)-polypropylene triblock copolymers as solid polymer electrolytes for lithium batteries *Solid State Ion.* **263** 87–94
- [176] Sun J, Liao X, Minor A M, Balsara N P and Zuckermann R N 2014 Morphology-conductivity relationship in crystalline and amorphous sequence-defined peptoid block copolymer electrolytes *J. Am. Chem. Soc.* **136** 14990–7
- [177] Bergfelt A, Lacey M J, Hedman J, Sångeland C, Brandell D and Bowden T 2018  $\epsilon$ -Caprolactone-based solid polymer electrolytes for lithium-ion batteries: synthesis, electrochemical characterization and mechanical stabilization by block copolymerization *RSC Adv.* **8** 16716–25
- [178] Bergfelt A, Hernández G, Mogensen R, Lacey M J, Mindemark J, Brandell D and Bowden T M 2020 Mechanically robust yet highly conductive diblock copolymer solid polymer electrolyte for ambient temperature battery applications *ACS Appl. Polym. Mater.* **2** 939–48
- [179] Aldalur I, Martínez-Ibañez M, Piszcz M, Zhang H and Armand M 2018 Self-standing highly conductive solid electrolytes based on block copolymers for rechargeable all-solid-state lithium-metal batteries *Batter. Supercaps* **1** 149–59
- [180] Dörr T S, Pelz A, Zhang P, Kraus T, Winter M and Wiemhöfer H D 2018 An ambient temperature electrolyte with superior lithium ion conductivity based on a self-assembled block copolymer *Chem. Eur. J.* **24** 8061–5
- [181] Pelz A, Dörr T S, Zhang P, De Oliveira P W, Winter M, Wiemhöfer H D and Kraus T 2019 Self-assembled block copolymer electrolytes: enabling superior ambient cationic conductivity and electrochemical stability *Chem. Mater.* **31** 277–85
- [182] Sutton P, Bennington P, Patel S N, Stefik M, Wiesner U B, Nealey P F, Steiner U and Gunkel I 2019 Surface reconstruction limited conductivity in block-copolymer li battery electrolytes *Adv. Funct. Mater.* **29** 1905977
- [183] Coote J P, Kinsey T, Street D P, Kilbey S M, Sangoro J R and Stein G E 2020 Surface-induced ordering depresses through-film ionic conductivity in lamellar block copolymer electrolytes *ACS Macro Lett.* **9** 565–70
- [184] Bullock S E and Kofinas P 2004 Nanoscale battery materials based on the self-assembly of block copolymers *J. Power Sources* **132** 256–60
- [185] Bullock S E and Kofinas P 2004 Synthesis of an A/B/C triblock copolymer for battery materials applications *Macromolecules* **37** 1783–6
- [186] He X, Wang Z, Zhou W, Jiang X, Han Z and Chen D 2017 Imidazolium-functionalized norbornene ionic liquid block copolymer and silica composite electrolyte membranes for lithium-ion batteries *J. Appl. Polym. Sci.* **134** 1–8
- [187] Ping J, Pan H, Hou P P, Zhang M Y, Wang X, Wang C, Chen J, Wu D, Shen Z and Fan X H 2017 Solid polymer electrolytes with excellent high-temperature properties based on brush block copolymers having rigid side chains *ACS Appl. Mater. Interfaces* **9** 6130–7
- [188] Bates C M, Chang A B, Momčilović N, Jones S C and Grubbs R H 2015 ABA triblock brush polymers: synthesis, self-assembly, conductivity, and rheological properties *Macromolecules* **48** 4967–73
- [189] Longstaff M, Gardiner K, Zhuravlev R, Finney J and Waldow D A 2019 Characterization of morphology in ring-opening metathesis polymerized novel solid block copolymer electrolytes by atomic force microscopy and x-ray scattering *Electrochim. Acta* **298** 339–46
- [190] Xie H Q, Xie D and Liu J 1989 Solid polymer electrolyte complexes of polyoxyethylene-containing star-shaped block copolymers and copolymers with uniform grafts *Polym. Plast. Technol. Eng.* **28** 355–69
- [191] Niitani T, Amaike M, Nakano H, Dokko K and Kanamura K 2009 Star-shaped polymer electrolyte with microphase separation structure for all-solid-state lithium batteries *J. Electrochem. Soc.* **156** A577
- [192] Tong Y, Chen L, He X and Chen Y 2013 Mesogen-controlled ion channel of star-shaped hard-soft block copolymers for solid-state lithium-ion battery *J. Polym. Sci. A* **51** 4341–50
- [193] Guan T, Qian S, Guo Y, Cheng F, Zhang W and Chen J 2019 Star brush block copolymer electrolytes with high ambient-temperature ionic conductivity for quasi-solid-state lithium batteries *ACS Mater. Lett.* **1** 606–12
- [194] Nykaza J R, Savage A M, Pan Q, Wang S, Beyer F L, Tang M H, Li C Y and Elabd Y A 2016 Polymerized ionic liquid diblock copolymer as solid-state electrolyte and separator in lithium-ion battery *Polymer* **101** 311–8
- [195] Zardalidis G, Ioannou E F, Gatsouli K D, Pispas S, Kamitsos E I and Floudas G 2015 Ionic conductivity and

- self-assembly in poly(isoprene-b-ethylene oxide) electrolytes doped with LiTf and EMITf *Macromolecules* **48** 1473–82
- [196] Metwalli E, Kaeppl M V, Schaper S J, Kriele A, Gilles R, Raftopoulos K N and Müller-Buschbaum P 2018 Conductivity and morphology correlations of ionic-liquid/lithium-salt/block copolymer nanostructured hybrid electrolytes *ACS Appl. Energy Mater.* **1** 666–75
- [197] Javier A E, Patel S N, Hallinan D T, Srinivasan V and Balsara N P 2011 Simultaneous electronic and ionic conduction in a block copolymer: application in lithium battery electrodes *Angew. Chem. Int. Ed.* **50** 9848–51
- [198] Patel S N, Javier A E, Stone G M, Mullin S A and Balsara N P 2012 Simultaneous conduction of electronic charge and lithium ions in block copolymers *ACS Nano* **6** 1589–600
- [199] Patel S N, Javier A E and Balsara N P 2013 Electrochemically oxidized electronic and ionic conducting nanostructured block copolymers for lithium battery electrodes *ACS Nano* **7** 6056–68
- [200] Kim H-K and Srinivasan V 2020 Status and targets for polymer-based solid-state batteries for electric vehicle applications *J. Electrochem. Soc.* **167** 130520
- [201] Sadoway D R, Huang B, Trapa P E, Soo P P, Bannerjee P and Mayes A M 2001 Self-doped block copolymer electrolytes for solid-state, rechargeable lithium batteries *J. Power Sources* **97–98** 621–3
- [202] Ryu S W, Trapa P E, Olugebefola S C, Gonzalez-Leon J A, Sadoway D R and Mayes A M 2005 Effect of counter ion placement on conductivity in single-ion conducting block copolymer electrolytes *J. Electrochem. Soc.* **152**
- [203] Rolland J, Poggi E, Vlad A and Gohy J F 2015 Single-ion diblock copolymers for solid-state polymer electrolytes *Polymer* **68** 344–52
- [204] Ghosh A and Kofinas P 2008 PEO based block copolymer as solid state lithium battery electrolyte *ECS Trans.* **11** 131–7
- [205] Ghosh A, Wang C and Kofinas P 2010 Block copolymer solid battery electrolyte with high li-ion transference number *J. Electrochem. Soc.* **157** A846–9
- [206] Fisher A S, Khalid M B and Kofinas P 2012 Block copolymer electrolyte with sulfur based ionic liquid for lithium batteries *J. Electrochem. Soc.* **159** A2124–9
- [207] Bouchet R *et al* 2013 Single-ion BAB triblock copolymers as highly efficient electrolytes for lithium-metal batteries *Nat. Mater.* **12** 452–7
- [208] Jangu C, Savage A M, Zhang Z, Schultz A R, Madsen L A, Beyer F L and Long T E 2015 Sulfonimide-containing triblock copolymers for improved conductivity and mechanical performance *Macromolecules* **48** 4520–8
- [209] Möhl G E, Metwalli E, Bouchet R, Phan T N T, Cubitt R and Müller-Buschbaum P 2018 In operando small-angle neutron scattering study of single-ion copolymer electrolyte for lithium metal batteries *ACS Energy Lett.* **3** 1–6
- [210] Villaluenga I, Inceoglu S, Jiang X, Chen X C, Chintapalli M, Wang D R, Devaux D and Balsara N P 2017 Nanostructured single-ion-conducting hybrid electrolytes based on salty nanoparticles and block copolymers *Macromolecules* **50** 1998–2005
- [211] Shao Z and Jannasch P 2017 Single lithium-ion conducting poly(tetrafluorostyrene sulfonate)-polyether block copolymer electrolytes *Polym. Chem.* **8** 785–94
- [212] Porcarelli L, Shaplov A S, Salsamendi M, Nair J R, Vygodskii Y S, Mecerreyes D and Gerbaldi C 2016 Single-ion block copoly(ionic liquid)s as electrolytes for all-solid state lithium batteries *ACS Appl. Mater. Interfaces* **8** 10350–9
- [213] Chen Y, Tian Y, Li Z, Zhang N, Zeng D, Xu G, Zhang Y, Sun Y, Ke H and Cheng H 2018 An AB alternating diblock single ion conducting polymer electrolyte membrane for all-solid-state lithium metal secondary batteries *J. Memb. Sci.* **566** 181–9
- [214] Zhang Y, Lim C A, Cai W, Rohan R, Xu G, Sun Y and Cheng H 2014 Design and synthesis of a single ion conducting block copolymer electrolyte with multifunctionality for lithium ion batteries *RSC Adv.* **4** 43857–64
- [215] Kawazoe T, Hashimoto K, Kitazawa Y, Kokubo H and Watanabe M 2017 A polymer electrolyte containing solvate ionic liquid with increased mechanical strength formed by self-assembly of ABA-type ionomer triblock copolymer *Electrochim. Acta* **235** 287–94
- [216] Nguyen H D, Kim G T, Shi J, Paillard E, Judeinstein P, Lyonnard S, Bresser D and Iojoiu C 2018 Nanostructured multi-block copolymer single-ion conductors for safer high-performance lithium batteries *Energy Environ. Sci.* **11** 3298–309
- [217] Kasemägi H, Ollikainen M, Brandell D and Aabloo A 2015 Molecular dynamics modelling of block-copolymer electrolytes with high  $t^+$  values *Electrochim. Acta* **175** 47–54
- [218] Inceoglu S, Rojas A A, Devaux D, Chen X C, Stone G M and Balsara N P 2014 Morphology-conductivity relationship of single-ion-conducting block copolymer electrolytes for lithium batteries *ACS Macro Lett.* **3** 510–4
- [219] Rojas A A, Inceoglu S, Mackay N G, Thelen J L, Devaux D, Stone G M and Balsara N P 2015 Effect of lithium-ion concentration on morphology and ion transport in single-ion-conducting block copolymer electrolytes *Macromolecules* **48** 6589–95
- [220] Aissou K, Mumtaz M, Usluer Ö, Pécastaings G, Portale G, Fleury G, Cloutet E and Hadziioannou G 2016 Anisotropic lithium ion conductivity in single-ion diblock copolymer electrolyte thin films *Macromol. Rapid Commun.* **37** 221–6
- [221] Porcarelli L, Aboudzadeh M A, Rubatat L, Nair J R, Shaplov A S, Gerbaldi C and Mecerreyes D 2017 Single-ion triblock copolymer electrolytes based on poly(ethylene oxide) and methacrylic sulfonamide blocks for lithium metal batteries *J. Power Sources* **364** 191–9
- [222] Devaux D, Liénafa L, Beaudoin E, Maria S, Phan T N T, Gignes D, Giroud E, Davidson P and Bouchet R 2018 Comparison of single-ion-conductor block-copolymer electrolytes with Polystyrene-TFSI and Polymethacrylate-TFSI structural blocks *Electrochim. Acta* **269** 250–61
- [223] Ahmed F, Choi I, Rahman M M, Jang H, Ryu T, Yoon S, Jin L, Jin Y and Kim W 2019 Remarkable conductivity of a self-healing single-ion conducting polymer electrolyte, poly(ethylene-co-acrylic lithium (fluoro sulfonyl)imide), for all-solid-state Li-ion batteries *ACS Appl. Mater. Interfaces* **11** 34930–8
- [224] Kitazawa Y, Iwata K, Imaizumi S, Ahn H, Kim S Y, Ueno K, Park M J and Watanabe M 2014 Gelation of solvate ionic liquid by self-assembly of block copolymer and characterization as polymer electrolyte *Macromolecules* **47** 6009–16
- [225] Steinle D, Chen Z, Nguyen H D, Kuenzel M, Iojoiu C, Passerini S and Bresser D 2021 Single-ion conducting polymer electrolyte for Li||LiNi<sub>0.6</sub>Mn<sub>0.2</sub>Co<sub>0.2</sub>O<sub>2</sub> batteries impact of the anodic cutoff voltage and ambient temperature *J. Solid State Electrochem.* (<https://doi.org/10.1007/s10008-020-04895-6>)
- [226] Chen Z, Steinle D, Nguyen H D, Kim J K, Mayer A, Shi J, Paillard E, Iojoiu C, Passerini S and Bresser D 2020 High-energy lithium batteries based on single-ion conducting polymer electrolytes and Li[Ni<sub>0.8</sub>Co<sub>0.1</sub>Mn<sub>0.1</sub>]O<sub>2</sub> cathodes *Nano Energy* **77** 105129
- [227] Zhai C, Zhou H, Gao T, Zhao L and Lin S 2018 Electrostatically tuned microdomain morphology and phase-dependent ion transport anisotropy in single-ion conducting block copolyelectrolytes *Macromolecules* **51** 4471–83
- [228] Shen K H, Brown J R and Hall L M 2018 Diffusion in lamellae, cylinders, and double gyroid block copolymer nanostructures *ACS Macro Lett.* **7** 1092–8